A STRUCTURAL HEALTH MONITORING SYSTEM FOR COMPOSITE PRESSURE VESSELS

A Thesis Submitted to the College of
Graduate Studies and Research
in Partial Fulfillment of the Requirements
for the Degree of Masters of Science
in the Department of Mechanical Engineering
University of Saskatchewan
Saskatoon

by
Bryan C. Lung

PERMISSION TO USE

In presenting this thesis in partial fulfillment of the requirements for a Postgraduate degree from the University of Saskatchewan, I agree that the Libraries of this University may make it freely available for inspection. I further agree that permission for copying of this thesis in any manner, in whole or in part, for scholarly purposes may be granted by the professor or professors who supervised my thesis work or, in their absence, by the Head of the Department or the Dean of the College in which my thesis work was done. It is understood that any copying or publication or use of this thesis or parts thereof for financial gain shall not be allowed without my written permission. It is also understood that due recognition shall be given to me and to the University of Saskatchewan in any scholarly use which may be made of any material in my thesis.

Requests for permission to copy or to make other use of material in this thesis in whole or part should be addressed to:

Head of the Department of Mechanical Engineering
University of Saskatchewan
Saskatoon, Saskatchewan S7N 5A9

ABSTRACT

Vehicles that run on compressed natural gas and hydrogen are currently being developed to reduce greenhouse gas emissions and smog. To meet the need for a safe, reliable fuel storage system, a low-cost, acoustic-ultrasonic system has been developed to detect damage in high-pressure storage cylinders made of Carbon Fiber Reinforced Polymers (CFRP). This structural health monitoring system could lead to lighter, lower cost cylinders, and improved safety in automotive applications that utilize hydrogen and natural gas.

Several Non-Deconstructive Evaluation (NDE) techniques were investigated in the course of this work, and low-cost piezo-film sensors were selected to monitor the cylinder. These sensors were integrated into the carbon fiber structure, resulting in a sensor network that can be used for real-time structural health monitoring of composite cylinders. The system was operated by exciting the piezo-film sensors with an impulse and then the corresponding structural response (or signature) was measured and analyzed. This was compared to a previously measured response and evaluated for changes which can indicate failures in the tank. The analysis reduces the changes in the structural response to a single damage coefficient, which can then be used for malfunction indication and decision making in an automotive on-board microprocessor control system.

The technology can be deployed at a reasonable cost, and has been designed to accurately detect damage with little or no maintenance required. Thirty cylinders were used in a test matrix to examine all possible failure mechanisms of the tanks, including: fatigue, cuts and gouges, impact and delaminations, stress rupture, heat damage, and combinations of these damage mechanisms. The damage detection system was capable of detecting damage long before a critical condition arose for all cases. However, further development and testing into larger cylinder designs and testing is still required to develop a final commercial product.

ACKNOWLEDGEMENTS

The author would like to thank Mike Sulatisky and Sheldon Hill of the Saskatchewan Research Council for their technical assistance and support throughout the project. The technical assistance of Craig Webster, Joe Wong, Carl Gung and Norbert Neufeld of Powertech Labs Inc. is also gratefully acknowledged.

The author wishes to express his gratitude to his co-supervisors Dr. R. Burton and Dr. S. Habibi, and to Marcy Green for all of her assistance in preparing the thesis. As well, the author would like to express gratitude to his wife for all of her patience.

Financial assistance was provided by the following organizations as a part of a larger research project:

- Natural Resources Canada
- Precarn Incorporated
- Climate Change Action Fund
- Saskatchewan Research Council
- Powertech Labs Inc.
- Charonic Canada Inc.

CONTENTS

TABLES

FIGURES

NOMENCLATURE

AE	Acoustic Emission
ANSI	American National Standards Institute
Code	A document that provides guidance in the construction, operation, or maintenance of components or systems
CFRP	Carbon Fiber Reinforced Polymer
CSA	Canadian Standards Association
d	piezo-electric constant, defined as the induced strain for a applied field
Δl	change in length (m)
Δt	change in thickness (m)
DC	Direct Current
C	capacity of the piezo-electric material
ε_o	dielectric constant of space (F/m)
ETFE	Empirical Transfer Function Estimate
F	force (N)
Failure Mode	The manner by which a failure is observed. Generally, it describes the way the failure occurs and its impact on equipment operation
FFT	Fast Fourier Transform
fr	resonant frequency (Hz)
g	piezo-electric constant, defined as the open circuit field for a given stress
h	height (m)
ISO	International Organization for Standardization
k	integer
K	relative dielectric constant
l	length (m)
M	integer
n	integer

NDE	Non-Destructive Evaluation
NGV	Natural Gas Vehicle
P	periodogram as calculated as the power spectral density
PAC	Physical Acoustics Corporation
PSD	Power Spectral Density
PVDF	poly-vinyl di-flouride
Q	applied charge (J)
S(ω)	spectral estimate
Standard	A document containing technical specifications or other precise criteria to be used consistently as rules, guidelines or definitions of characteristics, to ensure that materials, products, processes, and services are fit for their purpose
t	thickness (m)
U(ω)	normalized transfer function difference
V	voltage (V)
ω	frequency (rad./sec or cycles/sec)
w	width (m)
W	window characteristic
x	signal response
y	signal response

CHAPTER 1. INTRODUCTION

1.1 General

One of the most difficult issues in the development of alternative energy is in the storage of the gaseous fuel. Most often, the use of gaseous fuels, such as hydrogen and natural gas, can provide outstanding operating benefits and efficiency improvements over conventional fuels. However, the most expensive and complex component of the fuelling system is in the storage of these gaseous fuels.

In gaseous-fuelled vehicles, the most complex part of the fuelling system is traditionally the storage mechanism. In the fuelling system, the storage system constitutes the largest cost of the entire fuelling system, typically over 50% of the total costs [Sulatisky , 2002]. There are three other main design factors for the storage system. The first is the amount of stored energy in the system, the second, the volume of the storage system, and finally, the weight of the storage system. The high costs of the storage systems are commonly thought of as the main barrier in preventing the implementation of alternative fuels on a large scale [Sulatisky, 2002].

There are several mechanisms used to store gaseous fuels such as hydrogen. Hydrogen is considered as the most important and difficult gas to store, as the energy storage density (stored energy per unit volume) is lower than that of compressed natural gas, and much lower than conventional liquid hydrocarbon fuels. The methods used to store hydrogen include low-temperature cryogenic liquefaction, physical heavy metal hydrides, chemical storage in alkalai metal hydrides and high-pressure (compressed) gaseous storage [Bossel, 2003]. In order to weigh the advantages of one method over another, one must consider the energy input to store the hydrogen, stored energy density of the hydrogen,

and of course the practical limitations of each method. Each of these methods is discussed in the following paragraphs.

The low-temperature cryogenic liquefaction method of storing hydrogen allows for a reasonable amount of hydrogen to be stored in a given volume. This equals approximately 28% of the energy storage of gasoline for a given volume. However, liquid hydrogen must be stored in complex pressure vessels or cryogenic vessels. Hydrogen exists as a liquid at 20.3K at atmospheric pressure. This requires complex liquefaction plants to liquefy hydrogen. There are substantial costs associated with cryogenic storage, which involve refrigeration and evaporative losses of the gases. Using the finest current technology 40% of the higher heating value of hydrogen, at best, is used for liquefaction [Bossel, 2003]. In addition, the hydrogen boil off is 3 to 4% per day. For example, if a car is parked at the airport for 14 days, then the loss would be 50 to 60% of the stored hydrogen. Hence, there are operational, storage, and parking issues associated with liquefied hydrogen.

The second method of storing hydrogen uses physical metal hydrides. This method is based on the physical adsorption in spongy matrixes of special alloys as physical metal hydrides, such as $LiNi_5$ or $ZrCr_2$. In general, the energy balance with metal hydrogen requires compression to add the hydrogen, which releases heat. To extract H_2, heat is added. If properly designed to interact with the environment, this heat can be extracted from the environment. Typical compression pressures are 30 bar (440 psi), which requires significantly less energy than hydrogen stored as a high pressure compressed gas or for liquefaction.

However, physical metal hydrides (PMH) are quite impractical for mobile storage applications as they are very heavy. Currently, PMH's can only store hydrogen amounting to one percent of the total mass of the storage system. For example, 2 kg of hydrogen will require an amount of PMH of up to 200 kg to store this hydrogen. This stored hydrogen is equivalent to about 8 L of gasoline, which shows that it is quite impractical to use PMH for mobile sources of hydrogen.

The third method to be discussed with regards to storing hydrogen is storing the hydrogen chemically in alkaline metal hydrides. There are many different compounds available, but they are never found in a natural state. Energy is needed to form these compounds and bond the hydrogen to the alkaline metal hydrides. When the hydrogen is extracted, water is added to the hydrides, which releases the hydrogen, as well as reducing water to hydroxide. This releases energy, but this low grade energy is not useful and is lost to the environment.

Energy studies have shown that 60% of the energy of the hydrogen is required, theoretically, to produce and store the hydrogen as an alkali metal hydride [Bossel, 2003]. Accounting for losses in efficiency of real life, this number is actually much higher, and poses practical problems in application. In use, the hydrides react vigorously with water, releasing large amounts of hydrogen and energy, resulting in volatility. This can pose a safety issue, requiring complex containment systems to be put in place, especially for mobile applications.

High-pressure (compressed) gaseous storage is the last method of storing hydrogen to be discussed. Compression of gases requires energy. This energy is related to adiabatic compression relationships for real gases. By utilizing multi-stage compression, approximately 8% of the energy stored in the hydrogen is used to compress the hydrogen to 200 bar (2900 psi). To achieve 700 bar (10,200 psi), approximately 12% of the energy stored in the hydrogen is used for compression. Although complex high-pressure storage tanks are required to store the hydrogen at these pressures, this method of storage appears as one of the most attractive methods of hydrogen storage.

The focus of this research project is based on existing technologies, and as such, the discussion of future methods of storing hydrogen are not considered as they are not commercially available for gaseous storage. The project, thus, focuses on compressed gaseous storage of alternative fuels such as natural gas and hydrogen.

Safety studies have shown through “Failure Modes and Effects Analyses” that the most critical component of the vehicle fuelling system is the storage tank for gaseous fuels [White, 2002]. This includes both hydrogen and natural gas. The main reason for this is due to the high energy density of the stored fuel in the pressure vessel. Thus, improving safety of the pressure vessel has a profound effect on improving overall vehicle safety of the alternative fueled vehicle.

In general, the public views alternative fuelled vehicles very critically. Accordingly, one catastrophic failure of a high-pressure fuel tank tends to attract large media coverage. As this industry is very sensitive, most manufacturers that work in the alternative fuels area are very cautious to avoid having any failures of any kind. History has shown that when components fail, reliability of the whole industry comes under scrutiny which can bankrupt companies very quickly. The insurance and liability risk avoidance associated with manufacturing any product is becoming an increasingly important component in a manufacturer’s assets. Any product that improves safety reduces insurance and associated manufacturing costs. Furthermore, a product that can help prevent a catastrophic failure of a high-pressure cylinder by identifying faults before they become a problem would be an asset to any manufacturer.

In order to evaluate the best fit for the application of such a diagnostic technology, the different high-pressure storage tanks need to be examined.

1.1.1 Storage Tanks

Currently, the most economical method of storing gaseous fuels for transportation is through compression and high-pressure storage of these gases. However, to maintain driving range and utilization of space in vehicles and while minimizing weight, it is advantageous to use exotic materials to optimize the gas storage / weight ratio. This has been the driving function for the development of the carbon fiber storage tank.

There currently are four types of cylinders developed for the compressed gas market, as illustrated in Figure 1.1[ANSI/CSA, 2000]:

- Type I: All – metal pressure vessels, commonly called monolithic pressure vessels,
- Type II: Metal pressure vessels that are hoop-wrapped on the body with fiber reinforcement,
- Type III: Metal-lined pressure vessels completely wrapped fiber reinforcement, and
- Type IV: Plastic or non-metal lined pressure vessel with complete wrapped fiber reinforcement.

Figure 1.1: Different Pressure Vessel Classifications

Each different type of pressure vessel has different strengths. The monolithic pressure vessels (Type I) were the first common pressure vessel used for high pressure storage and their failure modes are very well understood. [Bhuyan and Su, 1998,Teply and Herbein, 1985] As an example, the fatigue life is very predictable, and designs incorporating leak-before-burst criteria can be accomplished. Other advantages for monolithic designs include a very high compressional design strength, which means that the tank is less susceptible to handling damage when the tank is empty. However, the tanks are very

heavy when compared to their composite counterparts. Type I pressure vessels are typically made out of either aluminum or steel.

The second type of pressure vessel (Type II) was the first example of the composite pressure vessel design. Type II pressure vessels consist of a metal cylinder with a hoop-overlay of composite material. This composite material usually consists of carbon fiber, fiberglass, or blends of the two materials. The use of the composite overwrap to retain the hoop stresses allows the walls of the metal lined tank to be reduced in thickness where the composite overlay is present. The result of this design feature is reduced metal in the liner, resulting in reduced weight when compared to their monolithic counterparts. These pressure vessels were the first commercial composite pressure vessel used for vehicular high-pressure gaseous storage. However, incorporation of composites typically results in increased manufacturing and certification costs.

The third pressure vessel design (Type III) consists of a metal liner, usually aluminum for prevention of oxidation corrosion, and a composite wrap overlay on the cylinder. The composite overlay, different than the Type II cylinder, consists of both hoop and transverse wraps on the cylinder. This results in complete coverage of composite material over the surface of the cylinder. The composite can be composed of different materials, typically carbon fiber or fiberglass, with blends of the materials also used. The advantage of this type of design is a reduction in weight of the cylinder, as the metal liner thickness can be reduced. The metal liner of the cylinder serves primarily as a membrane to contain the pressurized gases, as the composite wrap is not leak-tight. The composite overlay only retains the stress of the compressed gases. This system works primarily because the composite has a very high modulus of elasticity in comparison to the metal liner, resulting in the composite overlay taking the bulk of the load in the structure.

The fourth pressure vessel design (Type IV) consists of a plastic-lined pressure vessel with composite overwrap. This pressure vessel design is considered one of the most advanced due to the plastic liner having superior fatigue resistance relative to metals.

The spread between the modulus of elasticity for the plastic liner and the composite overwrap ensures minimal fatigue cycling on the plastic membrane. The plastic liner only serves as a retaining bladder for the pressurized gases stored inside the cylinder, as the composite wrap is not leak-tight. However, problems associated with the plastic liner have limited the application of these types of cylinders in the market. In particular, compatibility of the plastic liners with the automotive fluids (oils, solvents, gases, etc.) have caused problems, along with other environmental extremes in service.

The pressure vessels chosen for this project were of a Type III design. In particular, the tanks are designed and manufactured by Dynetek Industries of Calgary, Alberta. These tanks are composed of carbon-fiber reinforced polymer (CFRP) wrap over an aluminum liner. The liner itself serves as a bladder to contain the gas. The structural strength for pressure comes from the CFRP wrap.

Most pressure vessels, when pressurized are, in actuality, very difficult to damage from impact alone. This is a result of the pressure vessel having a large compressional strength due to the high pressures of gases stored within. Generally, when under pressure, the cylinders are susceptible only to damage with localized impact (penetration), or cutting action. The cylinders, however, are most vulnerable when they are empty due to the lack of structural strength. Much like a wire rope, the vessels can be kinked and damaged easily when not under load. One has to use extreme caution when handling empty cylinders, as they are extremely susceptible to damage if they are dropped, as is illustrated in Figure 1.2.

As illustrated in Figure 1.2a, the cylinder has been handled improperly and dropped when empty. As the composite can be easily damaged when handled, incidences of catastrophic failures are further compounded by the fact that damage to the composite structure cannot be easily assessed visually. In Figure 1.2b, the damaged cylinder which appeared to have only a slight scuff on the surface of the cylinder, was then subsequently pressurized. Before the tank obtained its full service or operating pressure, the cylinder failed. Depending on the extent of the damage, this failure can range from a slight

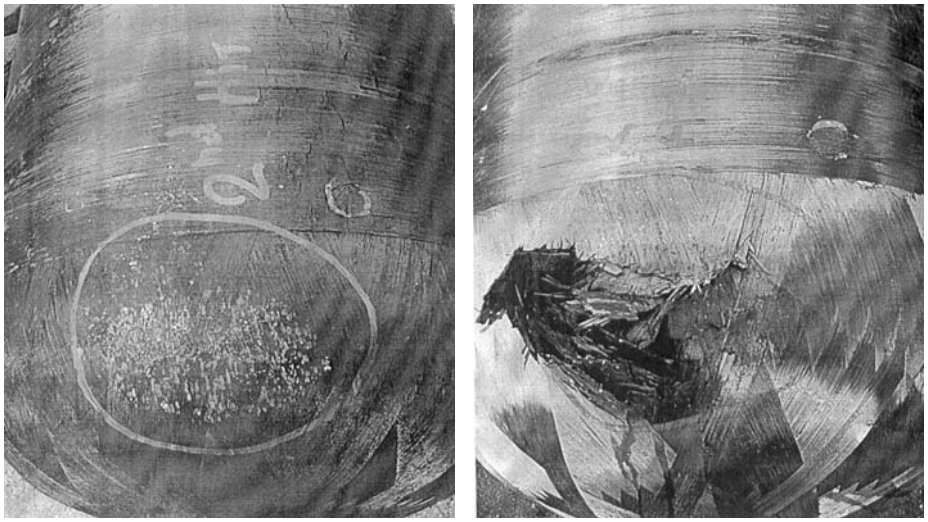

(a) (b)

Figure 1.2: Drop Damage
Drop damage before pressurization (a) and after pressurization (b)

release of gas pressure to a full catastrophic failure with debris and other projectiles causing damage.

Unlike conventional Type I tanks, external damage to the composite tanks is not very noticible, and cannot be easily found when the tanks are visually inspected. However, with Type III and IV tanks, the composite wrap retains nearly all of the structural support for the pressure vessel, thereby decreasing the visual signs of damage. Accordingly, when either the epoxy matrix or the fibers are damaged, this drastically reduces the structural integrity of the cylinder. However, advantages to the composite structure remain. As illustrated in Figure 1.2b, the failure with localized damage remains localized and catastrophic failure is avoided, as would not be the case with Type I pressure vessels. Therefore, it is important to understand how the cylinders fail in order to prevent failures of composite cylinders.

1.1.2 Tank Failure Modes and Codes

In order to design a system to properly protect the tank from all operating variations and failure modes, it is crucial to understand tank failure modes. Not obtaining a clear understanding of these failure modes can result in an ineffective fault diagnostic system,

which is potentially more dangerous than a cylinder without such a system. The areas of concern for failure include:

- Impact damage causing delaminations,
- Cut and gouge damage causing fiber damage,
- Elevated temperature from heat or fire,
- Composite and liner fatigue, and
- Sustained load, or stress rupture.

Most of the above failure modes take place in a similar manner. The end result of cuts, fatigue, and impact most often result in delaminations of the layers of composite overwrap. This delamination is the separation of the fiber layers through the degradation of the resin matrix. The resulting flaw allows movement of the fibers on top of each other, causing spread of the delamination as well as fretting and breakage of the fibers.

In order to fully understand the failure modes of the cylinders, reference to the relevant design codes and standards that the CFRP pressure vessels should be made. These codes have originated primarily as a reactive measure to address failures that have happened in industry. Currently, one of the strictest codes used in the industry is the NGV2-2000 code adapted for hydrogen [ANSI/CSA, 2002]. This code requires the following tests to be made in order to certify a new tank design:

- Drop Test: 1.83 m height from the lower end at 45° from vertical
- Flaw Tolerance Test: two cuts: 25 mm x 1.25 mm and 200 mm x 0.75 mm – both cut in the longitudinal direction into the composite sidewall
- Bonfire Test: flame source encompassing cylinder at a minimum temperature of 430°C
- Stress Rupture: 1.25 times service pressure for 1000 hours
- Fatigue Cycling: contains a test matrix of environmental, ambient, and tolerance requirements.

Details of the NGV-2 2000 code for composite pressure vessels for vehicle use are summarized in Appendix A. The failure modes that this code identifies will briefly be discussed in the following paragraphs.

A major failure mode is damage, which is due to delaminations. Delamination is most often caused by impact damage due to drops, vehicle collisions, and other related events. The delaminations can be audibly detected by tapping on the surface of the structure. If a change in pitch is heard when the surface over the damaged area is tapped, then a delamination exists. It is very difficult to correlate the degree, size and effect of the delamination on the structure using this method. Factors, such as the tightness of the wrap, mounting brackets, the pressure contained within the tank and the stored fluid type and density will all affect the sound of the tank as it is tapped, as well as the size and sound from the delaminated spot. This is a very difficult method to determine the structural integrity of a cylinder.

Delamination typically causes failure of the cylinder that is proportional to the degree and size of the delamination. If, for example, the delamination is very severe, it is possible to have the tank fail upon pressurization. However, with the current design of pressure vessels, and in particular the Type III aluminum-lined CFRP Dynetek pressure vessels, this rarely, if ever, happens regularly. Typically, what happens with a delamination is the structure is weakened, causing movement. This movement causes a gradual enlargement of the delamination. Eventually, the tank will fail due to liner fatigue because of elevated stresses in the liner as a result of the CFRP weakening. The failure of the liner results in leakage of the stored fluid. In the designs that do not have this advantage of a semi-load bearing liner, delaminations can cause elevated stress levels leading to rupture of the tanks.

A second failure mode is associated with cut and gouge damage to the composite fibers that make up the load-bearing part of the cylinder. Cut and gouge damage on the tanks will produce failure of the tank. As with impact damage, the degree of damage will

determine the failure mechanism of the tank. Typical causes of cuts and gouges are impacts or collisions in service with road debris, curbs, and other objects. The presence of a cut or gouge in the tank simply removes load-bearing fibers from the tank. The removal of these load-bearing fibers reduces what is known as the burst pressure of the tank. This does two things: first, if the reduced burst pressure falls below the service pressure, the tank will fail upon pressurization; second, the reduction of the load-bearing fibers will cause stress levels to be increased throughout the structure. As a result, the weakest point in the structure will fail first. Typically, this will be the aluminum liner in the tank, as the liner will tend to take some of the load as the structure begins to flex as the pressure is cycled.

The failure mode associated with cut and gouge damage can be considered similar to the failure mode of delaminations. They are similar since the cut and gouge damage causes delaminations in the structure as the elevated fiber stress levels cause the structure to move and shift. In comparison, the following failure mechanisms are different as they cause different failure modes.

A third failure mode is often the most difficult to detect or predict. Elevated temperature is of concern to CFRP structures due to failure of the matrix. Typically, the breakdown temperature of the epoxy matrix used in these tanks is approximately 450°C. At this temperature, the epoxy disintegrates and has little or no structural integrity remaining. Localized heat damage, through the use of a propane torch for example, can cause failure of CFRP pressure vessels as the matrix is removed, causing a lack of structural strength of the tank. This can be caused as well by heating on members on or near the tanks such as strapping, bolts, fittings, and other members. Oxy-acetylene torches can easily reach the breakdown temperatures of the matrix, and are capable of damaging the structure. However, the visual range of damage can vary from a blackened spot that can be polished or wiped off, to the breakdown of the composite fibers due to lack of a proper matrix.

Composite fatigue is another type of failure mechanism for carbon-fiber tanks. The fatigue life of the tank is always design-dependent and difficult to determine. In the case

of aluminum-lined tanks, the fatigue of the liner is the failure mechanism that dominates the cylinder life when properly designed and manufactured. However, when this does not happen, the composite material can fatigue and lose its structural integrity. This is often seen in the case of Type I pressure vessels that unexpectedly rupture in service. Factors such as temperature, contained fluid type, pressure cycles and other environmental conditions help determine the structural life of the pressure vessel.

Stress rupture is the final failure mechanism of concern for these pressure vessels. The CFRP structure exhibits a failure mechanism unique to this type of tank. The closest type of failure mode in Type I cylinders is creep. What tends to happen is that when the tanks are subjected to an elevated pressure (typically about two times service pressure and above) they have a finite life. If left past their life, the tanks will tend to rupture, similar in action to creep. It is important to evaluate the stress rupture life of the tank, as this can produce unexpected failures. Alternatively, this can be prevented through proper operation and maintenance of the pressure vessels.

1.2.3 Tank Diagnostics Systems

There are two components of the tank cylinder that are of interest in this particular study. The first is the composite wrap, composed of carbon fiber reinforced polymer; the second is the liner within the tank. Each component has a specific purpose: the composite wrap bears the force of the high-pressure inside the tank, and the liner contains the gas within the wrap preventing leakage. If the liner fails, the tank leaks; it does not rupture, but simply leaks gas with what could be considered excessive permeation through the structure. This can be easily detected by a reduction in pressure, similar to a leak anywhere on components or fittings.

The industry demand for on-board storage cylinders of lighter weight has led to the increased use of high-strength composite materials. Compared to Type I tanks, these high-pressure (up to 250 bar, 3,630 psi) composite-wrapped tanks have proven to be lighter with often less than one-quarter of the vessel mass of its equivalent monolithic

counterpart. However, usage of these composite tanks have shown that they are more susceptible to in-service damage. A regulatory system for the periodic inspection and/or re-testing of storage tanks in fuel cells or natural gas vehicles does not exist in Canada or the U.S. In addition to the need to ensure cylinder integrity, fuel cell vehicles and natural gas vehicles suffer from reduced driving range when compared to conventional gasoline or diesel fuelled vehicles. Hence, a reliable fault sensing system will permit more aggressive tank designs. In a futuristic vehicle, it is most desirable to have a tank with a life of 20 years at one-half the price than a tank with an 80-year life that weighs too much. A proper diagnostic and prognostic system would mean that storage tanks would not have to be over-built with safety factors on top of safety factors.

Currently, there are no commercially available diagnostic systems for these types of structures. The current state-of-the-art technology utilizes ultrasonic technology, requiring an ultrasonic sensor to transmit a signal into the structure. A reflected signal is received, and the timing of the signal is used to identify cracks, delaminations, and other flaws in the structure. However, these technologies require the cylinder to be removed from service, and placed in a rotational apparatus that allows the ultrasonic sensor to pass over the entire surface of the structure [Van de Loo, 1999]. This does not provide a continuous method of determining the structural integrity of the cylinder, but rather a periodic assessment, and would not be suitable for a diagnostic system in a vehicle.

In the past, investigations into acoustic emission have been utilized for composite pressure vessels [Osamu, 1990]. Essentially, acoustic emission works on the principle that as a composite structure is stressed, at some point before failure of the structure, the fibers will yield and start to break. Each fiber breakage is defined as an event, and as the structure is stressed closer to the point of failure, the time rate of events significantly increases. In a well defined experiment, acoustic emission can be used to define a critical threshold, or knee in the events/time basis at which point the structure has started to degrade. Although providing good potential for damage indication in pressure vessels, the “Kaiser effect” [Nesvijski and Sarkis, 2000] still limits the application of this technology. The Kaiser effect states that in order to evaluate the structure, it needs to be

stressed into a state beyond its previous stress levels. In essence, the structure has to be overstressed in order to evaluate it, causing potential damage to the structure, while only providing a periodic assessment of the structural integrity.

Investigations are currently being made into strain monitoring. Research is being conducted into fiber-optic based systems, using such technology as Bragg Filters and transmission from one fiber to a second in a twisted fiber pair to measure local strain in the structures [Foedinger et al., 1999, Udd et al., 2000]. These types of systems allow for localized strain monitoring in the structure, but are only able to determine damage local to the sensing media.

Although ultrasonic and fiber optic technologies are dropping in price, the implementation of these technologies in mass production remain in the distant future. As with any supplemental system, the costs must remain significantly lower than the product that it is supplementing. This limits the application of such ultrasonic and fiber-optic technologies. Furthermore, implementation of acoustic emission technologies remains in a very small niche market, as this technology can be very sensitive to automotive and environmental noise.

A system is still required that will allow continuous assessment of the structural integrity, while providing reliable evaluation that is independent of pressure, application and other environmental factors. What is needed, then, is a monitoring and diagnostic system that can ensure the structural integrity of storage tanks, with the capability of preventing the pressurizing of the tanks should a problem be detected, or if the design life span of the cylinder is exceeded. Such a “smart cylinder” will make it possible to keep track of their location, and to remove them from service once their design life is over. Integration of such a fault sensing system into vehicle controllers, fuelling systems and fuelling stations can lead to numerous advantages over existing technology.

The application for such a diagnostic system can be broken down into two major areas. The first is in the application for on-board vehicle use. The second application is in the

use of lightweight tube trailers for portable storage of high pressure gases. Two driving forces will help to enable this technology: first, economics, as design and costs may eventually be optimized by providing continuous integrity monitoring, and second, operational safety levels which can be improved.

Volume and weight are important parameters in the design of storage cylinders. The volume is critical to the mass of gas stored, while unnecessary cylinder mass causes reductions in efficiency, increased power requirements, and ultimately reduces the design efficiency. Thus, the use of composite (CFRP) pressure vessels becomes good design practice because of better material properties.

As the hydrogen industry begins to grow, infrastructure for fuelling vehicles will be required, and the cost needs to be optimized. Currently, there are very few known or proven methods to examine the structural integrity of these composite pressure vessels. Accordingly, visual inspections are used every three to five years, as well as a complete removal of the tanks and a hydrostatic proof to 1.25 times the service pressure. Introduction of a continuously monitored integrity observation system would allow for these tanks to be used in operation until their fatigue life is significantly reduced, or substantial damage to the composite wrap is inflicted. Compared to other methods of bulk hydrogen storage, compressed gas has the potential to become the most economical if properly developed.

As with most new and innovative technologies, damage detection has been used in the aerospace field for many years. Movement of such safety systems into automotive applications is now possible with the movement to fuel injection and increased computer control in the automotive fuel systems. Once the technology can be applied with significantly reduced cost on a mass – production scale then costs decrease and the technology becomes an accepted practice. Accordingly, the design must meet these demands, with a minimal cost for sensors, instrumentation and signal conditioning equipment. Advanced software design can be used to supplement by incorporating such

concepts as intelligence, expert systems, smart systems, and optimal design and control of all aspects possible.

1.2 Project Objectives

The objective of this project is to develop an on-board tank damage detection system. The system must be capable of evaluating the current structural integrity of the cylinder. In particular, the system must be able to identify damage present in the composite wrap, or load-bearing portion of the cylinder.

The Dynetek DyneCell cylinder has been chosen as the preferred cylinder design for the application of the damage detection technology. The design has shown itself to be robust, reliable, and predictable for in-service applications, creating a good platform to base the fault diagnostic work. The detailed project objectives include:

1. To define methods of failures in automotive gaseous storage cylinders,
2. To evaluate the current state of the art in Non-Destructive Evaluation (NDE) techniques for composite cylinders,
3. To develop a technique to identify the presence of a fault in a cylinder,
4. To experimentally evaluate the feasibility of the technique, and
5. To present the design of the fault detection system.

1.3 Thesis Outline

The format of this thesis shall be as follows: Chapter 2 introduces the relevant failure mechanisms and non-destructive techniques available to monitor the cylinders. Chapter 3 discusses sensor selection and sensor designs. Chapter 4 illustrates the test methods used, while Chapter 5 discusses the data analyses used in the system. Chapter 6 gives the results, and Chapter 7 gives the discussion. The thesis conclustions and recommendations are made in Chapter 8.

CHAPTER 2. FAILURE MECHANISMS OF CYLINDERS AND NON-DESTRUCTIVE EVALUATION TECHNIQUES

2.1 Introduction

Over the past 30 years, the high-pressure gas cylinder technology has been emerging using artificial high-strength fibers in engineering products. The trend started with the introduction of glass fibers, and was followed by aramids (nylon-based fibers), and more recently by carbon-based fibers [Bar-Cohen, 2000]. Restricted initial availability and costs have meant that artificial, high-strength fibers have only been provided for strategic uses in military and aerospace applications where high strength and low weight overrode other considerations.

As fiber availability increased, other specialized uses have emerged, such as sporting equipment, where it is currently the norm [Walters, 2003]. High-strength fibers have also become established in the field of high-pressure gas cylinder manufacture. As with other applications, fibers have made initial commercial impact in those cylinder uses where weight is paramount, such as firefighting tanks, and alternative fuels such as compressed natural gas and hydrogen. Although at the present time costs are too high for widespread application of composites into industrial gas storage and distribution, the growth trends will certainly continue.

To properly understand the requirements for the diagnostic technology of high-pressure gas cylinders, it is essential to understand the cylinder failure mechanisms. These mechanisms indicate what type of damage a diagnostic system will be required to detect, how to design the system for the operational modes, as well as what type of damage will be used to assess the system. This, then, is the objective of this chapter.

The following steps were determined for the development of the proposed diagnostic technology:

- evaluate relevant failure mechanisms
- perform background investigations into current non-destructive evaluation (NDE) techniques
- select the best NDE candidate for this application
- select, locate and place sensors on the pressure vessel
- identify signal inputs and outputs
- analyze and reduce data
- perform input compensation
- evaluate system reliability and accuracy

In this chapter the first three steps are discussed. The remaining items are discussed in subsequent chapters.

2.2 Failure Mechanisms

A feature of the composite-wrapped cylinder is that over-reinforcement leads to a change in the bursting from a hoop failure mode with longitudinal tearing of the body (as always occurred in an unwrapped cylinder) to a longitudinal failure mode with transverse fracture of the cross section, resulting in the cylinders' separation and projection. This latter failure mode is, on safety grounds, considered unacceptable. On the other hand, a cylinder carrying insufficient reinforcement will not fully exploit the potential benefits offered by composites.

It follows that a critical understanding of the factors influencing the change of burst mode is of importance to the design and manufacture of cylinders. A further significant feature of wrapping is that pre-stressing can be readily employed to provide favorable load sharing conditions between the metallic cylinder (or liner) and the fiber/resin overwrap.

While not affecting ultimate bursting conditions, pre-stressing can significantly improve cyclic fatigue performance of the liner by reducing tensile hoop stress in the normal elastic operating range. A convenient method of creating pre-stress is by autofrettaging the wrapped cylinder, involving deliberate overpressurization into the metallic liner's plastic range during manufacture [Walters, 2003].

Since composite cylinders are often used in the same markets and for the same purpose as traditional all-metal cylinders, standards for composites are intended to provide the same overall level of safety, and as far as possible are written in a similar way – with one exception, namely the approach to cylinder design. With metallic cylinders, it has been the long-held practice to provide within the standard a specific clause on the design including stress formulae derived from well-established materials theory [Bhuyan and Su, 1998]. This approach is unambiguous, ensuring that the stress in the body of the cylinder due to internal pressurization never exceeds a given safe proportion of the material's strength properties under normal operating conditions. However, with the greater complexity of composite cylinders, it has generally been judged too difficult to follow a similar track [Walters, 2003]. Instead, the concept of a performance-based design has been introduced whereby the adequacy of a new cylinder is proven by carefully selected tests intended to represent extremes of service conditions [ASTM, 2001].

While this effectively experimental performance-based approach to design leads to a safe composite cylinder, it is inevitably resource consuming and costly in the amount of testing required compared with prescriptive design. With infant technology, this method of design is the most suitable, but as the technology develops, there is a strong case to move to predictive design to reduce the test burden and introduce a common, predictable method for cylinder design, testing and application [Walters, 2003].

In the present state of the art, where performance-based testing is the normal, it is a fact that regulating bodies in several prominent industrialized countries insist on a design assessment by the composite cylinder manufacturer as part of the approval process

[ASTM, 2001,ANSI/CSA, 2000]. At present, this requirement is met by employing proprietary computer programs using numerical modeling (ANSYS, FEMLAB, COSMOS) techniques to optimize prescribed concurrent conditions for a particular cylinder, in the form of a design statement. This approach falls short of comparable analysis done with all-metal cylinders, and one can argue that such calculation add little value to the experimental testing already required [Walters, 2003].

Although no broad theoretical design philosophy has existed for composite cylinders, design tools in the form of optimization software programs have been developed, and are used privately by cylinder manufacturers. The best known of the early versions was that by NASA [Johns and Kaufman, 1964] licensed to several North American cylinder manufacturers.

Critical to this study were the relevant failure mechanisms for the cylinders. Such failure mechanisms were identified for the Dynetek Dynecell cylinder by testing as follows: [Teply and Herbein, 1985, Webster, 1999]

a) Impact damage testing
b) Cut and gouge testing
c) Heat damage testing
d) Fatigue testing through pressure cycling
e) Stress rupture testing
f) Environmental testing

These will now be considered. In addition, the test procedure used to implement tests to investigate these failure mechanisms will also be considered.

2.2.1 Impact Damage Testing

It is important to develop a method to detect damage caused by impact, because such damage is often not apparent through visual examination. Furthermore, depending on the extent and localization of the damage, many of the existing NDE systems will not detect such damage. Currently, the best mechanism for detecting delaminations is to tap on the surface, and if a 'woody' sound is heard in a localized spot, then delamination probably exists at the point. A good example of the seriousness of this damage mechanism was shown in Figure 1.2. External damage is not noticeable, but upon pressurization, the pressure vessel failed.

The damage mechanism that occurs from impact damage is the delamination of the composite structure. The tank is most sensitive to delamination and impact damage when the tank is not pressurized. Under pressure, the force balance between the internal gas and the composite structure make the tank very rigid and able to resist delamination damage. Impact damage produces a small dent in the aluminum liner, and then cracks, producing fatigue crack initiation points through localized stress risers in the carbon fiber reinforced polymer (CFRP). The damage mechanism is very similar to that of a wire rope. It is very strong in tension and weak in compression. If you try to apply compression in the wire rope, you kink the rope, causing strand breakage that will ultimately destroy the structural integrity of the wire rope.

NGV2-2000 is an industrial standard for the development and certification of composite pressure vessels used in vehicle applications. This standard was originally developed for natural gas monolithic (Type I) and composite pressure vessels and has been adapted to hydrogen applications as well. Relevant sections are summarized as Appendix A. Section 18.8 of the code shows that for delamination to occur, a cylinder must be dropped at a 45° angle from the horizontal, and from a height of 1.8 m (6.0 ft) to the lowest part of the cylinder. Of particular interest is the fact that it is not the initial impact from the drop that causes the delamination (see Figure 2.1). When the tank is dropped at a 45° angle, the initial impact strikes high on the rounded shoulder, where the aluminum liner is

thickest and at a smaller diameter (thus making it stronger). The delamination damage occurs on second strike, due to two influences on the tank. The first is that when the tank strikes on the initial impact, the momentum converts from linear to rotational energy, where the point of rotation is at the center of gravity of the tank (since it is symmetrical). This is caused by the force imbalance of the impact hitting the tank at one end. The second contributing factor is that now that the tank is rotating instead of moving along a straight line. This impels the strike of the second impact below the shoulder of the tank to a point on the sidewall of the tank. It is here, where the diameter is largest and reinforcement is minimal, that delaminations most naturally occur.

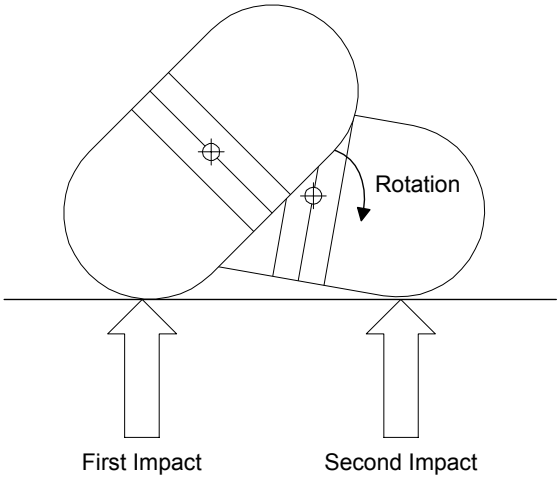

Figure 2.1: Impact Damage Path from 45° Drop Angle

This knowledge lead to the design of the standards to concentrate on areas of weaknesses in the tank designs. Accordingly, the test method utilized in this thesis followed in part the relevant standards. Varying levels of delaminations were then tested, starting at heights of 0.61 m, 1.22 m, 1.83 m and 3.05 m. In between each of these tests, the cylinders were examined both audibly as well as with the damage detection system being developed in this project in order to quantify and classify the delamination faults in the tank. Furthermore, testing was done with the tank to quantify the tank damage in terms of fatigue life and burst pressure.

Gravel impact damage testing was conducted primarily as a mechanism for determining additional environmental influences on the tank. Typical installations of high-pressure storage tanks place them underneath the vehicle in operation. Hence, they are subjected to gravel spray on roads and other road debris. When the tank is pressurized, these factors typically produce very little reduction in structural integrity. Most often surface finish is compromised and may overshadow other damage mechanisms, such as freeze-thaw cycling and chemical corrosion. Evaluation of this damage mechanism (gravel impact) is important because of the possibility that serious delamination damage is overlooked because it is masked by insignificant surface damage from gravel impact.

Investigations were conducted that applied small, insignificant surface damage to the tank. The damage detection system must be able to distinguish between this slight damage and other significant damage. This testing was done such that the surface damage due to gravel impact was applied, and then the tank was subjected to massive delamination damage to determine if the system did identify the difference between superficial damage and serious damage.

2.2.2 Cut Damage Testing

Cuts and gouges provide a significant problem for composite CFRP tanks. Because of the very nature of the composite tank, the structural integrity is found predominantly in the fibers that make up the composite wrap. The aluminum liner serves as more of a sealing mechanism to contain the gases within the pressure vessel. Accordingly, there are combinations of two wrap types in the manufacture of CFRP tanks. The first is hoop wrap, which is fiber wound in the hoop direction, and the second is a helical-type wrap. The hoop wrap provides strength to the tank in the radial direction while the helical wrap holds the tank together longitudinally. The tank is wrapped with a typical fiber tension of 20 to 30 N (5 to 7 lbf) and when the fibers are cut, they ‘spring’ back, in response to this tension. This, in combination with the drying and shrinking process of the laminate and the autofrettage process causes significant preload in the fibers.

The NGV2-2000 standard (summarized in Appendix A) calls for two cuts to be placed in the tank. The first cut is 25mm long by 1.25mm deep, and the second cut is 200mm long by 0.75mm deep. Both of the cuts are to be made in the longitudinal direction, as the stresses in the hoop direction are typically twice those of the stresses in the longitudinal direction. The standard then states: "The flawed container shall then be pressure cycled, from not more than 10% of 1.25 times the service pressure to not less than 1.25 times the service pressure for a number of cycles equivalent to 750 times the design life of the container in years, with a minimum number of cycles of 11,250."

As can been seen from the above standard, the requirements for the tank to withstand cut and gouge damage are extreme and excessive. This serves as a good minimum threshold of damage for the damage detection system to pick up. Varying degrees and depths of cuts were examined for conditions under and above what the standard calls for, and used to verify and quantify the damage present in the tank. This is illustrated in Figure 2.2.

Figure 2.2: Typical Cut and Gouge Testing

2.2.3 Heat Damage Testing

Heat damage is another one of the damage and failure mechanisms affecting composite tanks. In particular, localized heat damage can cause a loss of structural integrity in the tank. As mentioned previously, typical upper breakdown temperatures of the matrix are around 450°C.

This damage type is typically identified in the codes and standards as “Bonfire Testing”, as summarized in Appendix A. It is considered a crucial component of the test matrix for the design certification of cylinders. The bonfire test objective is to determine the failure mode of the pressure vessel under heat damage. However, the damage inflicted in this test is typically too massive to get an accurate reading on threshold values. A typical bonfire test is shown in Figure 2.3. As can be seen, the tank is completely immersed in flames, and any sensors, connections or wires that are unprotected are burned off.

Figure 2.3: Bonfire Testing

In this area of work, it was decided to examine localized heat damage spots on the tank to evaluate the damage detection system. Causes of localized heat damage can be due to oxy-acetylene torches used for removing bolts, straps, connections, and other metal components. Furthermore, pressure vessels have been used in areas where fires are

present. As an example, construction sites, firefighting, and industrial processes all pose significant risk to damaging the pressure vessel.

A small propane cylinder was utilized to apply to localized heat damage, which was timed while being applied to the tank. The flame temperature reached a maximum of 650 °C (1200 °F) and was very localized. This resulted in the disintegration of the matrix from the tank in these localized heated spots. The amount of damage could be measured by inserting a sharp object between the fibers to determine the heat penetration depth.

2.2.4 Fatigue Damage Testing

The fatigue damage in the tank must be very well understood and accounted for. This is the fundamental area defined in the NGV2-2000 code in Appendix A. Accordingly, this is the intended use of the tank, and as such, it is one of the most important variables in the tank design and application.

Fatigue testing was straightforward; testing was carried out after, during, and simultaneous to all other testing (drop, cuts, heat, sustained loading), as a mechanism for evaluating damage after several control tanks were evaluated.

2.2.5 Stress Rupture Damage Testing

Stress rupture, also known as sustained loading, is unique to composite cylinders [Teply and Herbein, 1985]. This failure mode is by definition closest to what is referred to as creep in metals. If the tank is exposed to an elevated pressure over a long period, then the composite fibers tend to fail. Initial designs of high-pressure composite cylinders typically failed during this test as they would catastrophically rupture after a period of time.

The test procedure is to bring the cylinder up to three times its service pressure (630 bar or 9100 psi for 210 bar cylinders), and hold the tank for 8 hours. Three times service

pressure was chosen as the typical pressure for sustained loading for cylinder designs where the burst pressures range from 3.8 to 4.5 times service pressure. The structural integrity observations were taken, and if the damage was non-detectable, then further exposure to over-pressurization was applied.

2.2.6 Environmental Testing

In order to evaluate the reliability of the damage detection system, environmental variables were examined to characterize the response of the damage detection system to these modifying influences. Environmental testing included evaluation of the following parameters:

1. cylinder mounting conditions – foam bed, neck mount and strap mount,
2. stored fluid type – system effectiveness was examined with water and nitrogen,
3. stored fluid temperature – ranges were from –40 ^{o}C to 80 ^{o}C,
4. humidity and water variations, and
5. pressure testing.

Both individual and combination testing of the above environmental conditions were made. Combined testing, for example, involved cuts, drops, and fatigue taken together. Compressed gases were used for environmental testing, and no significant deviations in measured parameters were noted. As predicted, electrical impedances changed with temperature, but the acoustical properties of the cylinder remained stable in the frequency ranges of interest.

2.3 Non-Destructive Evaluation (NDE) Techniques

Several different non-destructive evaluation (NDE) techniques were evaluated for the potential to be used as a damage detection system. These techniques included: acoustic emission, fiber-optics, and ultrasonics (resonance, guided waves, and bulk waves). Consideration was given to each of the techniques based on technical complexity, cost, reliability, difficulty to work with, sensitivity, and sensor range. The notable difference

in the methods includes the frequency band (acoustic: 0 – 20 kHz; ultrasonic: 20 kHz and up) and the transmission medium. The following summarizes some of these techniques.

Acoustic emission (AE) has been a growing area of non-destructive technology in recent years. Advances in the acoustic emission technology have been made from improvements in both sensor and analysis techniques. This technique has been primarily used to detect defect growth in metals and composites [Holoryd and Randall, 1993]. It is based upon the detection of high frequency stress waves (structure borne sounds), which are naturally produced by the failure of materials at a microscopic level. These emissions occur in the form of a transient burst, each corresponding to a localized microfailure within the body of the material. These emissions are very broadband, and contain frequency content ranging from DC to megahertz.

AE techniques have been increasingly used for non-destructive evaluation. Compared with other NDE methods, AE has the advantages of:

- having low processing times,
- utilizing continuous monitoring, and
- being capable of revealing the status of defects and their dynamic growth.

Source mechanisms targeted by AE monitoring include crack extension and plastic deformation, which are active in defect growth. AE transducers, however, are also sensitive to stress waves generated by a host of other source mechanisms such as impacts, friction, turbulence, and cavitation. These troublesome mechanisms help to disguise AE results and often require advanced monitoring techniques to separate the useful information from this background noise. One study attempted to utilize neural pattern recognition techniques to sort through the recorded AE features (amplitude, energy, frequency, etc.) from the background noise to separate damaged (cracked) liquid hydrogen cylinders [Tsimogiannis et al., 2002]. However, the highly mixed data proved the sorting to be inconclusive and produced many ambiguous results. Utilization of AE technology in a practical field application has still been elusive as a reliable system.

One particularly important application of AE monitoring is in the application of filament wound tanks or cylinders. Many studies involving AE monitoring have concentrated on understanding and differentiating the failure processes, including but not limited to, characterization, signatures and failure modes, damage location, and predictions of residual strength.

Current research is underway to use AE to predict burst pressure in damaged systems, and utilizing AE signatures to identify failure modes and mechanisms. Triangulation of the AE event is used to identify the damage location, and intensity is used for a measure of the extent of damage. Recently, pattern recognition, neural networks, and wavelet analysis have been used to differentiate types of AE signals (from the fiber, or matrix) and the failure modes [Javed and Littlefair, 1993, Zhang et al., 1999, Dode and Roa, 2002]. However, on the AE parameterization and signal analysis, the counts-amplitude relationship is believed to play the most predominant and significant role [Van de Loo, 1999, Kotsikos et al., 1999], but these new parameters based on signal analysis are becoming more important. However, the direct link between AE signal parameters and a specified failure process is still illusive. In a real-world application, the conventional parameter of accumulated counts represented by the number of excursions above a preselected threshold is still the most widely proven, accepted, and used method of AE as a NDE method.

Piezoelectrics are most often used in AE sensors due to the high sensitivity and very low response times. Use of low-cost polyvinyl di-fluoride (PVDF) piezo-electric films in AE and other applications is starting be used in NDE investigations. Advantages of PVDF films over conventional piezoceramics include low costs, ease of application due to maneuverability of the sensors, high ductility with the failure (up to 40%), a broad frequency response, and numerous other advantages. Further from the application side, specialized Fiber Bragg grating sensors are being developed, which are sensitive to AE events [Perez et al, 2001]. In particular, careful selection of Bragg filter spacing allows for resonant frequency tuning for a particular sensitivity to certain AE frequencies. Use of fiber optics may allow for future adaptation of telecommunications based multiplexing,

resulting in elimination of numerous wires and interconnects found in electrical-based systems.

Irrespective of the source process, the stress wave activity that is generated is inherently transient in nature. The wave front associated with each transient burst propagates readily through most metallic structures, and undergoes many reflections prior to its decay beyond the limit of detection. It is common for AE activity to achieve a stochastic distribution known as a diffuse field. Under these circumstances, the position of the source within the component and the positioning of the sensor to detect it are not critical and in practice, this gives great flexibility in the mounting of the AE receiving sensor [Holroyd and Randall, 1993].

A Lincoln Composites Inc. patent, [Duvall, 1996] covers such a conceptual system, including damage sensors, fill control, and pressure monitoring (for fuel gages). However, details into the acoustic emission damage detection is sparse in the patent, and do not take into account operational limitations, primarily caused by the Kaiser effect.

The Kaiser effect was first investigated by Wilhelm Kaiser [1950], and describes the phenomenon that a material under load emits AE waves only after a primary load level is exceeded. During reloading of these materials, they exhibit elastic behaviour until the previous maximum load is reached. As the Kaiser effect is permanent for CFRP material, little or no acoustic emission will be recorded before the previous maximum stress level is reached. This is done while monitoring the system for excessive noise levels (which is caused by fibers breaking). If this noise exceeds some predefined level for the specific material, then the system is said to be in the process of failing. Thus, application of AE monitoring techniques are suited to a controlled analysis where the structure can be loaded and evaluated under controlled conditions to ensure removal of background noise and ensuring adequate loading of the structure.

Optical fibers are wave-guides which can transmit light over a distance of several miles with almost no loss. They consist of a core, a mantle, and an exterior coating. At specific

locations within the core, modifications can be made by a single exposure to superimposed rays of ultraviolet light. This is done to produce what is known as a Bragg grating filter. At these specific locations, the Bragg reflection occurs, and specific wavelengths (only a small portion of the incident infrared light) is reflected in this grating. As a result, the wavelengths at which this reflection occurs are a function of the elongation of the glass fibers, and can be used via spectroscopic mechanisms to measure localized deformations in the structure. A network of Bragg grating sensors can thus provide information on deformation and load patterns throughout an entire component.

Low-power ultrasonic methods are the most conventional and traditional mechanisms for non-destructive evaluation used in industry. These techniques utilize the ability of a discontinuity in a material to reflect part of the energy hitting it in a solid material. There are three major types of ultrasonic systems including: pulse-echo, through-transmission, and resonance [Finlayson et al., 2003]. The pulse-echo system uses a pulse that is transmitted into the material and is reflected by an interface. If the time of travel is measured, the depth to the interface can be calculated. Through-transmission systems place continuous pulsed or modulated waves on a transducer coupled to one side of a part with pickup on the other side. If a flaw interrupts the waves, the waves do not penetrate the part. The resonance system utilizes a single transducer and varies the frequency applied to it. Within the applied frequencies is a single wavelength with a driving input energy that causes resonance. This condition is combined with the material properties to determine delaminations in structures.

An example of fiber optics can be shown in the development of Bragg Grating filters. As illustrated in Figure 2.4, the fiber optic cable is embedded into the composite structure. As the structure is cycled (loaded and unloaded), the fiber moves with the structure, subjected to the same strains that the structure bears. Through the use of multiple-strand fiber bundles and Bragg grating pass-band filters, either total strain, or localized strain can be measured optically in the fiber. This is accomplished through manufacturing the Bragg filters to reflect a specific frequency, and utilizing peak or phase shifting of the light to measure the displacement between filters. [Udd et al., 2000]

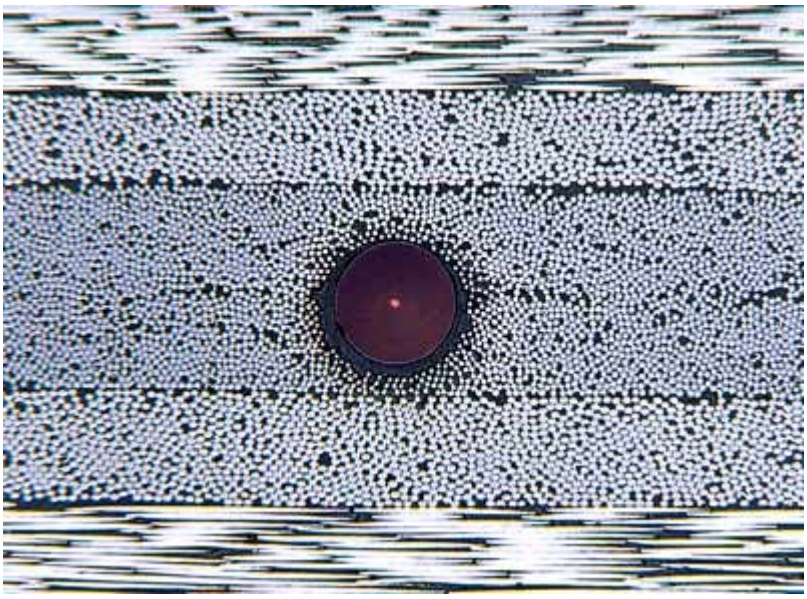

Figure 2.4: Embedded Fiber Optic Cable in Composite Structure

Recently, progress has been made on utilizing polarization maintaining optical fibers with Bragg grating filters to measure multi-dimensional strain. Although very complex in application as well as manufacture, these types of sensors are starting to be utilized in aerospace applications.

Ultrasonic-based systems are the most commonly used NDE systems. These systems usually incorporate a sensor and moving mechanism that will enable the sensor to pass over the entire surface of the structure. Resonance ultrasonic systems are commercially available and are used to find small cuts or delaminations in composite structures. The system is set up to measure the reflectance time, used to calculate a nominal thickness of the structure. If the thickness varies slightly (from the presence of a crack, cut, or delamination) then a flaw has been identified. However, further investigation is often required, applying visual inspection methods such as dye penetrants or magnetic particle inspection to confirm the presence of a flaw [Avallon and Baumeister, 1996].

Pulse-echo ultrasonic systems are very similar to resonance ultrasonic systems. However, instead of identifying the resonance frequency, a pulse is sent, and the echo is

timed. When the ultrasonic wave hits the interface of a discontinuity, such as a cut, crack or delamination, the normal time is interrupted and the discontinuity has been identified. This system is also commercially available, and requires the movement of the transducer directly over the discontinuity for reliable identification [Deutsch et al., 1998].

The through-transmission system is also very similar to the two other ultrasonic techniques. However, access to both sides of the test material is required for this technique, which requires a transmitting and a receiving sensor. A new similar process, termed guided wave ultrasonics, is currently being developed into a commercial system [Rose, 2002]. The basis of this technique utilizes the introduction of the wave at the angle of incidence for the material, accomplished by utilizing what is known as a wedge transmitter. The wave is thus forced into a reflective mode where it can travel longer distances throughout the structure. Defects in the structure then appear as 'oscillatory' characters in the received signal. Unfortunately, costly probes are required to be designed and manufactured for different applications, geometries, and material types to correctly produce the guided wave.

Numerous other methods of ultrasonic NDE techniques have been in development over the last 30 years [Rose, 2002, Bar-Cohen et al., 1998, Bar-Cohen et al., 1996]. These include: the use of lamb (flexural surface) waves in a composite component immersed in water to detect flaws; the use of shear waves by spiral electromagnetic transducers to identify flaws in complex metal parts; and the use of acoustic bridges to aid detection. Numerous other techniques are also under development. However, many of these techniques are subject to environmental and surface phenomena and complex analysis is often required due to geometry and material complexity. It is beyond the scope of this review to detail many of these techniques, but it can be stated that the practical application of NDE techniques in this thesis has eliminated the choice of such techniques.

2.4 Concluding Remarks

Table 2.1: Summary of NDE Techniques Evaluated

	Acoustic Emission	Fiber Optics	Ultrasonics
Industry Working Knowledge	Good	Good	Good
Reliability	Low	High	High
Sensitivity	Low	High	High
Sensor Range	High	Low	Low
Manufacturing Difficulty	Low	High	High
Cost of Technique	High	High	High
Development Required	Low	High	Low
Type of System	Passive	Passive	Active

Table 2.1 shows the results of the background information gathered on existing NDE techniques. Examples of each type of NDE were given and discussed in this section. Acoustic emission is often most associated with pressure vessel applications because the stress and strain on these structures is clearly understood. The application of the acoustic emission system is very simple – it consists of listening to the structure as it is being loaded. By the Kaiser effect, the sound of the fibers breaking will produce predictable sound levels in the structure. When the sound levels exceed a specified rate and amplitude combination, then the structure is known to be failing, but by this time it is sometimes too late.

After careful examination and identification of above equipment, a new technique, based on the blending of several existing technologies, was pursued. As will be discussed in later sections, a technique utilizing bulk ultrasonic wave transmission was developed utilizing a low-cost sensor matrix.

CHAPTER 3. SENSOR DESIGN

3.1 Sensor Selection

An important stage in the development of the damage detection system was to identify the main sensor types available and the relative merits of each. This will be considered in this Chapter. From the possible ultrasonic systems, there is a requirement to convert mechanical energy in the form of waves into electrical energy. This requires a piezo-type sensor; in particular, one that has the following characteristics:

- inexpensive,
- reliable,
- simple to install during the manufacture process, and
- ability to be installed on the tank (embedded on a curved surface) or built into the tank end-boss.

Three different sensors were selected as potential candidates for the tank diagnostic system. These included the conventional piezoceramics, piezo-film, and flexible ceramic matrices. The first type is the conventional piezoceramic sensor, an example of which is shown in Figure 3.1. Recent developments in sensor technology (spawned initially from accelerometer developments) have reduced the size and cost of these sensors.

Figure 3.1: Conventional Piezoceramic-Type Sensor

The piezoceramic sensors examined in this study were manufactured by Physical Acoustics Corporation (PAC) and Digital Wave Corporation. The sensors require a coupler to the structure being examined – typically vacuum grease or hot glue. Typical units have a sensitivity range up to several hundred kilohertz and are used for acoustic emission evaluation of structures. Sizes and costs have been drastically reduced, but they still remain bulky to use and in this case would need to be installed into the cylinder endboss. The typical sensor costs are around $1000 for a single sensor.

The second sensor type examined is known as a piezo-film. It is composed of a polyvinyl di-fluoride (PVDF) material and is coated with a silk screening process. The sensors, a sample of which is shown in Figure 3.2, have the advantage that they cover a larger surface area than the conventional sensor types. This results in higher sensitivity as well as a reduced amount of amplification required for this application. Furthermore, they are very thin, flexible and robust.

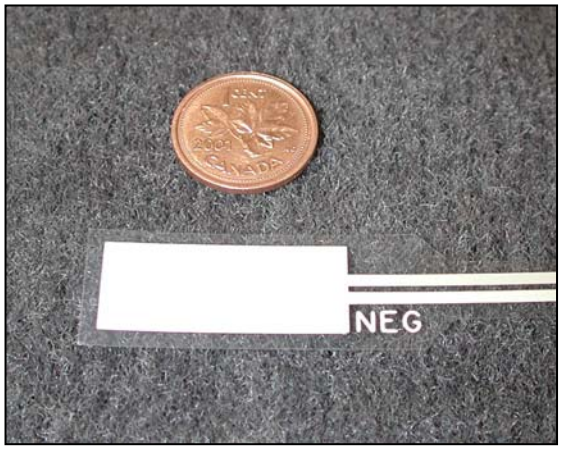

Figure 3.2: Piezo-film Sensor

The typical applications for piezo-film sensors include accelerometers, SONAR, ultrasound applications, switches, and infrared sensing. These sensors are considered a relatively new product, and many new applications are being developed for them. The cost of the sensors is less than $1 in quantities of 1,000 units.

The third sensor type is a combination of the sensors as illustrated in Figure 3.3. Developed by Sensortech Technology Limited, a Canadian company located in Montreal (www.sensortech.ca), these sensors are a joined multiple array of piezoceramic sensors. The linkage and size of the sensors allow the pad to be somewhat flexible.

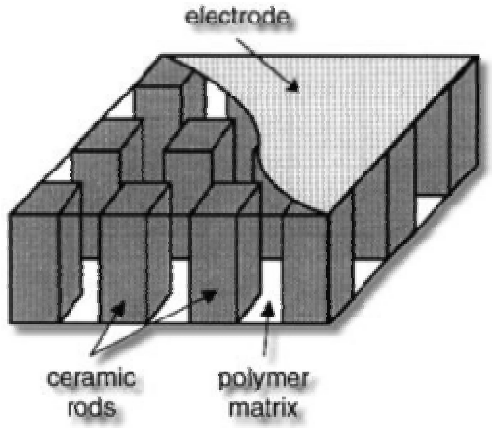

Figure 3.3: Flexible Ceramic Sensor

As the application of piezoceramic sensors is well known, and because they are considered reliable, they were selected to do the initial work. Comparisons were made between this sensor and the piezo-film sensor. Installation of the sensors into the tank was considered as one of the most important features of the sensor. Coupling the sensor to the tank in both a low-cost and reliable method is critical to the success of such a health monitoring system. Analysis of the operation of the different sensors showed similar operational properties; however, special machining during manufacture would be required for the use of piezoceramic sensors to mount the sensors into the tank end-boss. Flexible ceramic matrix sensors are still very expensive to purchase and only available in limited quantities. In order to properly satisfy the requirements of utilizing a low-cost sensor, the piezo-film sensor was selected for this application. To implement the sensor into the health monitoring system, investigations into the sensor sensitivity and placement are now detailed.

3.2 Sensor Location and Placement

The sensor location and placement are paramount to having a successfully designed system that exhibits robust and reliable operation. The sensors do have a limited range, and this presents the possibility that the damage might only be observable when it is present in a direct line between the sending and receiving sensor (ignoring reflection and diffraction effects).

Central to the use of piezo-film for acoustic actuation and signal examination, the fundamentals of piezo-film must be examined. Piezoelectric materials are anisotropic, and thus differ both in their electrical and mechanical properties and responses depending on the axis of applied electrical field or mechanical stress or strain. Figure 3.4 shows the numerical classification of axes generally used for piezoelectric calculations.

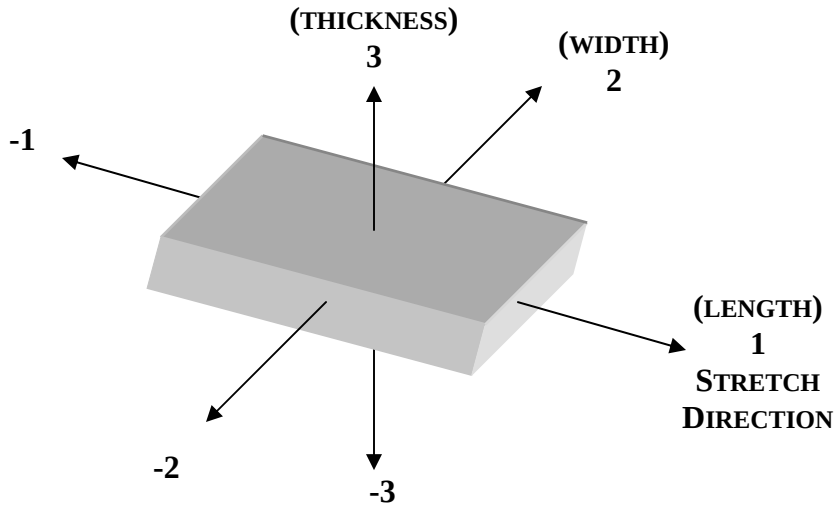

Figure 3.4: Numerical Classification of Axes

Piezo-film transducers offer a wide dynamic range (from near DC to 2 GHz) with low energy requirements attributed to the soft polymers used to produce the transducers [Measurement Specialties Inc, 1999]. The sensor is best suited as a high ultrasonic transmitter when operated in the plane 33 (referred to as d_{33}), or the thickness mode in Figure 3.4. The maximum transmission occurs near resonance, in this case, near 21 MHz.

The basic half-wavelength resonance is defined as:

$$f_r = \frac{v}{2t}, \tag{3.1}$$

where,

v is the speed of sound in the medium (in this case the polyvinyl di-flouride), and t is the transducer thickness.

For the given transducer characteristics, this is equal to:

$$f_{r3} = \frac{v}{2t} = \frac{2200 m/\sec}{2 \times 52 \mu m}$$
$$f_{r3} = 21.2 MHz \qquad (3.2)$$

The resonances in the other modes can be calculated similarly, leading to f_{r1} = 4.7 kHz in the stretch direction (d_{11} in Figure 3.4) and a resonance frequency of f_{r2} = 68.7 kHz in the width direction (d_{22}). These lower resonances are generally used for application in lower-frequency applications.

Operation of the piezoelectric material often leads to the question of how much voltage is developed for a given pressure or force, or conversely, how much force can be generated from a given voltage. The derivations of these expressions can be done based for the case of a piezoelectric element (assembled in the d_{33} direction), with the nomenclature defined in Figure 3.5.

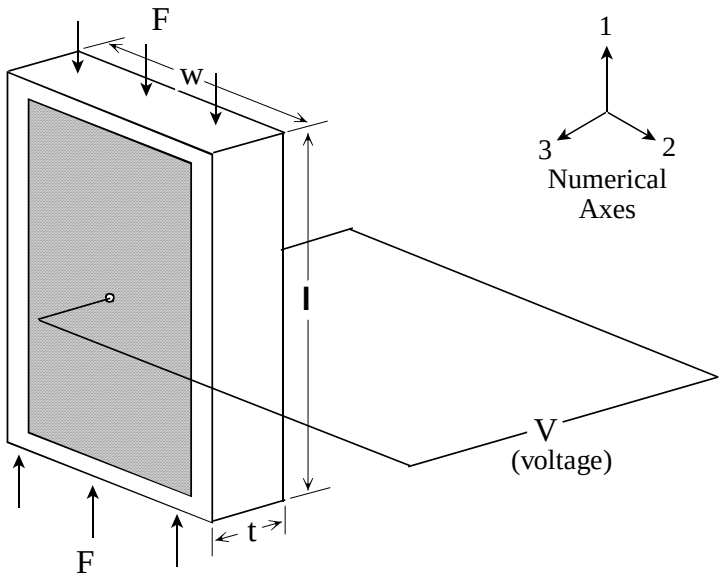

Figure 3.5: Piezoelectric Plate Analysis

The operation of the piezoelectric film is related to the piezoelectric "g" constant [Measurement Specialties Inc, 1999]. This is defined as the open circuit field developed for a given applied stress. For this analysis, the open circuit field is nearly considered as the ratio of the voltage to the distance between electroded surfaces. The stress can be considered as the force divided by the area in which it is applied.

Consider the structure shown in Figure 3.5. The voltage is measured or applied in the 3-axis, and the force is created or applied in the 1-axis, yielding the subscripts 31 for this example.

Thus, by definition, the constant g_{31}, is:

$$g_{31} = \frac{V/t}{\frac{F}{wt}} \tag{3.3}$$

where,

V is the voltage,

t is the distance between the electroded surfaces,

w is the electrode width, and

F is the force applied.

Now for the action of generating force from an applied voltage, the definition of the constant g is also,

$$g = \frac{\text{strain developed}}{\text{charge density}} \tag{3.4}$$

The strain is the relative charge in length, in this case $\Delta l/l$ for the g_{31} direction. The charge density is the charge over the area in which it is applied, thus,

$$g_{31} = \frac{\Delta\ell / \ell}{\frac{Q}{\ell w}} \tag{3.5}$$

Q is the applied charge, also defined as,

$$Q = VC \tag{3.6}$$

where,

V is the voltage applied, and
C is the capacity of the piezoelectric material (also related to the capacitance and dimensions of the plate)

This is defined as

$$C = \frac{K\varepsilon_o \ell w}{t} \tag{3.7}$$

where,

K is the relative dielectric constant of the plant, and
ε_0 is the dielectric constant of space.

Substituting equation (3.6) and (3.7) into (3.5) yields

$$g_{31} = \frac{\frac{\Delta\ell}{\ell}}{\frac{VK\varepsilon_0 \ell w}{t}\left(\frac{1}{\ell w}\right)} \tag{3.8}$$

or,

$$\Delta \ell \quad = \quad g_{31} K \varepsilon_o \frac{\ell V}{t} \tag{3.9}$$

So, based on the piezoelectric "g" constant, the dimensions, the dielectric constant, and the voltage applied, the charge in length can be calculated for a given voltage.

This can be further simplified with the definition of a piezoelectric "d" constant, defined as,

$$d \quad = \quad \frac{strain\ developed}{applied\ \ field} \tag{3.10}$$

This can be shown as,

$$d_{31} \quad = \quad K \varepsilon_o g_{31} \tag{3.11}$$

By substituting equations (3.11) into (3.9), the calculation for the change of length becomes:

$$\Delta \ell \quad = \quad d_{31} \left(\frac{\ell V}{t} \right) \tag{3.12}$$

This same analysis can be used to show expansion in the thickness plane,

$$\Delta t \quad = \quad d_{33} V \tag{3.13}$$

Because the piezoelectric film is constructed of a laminate assembled in the thickness (3-direction), the motion caused by charge to the piezoelectric film is always in the 3-direction (i.e. d_{31}, d_{33}). The piezoelectric constant "d" is generally used to define

parameters of the piezoelectric. Coupling of the two directions is defined as a percentage of the material dimensions, determined experimentally for a particular transducer. Note that the dimensions and slenderness of the transducer (l/t) plays an important role in the actual motion of the transducer when subjected to a voltage. Thus, it becomes important to select both the proper transducer properties and the correct dimensions for a particular application.

However, working through these calculations is of limited use in the application of these sensors in a resonant application. Every body has a natural resonance, as shown in the previous calculations. This resonant frequency is that in which the material prefers to vibrate most freely. If excited at this frequency, the body in question vibrates at greater amplitude than it would at other frequencies. The equations developed above describe the behaviour of piezoelectric materials only for non-resonant steady state operation. In the transient operation of these sensors, the driving force is applied as a high-frequency impulse, with both low and high frequency content. This will cause the piezoelectric material to produce the highest power and amplitude at its resonant frequency. The placement and installation of the sensor fixes the mode of resonance in which the sensor vibrates, also indicating the frequency range that will be expected.

The placement of the sensor has the potential to make the difference between the system operating reliably or operating in a non-functional mode. Numerous trials were made, and the following variables in the sensor placement were examined:

- surface sensor mounting,
- embedded sensor mounting,
- rotation of the sensor,
- location of the sensor on the tank sidewall, and
- tank neck and tank shoulder sensor mounting.

This was accomplished through a series of tests on complete tanks, tank sections, plates, bars, and rods.

Initial testing was accomplished on a plate with a Lexan base, which has similar polymer properties as the tank matrix in the carbon-fiber structure. The plate and sensor location are illustrated in Figure 3.6. Localized damage was inflicted, as well as massive damage on the structure. This was accomplished through cuts, holes and fracture of the plate. The initial results indicated that damage detection was limited, but not totally unsuccessful.

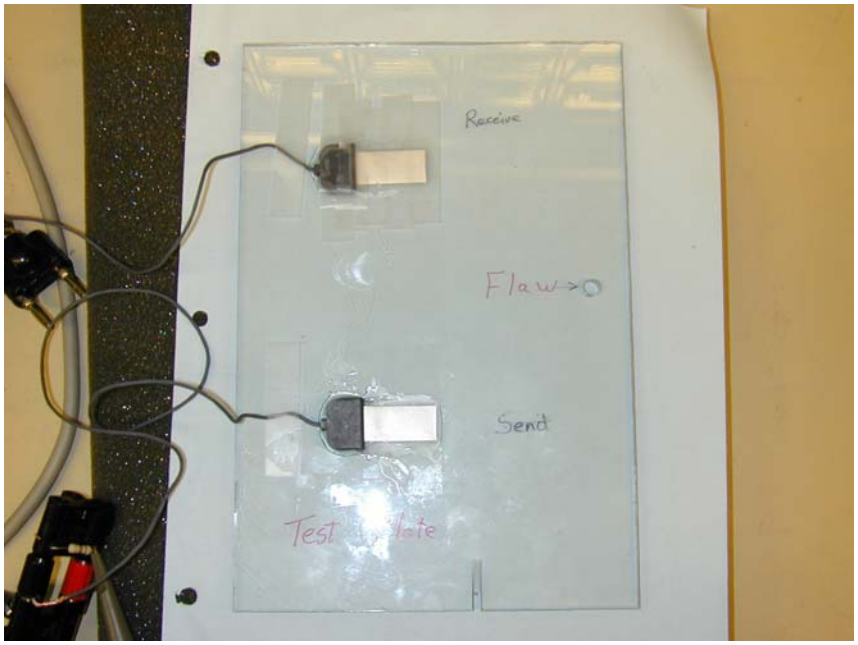

Figure 3.6: Lexan Test Plate Apparatus

Investigations were made into sensor application mechanisms using vacuum grease, epoxy, contact cement and other adhesive applications. In general, it was found that for the strongest signal, an epoxy binding provided the least acoustical impedance at the sensor to structure interface. This method of fixing the sensor will restrict its motion in all three primary directions, as well as some other minor modes of vibration, thus creating a very complex mode of vibration. The sensor response should contain peaks at each of the resonant frequencies, and will be indicative of the cross-coupling that exists between the different modes of vibration.

Figure 3.7 shows the received signal from an impulse input to the setup as illustrated in Figure 3.6. This information is shown only as an example to the type of tests conducted to evaluate variables in sensor technology, sensor placement, location of the flaw, and method of attachment. The impulse response also facilitated input and response characteristics.

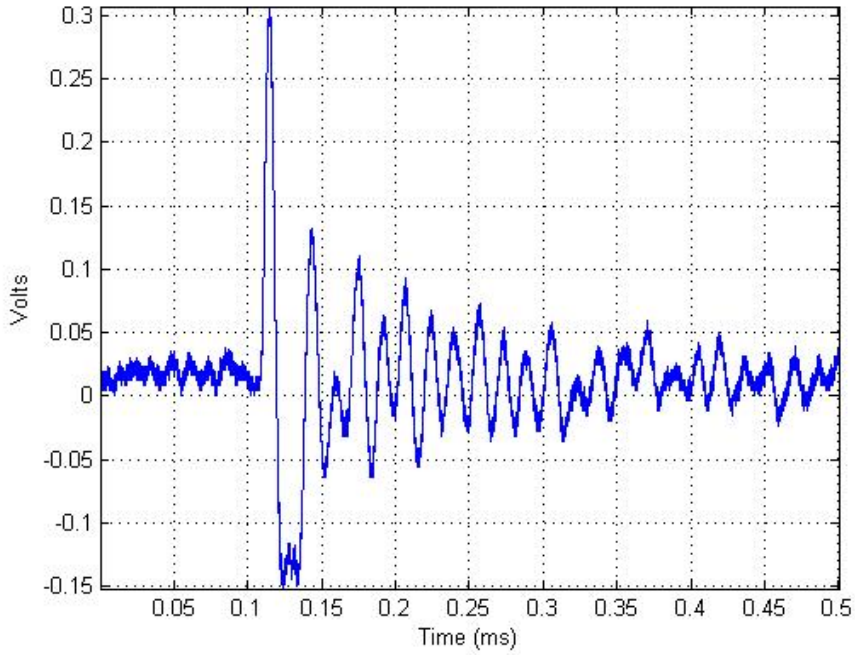

Figure 3.7: Signal on Plate Before Damage (Sampling rate: 1 MHz)

A slight variation in the signal was measured after the damage was placed in the plate (which was a hole flaw as shown in Figure 3.6). Notice that the signal has slightly changed as illustrated in Figure 3.8. These signals are examined in greater detail in Chapter 5.

Bars and rods were used to examine the compression waves in the tanks. Because the cylinder liner is constructed from aluminum, similarities in the compression wave were examined through tests on solid aluminum bars. This testing validated that cuts provide a small reflection of the compression wave in a solid bar, but is limited to use for monolithic types of materials. The complex structure that comprises the outer composite

shell did not appear to provide a good medium for reflections of cuts to be seen in the compression waves.

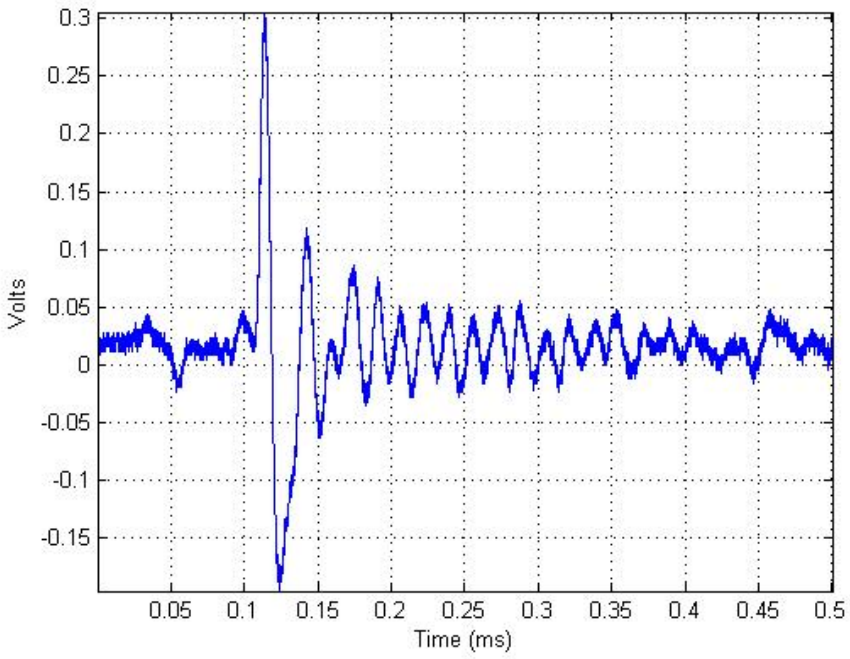

Figure 3.8: Acoustic Signal on Plate After Damage (Sampling rate: 1 MHz)

The apparatus shown in Figure 3.9, was used in the laboratory to help evaluate the feasibility of the different testing mechanisms. In brief, different mounting systems, different sensor rotation and combinations there of, as well as flaw characteristics (cut depth, rotation and thickness) were evaluated. The results were considered satisfactory for laboratory work, but were limited for application purposes due to sensitivity, high noise, and poor signal quality. Furthermore, small cuts and cracks were difficult to identify.

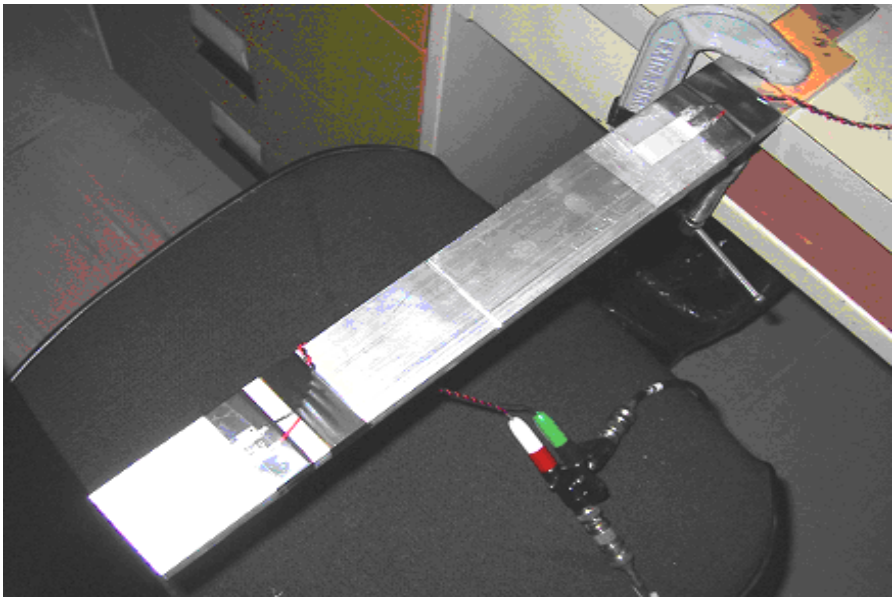

Figure 3.9: Cut and Compression Wave Testing in an Aluminum Bar

Figure 3.10 shows the apparatus for tank structure testing. Independent sensitivity studies were conducted based on sensor size, rotation, mounting mechanisms, location, and surface mounting verses integral mounting. These conditions are illustrated in Figures 3.11, showing sensitivity of sensor placement to flaw location. Figure 3.12 shows sensor size and rotational testing, and Figures 3.13 illustrates the sensor surface mounting testing. Figure 3.14 shows the final embedded sensor design and placement based on prior sensitivity testing.

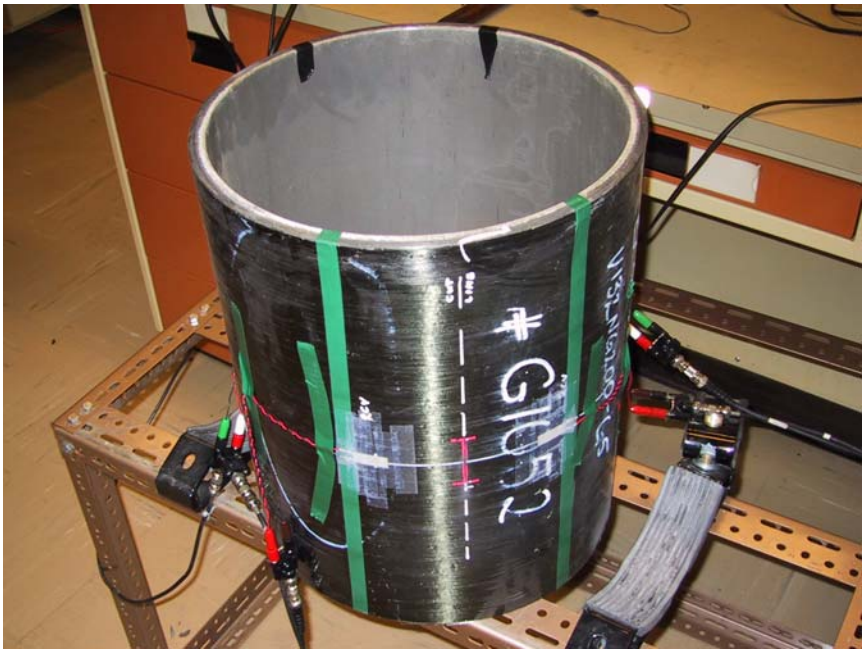

Figure 3.10: Localized Tank Section Testing

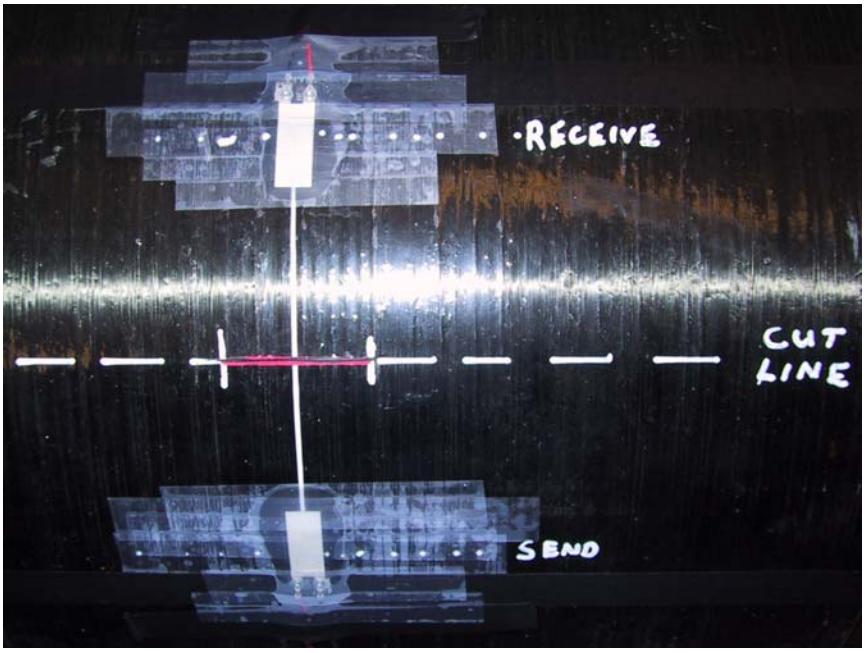

Figure 3.11: Sensor Sensitivity Testing

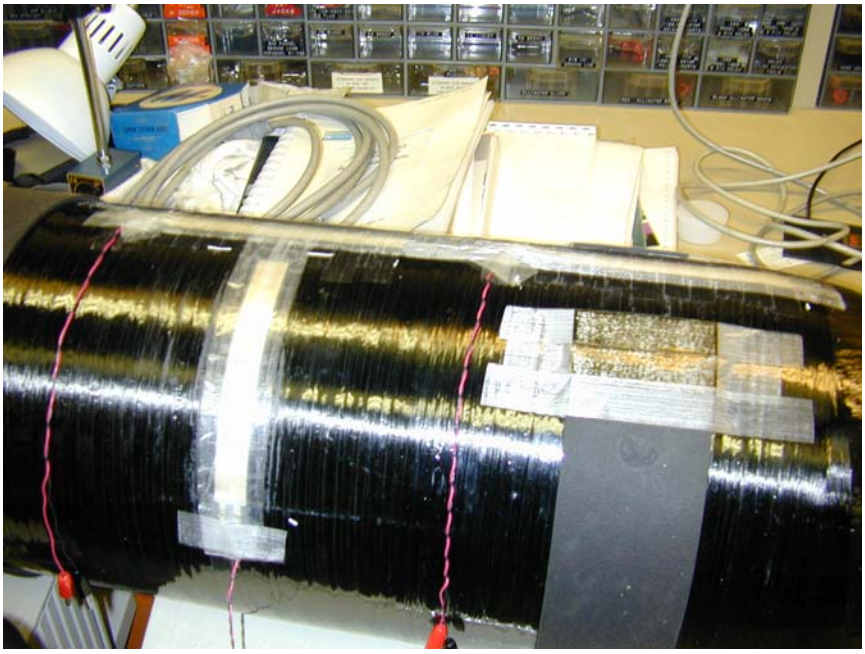

Figure 3.12: Sensor Rotation and Location Testing

Figure 3.13: Sensor Surface Mount Testing

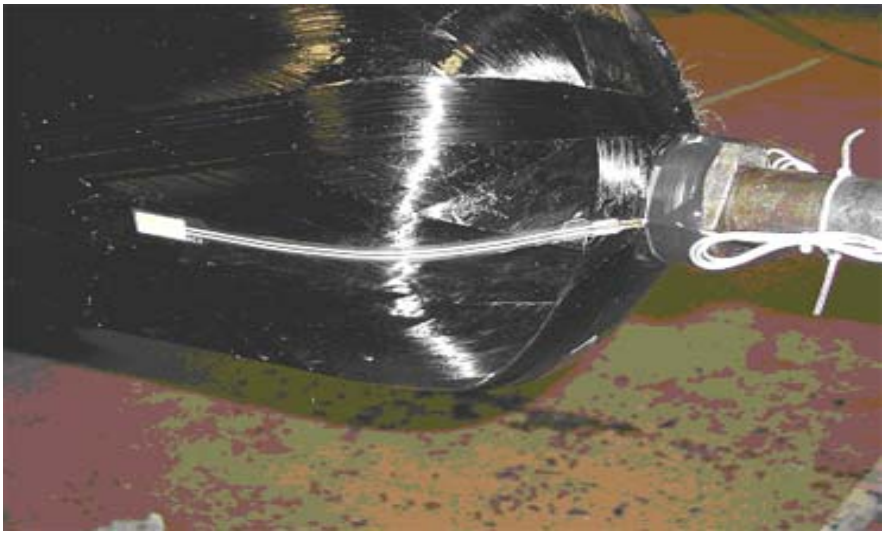

Figure 3.14: Embedded Sensor Manufacture

The sensor installation into the composite structure is illustrated in Figures 3.14, 3.15 and 3.16. Special sensors were obtained that contained a 152 mm (6 inch) flexible leads that allowed the electrical connectors to be placed off of the composite surface. This was done due to the inherent problems associated with placing a "thick" connector into the composite structure, which can potentially weaken the structure causing localized stress risers, and would certainly require recertification of the cylinder design with this hardware in place.

Figure 3.15: Embedded Sensor Design

Figure 3.16: Embedded Sensor Final Design Manufacture

The final sensor design is shown in Figure 3.17. This sensor design consists of a completely encased sensor with the final wrap of the carbon-fiber shell. There is relatively little chance of damage to the sensors or leads as they are wound predominantly into the cylinder structure. Furthermore, noise levels are reduced as the carbon fiber is an electrical semiconductor. This creates a condition very similar to a Faraday Cage, where electrical, electromagnetic, and radio-frequency noise is kept to a minimum. A summary of the manufacturing procedure can be found in Appendix B.

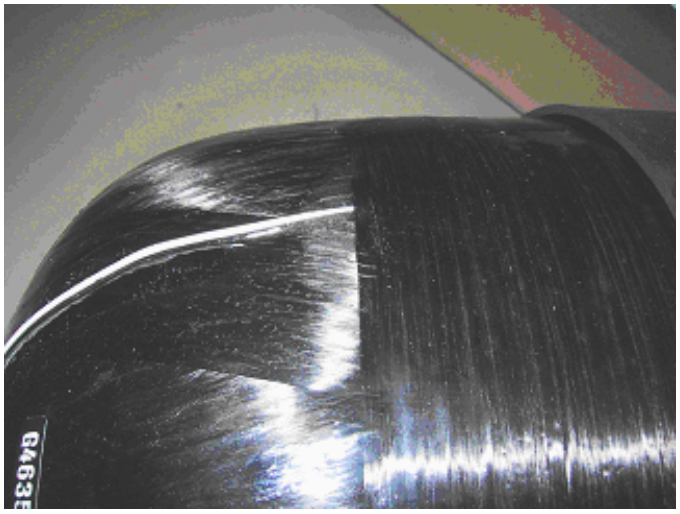

Figure 3.17: Embedded Sensor Final Design

Figure 3.18 illustrates the final sensor placement determined for the L033 series (33-L water capacity) pressure vessels. As can be expected with larger cylinders, the placement of the sensors may become more critical as the physical distances between the sensors increases. No examination of transmission distances was made, other than the sensor placement as determined in Figure 3.18.

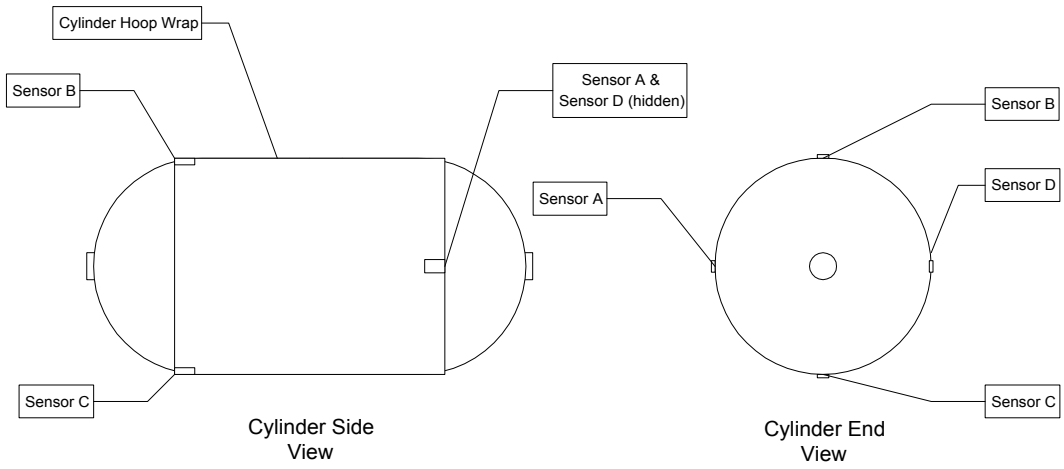

Note: Sensors are mounted every quarter (90 degrees) on alternate ends just underneath the final hoop wrap (thickness is approximately 6.5mm deep)

Figure 3.18: Test Sensor Setup

3.3 Sensor Application

The sensors are used both in transmit and receive mode. This is illustrated in Figure 3.19, a schematic representing the sensor operation. Note that it was observed that with surface sensor mounting, surface effects, reflections, and lack of penetration of the high-frequency waves into the cylinder caused unreliable operation and functionality of the system. However, the sensors were subsequently integrated into the cylinder, during the manufacture of the cylinder. This improved reliability and functionality of the system.

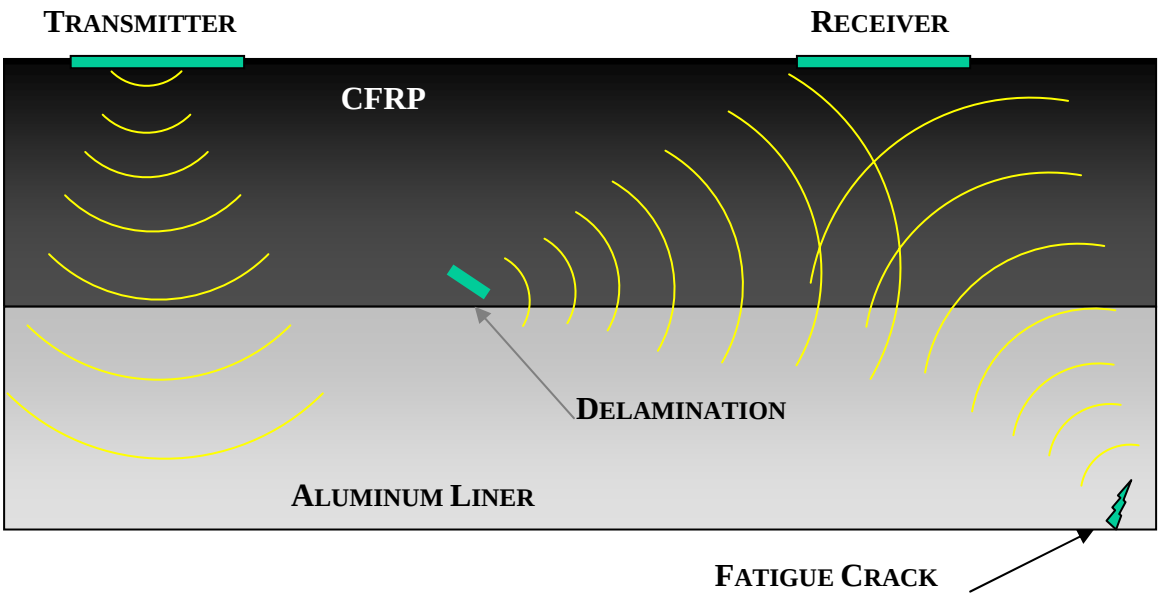

Figure 3.19: Schematic of Operation

The waveforms received in this application are a complex function of the resonant modes of vibration and installation, and are dependent on proximity and orientation of the sensors with respect to the transmission sensor. It is not a trivial task to analyze or model the complex relationship of the waveforms for the apparatus. In fact, variables in manufacturing can be significant (up to 10% by weight) and fiber layouts differ significantly enough to make a model extremely complicated to produce.

3.4 Concluding Remarks

Investigations were made into integrating low-cost piezo-film sensors into the composite overwrap of the cylinders. This allowed for noise and electromagnetic shielding of the sensors, which is inherent in the design of such a tank health monitoring system. Placement and sensitivity studies were completed that investigated the proper alignment and placement of the sensors into the tank. The methods by which this health monitoring system was tested, designed, and built are discussed in the following chapter.

CHAPTER 4. TEST METHOD

4.1 Introduction

In this chapter, a brief summary of this experimental setup is discussed, along with a discussion of the test matrix for the development and evaluation of the health monitoring system.

4.2 Test Apparatus and Procedures

All testing was conducted at Powertech Labs Inc. of Surrey, British Colombia. Powertech Labs is a world leader in the testing and design of high-pressure vessels. Capabilities at Powertech Labs include: high-pressure testing of cylinders for fatigue, stress-rupture, impact, cuts, gouges, and environmental testing requirements for the certification of the high-pressure tanks to various industry standards throughout the world.

Selected tests were chosen due to the failure mechanisms associated with tank deterioration as outlined in Chapter 2. The testing apparatus was assembled from existing and available testing equipment. The test apparatus consisted of the following components:

- Test chamber with blast doors;
- Hydraulic pump and reservoir, and interface to water for cycling;
- Pump controller and cycle counter; and
- Damage system detection

A schematic of the test setup is shown in Figure 4.1. Water, as opposed to oil, was used for pressure cycling the pressure vessel due to environmental concerns when the vessel eventually leaked. This was achieved by utilizing a hydraulic oil-water interface unit, which was composed of a free-floating piston inside a cylindrical chamber. On the hydraulic oil side, a positive displacement pump and servo-valve were used to control the tank pressures. Two data acquisition systems were utilized in this setup, one for controlling and counting the pressure cycles, and a second for measuring the damage detection system implemented in the testing. Data synchronization was achieved through time stamping the data and correlating the multiple data streams after the testing was completed.

The test setup consisted of the hydraulic system interfaced to the tank and associated control systems and lines. The pump was a Parker positive displacement pump with a flow rate of 19 lpm (5 gpm) and 15 kW (20 hp) motor, as shown in Figure 4.2. Maximum operating pressure was 345 bar (5000 psi). Control logic was supplied through a computer interface using National Instruments Labview™ and was achieved through an appropriately-sized Moog servo-valve.

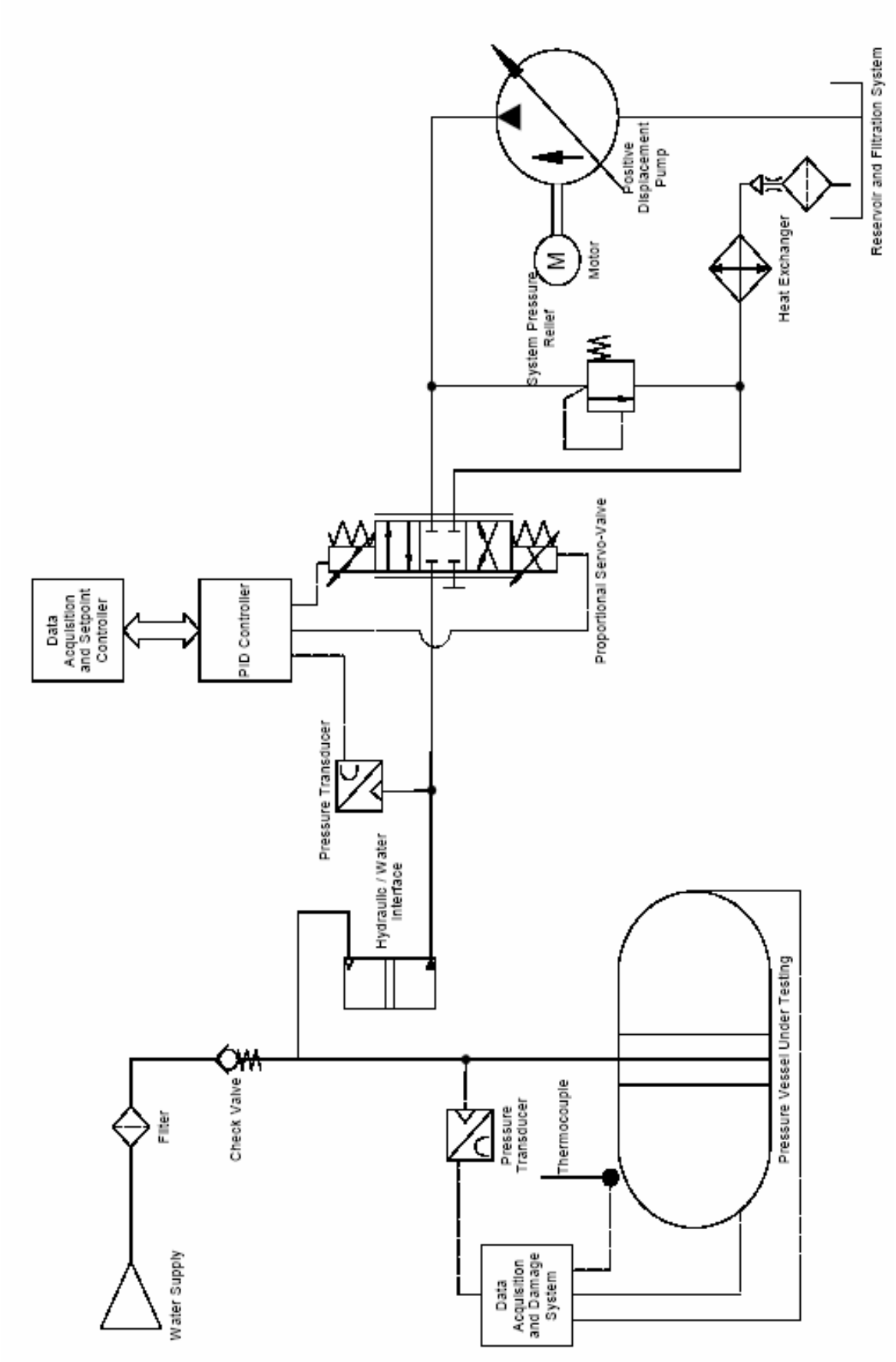

Figure 4.1: Test Setup Schematic

Figure 4.2: Hydraulic System

All tests were performed in the test chamber shown in Figure 4.3. There is a large amount of energy stored in a tank under high pressure, and safety precautions were made accordingly.

Pressure transducers were located outside the cylinder and test chamber and routed through high-pressure hosing and tubing, so that destructive tank testing could be conducted without any risk to personal safety.

Figure 4.3: Test Chamber with Blast Doors

The structure, as shown in Figure 4.4 was utilized to support the tank during testing. Provisions were made to facilitate testing of different mounting mechanisms (neck mounting and tank strap mounting). Furthermore, testing with different media was examined, including water and gaseous media.

Typical test media for these types of cylinders include water, oil, nitrogen, natural gas (predominantly CH_4) and hydrogen. Because internal tank stresses are identical in all cases, (the only major difference being in the catastrophic failure mode, where the compressibility of the gases allow for additional energy storage), water was used in all testing, with several cases of examination of gaseous media to provide supplementary and confirmation tests for the pressure vessels.

Figure 4.4: Support System

The tank damage monitoring system is shown in Figure 4.5. This system utilized two personal computers interfaced together in Matlab®. One computer was used for monitoring environmental variables and tank impedance, while the other was used to monitor the health of the pressure vessel. Signal generators were required, and all systems were interfaced to work in unison.

Figure 4.5: Tank Damage Detection and Analysis System

The data given in the system setup, as shown in Figure 4.6, shows the complex interface between the two systems required to keep the machines running in unison, without interference between the systems.

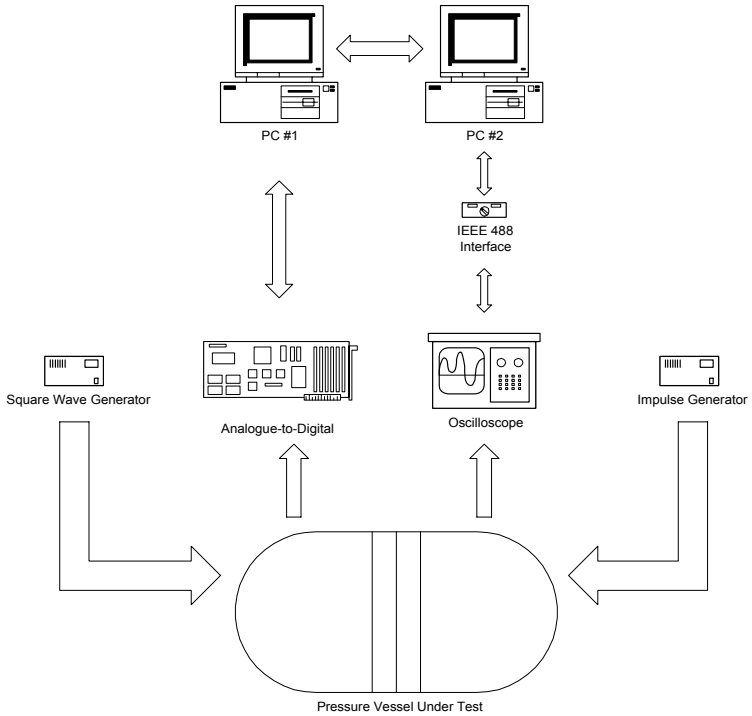

Figure 4.6: Data Acquisition Setup

4.3 Test Matrix

The test matrix, as shown in Table 4.1, was developed and defined for this particular tank application (33-L Dynetek composite tank). Two sets of sensor mounts were tested to evaluate damage: surface mount and embedded mounting. The first sensor sets were tested on a surface sensor mounting condition. For this type of sensor mounting, the top surface of the tank was cleaned off, and then the sensor was adhered to the surface of the tank at predefined locations.

Table 4.1: Test Matrix for Development and Evaluation

Test	Number of Tests	Tank Serial Numbers
Surface Sensor Mounting:		
1) Drop – Delamination Damage	1	G1414
2) Cut – Gouge Damage	1	G1408
3) Heat Damage	0	N/A
4) Stress Rupture	0	N/A
5) Fatigue Damage	2	G1416, G1408
6) Gravel / Impact Damage	0	N/A
7) Environmental	1	G1415
Embedded Sensor Mounting:		
1) Drop – Delamination Damage	2	G4636, G4697
2) Cut – Gouge Damage	5	G4635, G4697, G4604, G4642, G4694
3) Heat Damage	1	G4607
4) Stress Rupture	1	G4634
5) Fatigue Damage	4	G4646, G4604, G4695, G4697
8) Gravel / Impact Damage	1	G4694
9) Environmental	2	G4642, G4697

Note that the specific manufacturing information for the embedded sensor mounting tests (cylinder serial numbers G4607 to G4697) is included in Appendix C.

4.4 Summary

In this section, the test apparatus and test procedures were presented. In the next section, data management and signal processing required to gather and analyze the test results are presented.

CHAPTER 5. SIGNAL PROCESSING AND DATA MANAGEMENT

5.1 Introduction

An overview of signal processing and data management is given in this section. This overview is supplemented with Appendix D, which discusses in detail the signal processing that was used to analyze the waveforms.

5.2 Data Acquisition System and Data Management

In order to facilitate both signal processing development and data acquisition, a Matlab® based system was developed. The tank integrity data was collected at a sampling frequency of 250 MHz on four channels simultaneously. As can be expected, large amounts of data could be sampled, and required processing within the program.

A Matlab®-based graphical user interface was created, with the ability to perform the following tasks:

1) Sample the high-speed-data and control instruments onboard the computer system through data acquisition devices, IEEE 488 devices, and USB interfaces;
2) Sample environmental parameters such as temperature and pressure of the tank at the time of sampling;
3) Insert the data into a large database for data storage;
4) Back up system parameters and write data to file;
5) View and plot time, frequency and wavelet data;
6) Analyze and examine data and compare to baseline signatures for damage calculations; and
7) Capture and store baseline signatures.

Typical input signals to the piezo-film transducers are shown in Figure 5.1. Typical output or received signals are shown in Figure 5.2.

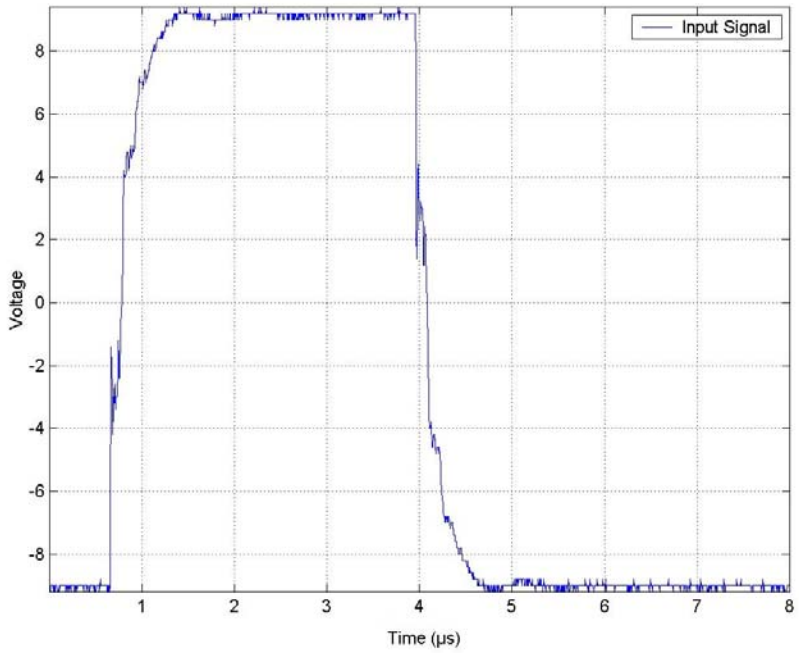

Figure 5.1: Input Signal

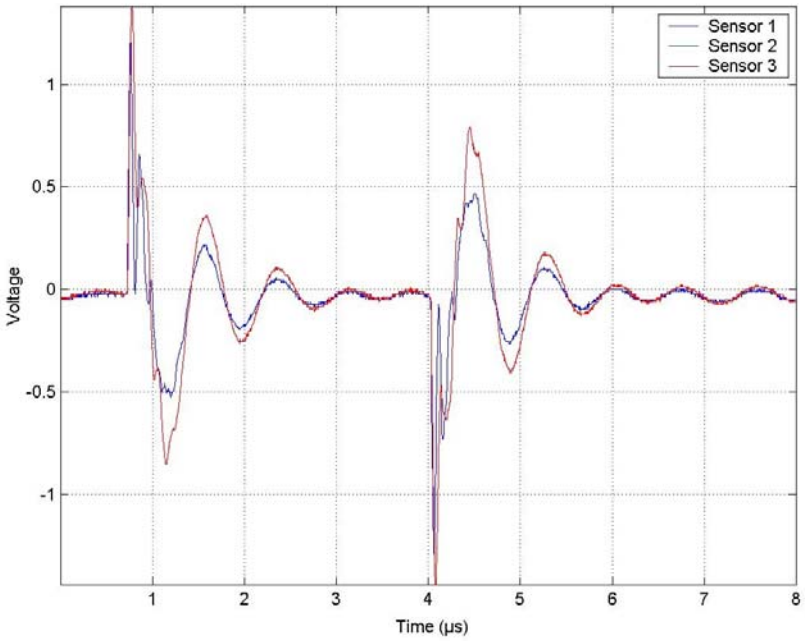

Figure 5.2: Received Signal Waveform

The relationship between the sent and received signals forms the basis for this detection system. In essence, the system is monitored by performing the following tasks in order:

1. Baseline the tank, while it is in its new or 'as new' condition. Comparisons of this baseline can be run between different tanks of the same design. This can also form a basis of quality control of the tanks. For example, it may be possible to identify flaws and deficiencies in the tanks from the manufacturing process (such as unautofrettaged tanks, dry or misaligned carbon wrapping, and poor metal properties in the tank liners). For a complete discussion of the manufacturing process, see Appendix B.
2. Test the relationship between the input and output signals. Store this data in temporary memory.
3. Analyze the current signal and the original 'baseline' signal and examine the differences in these data.

Different features in these signals can be visually observed. The analysis of these features and the resulting analysis procedure is detailed in Appendix D.

Figure 5.3 shows the typical composition of ultrasonic acoustic signals and their corresponding wave types:

1. Extensional signal: composed primarily of compression waves
2. Flexural signal: composed of transverse or surface waves
3. Reflections: A combination of surface waves, interference, superimposition and reflections of the previous two signal combinations.

The compression waves are composed of high-frequency waves that move very quickly through the structure. The transverse waves' propagation speeds are slower and reach the receiving signal with a greater time delay. They also tend to travel along the surfaces of the structure. Following the waveforms becomes a mixed-mode transform, resulting in the superimposed signals shown as reflections.

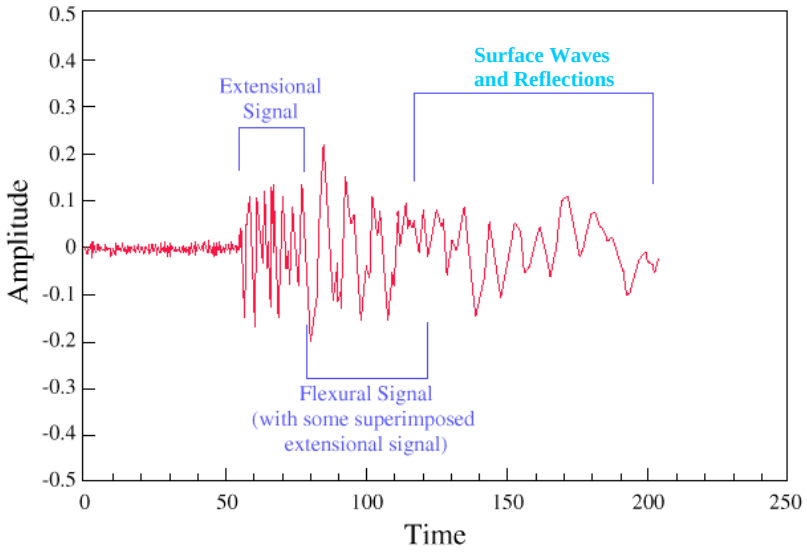

Figure 5.3: Typical Breakdown of Acoustic-Type Signals

The system schematic is described in Figure 5.4. This system gives a fairly accurate representation of system functionality. The structure of the system is then recorded by characterizing the relationship between the transmitting and receiving sensors. One of the major differences with this type of system is that due to the use of low-cost, thin-film sensors, the impulse and resulting waveforms are not typically guided, focused or directed into the structure when compared to existing ultrasonic systems that utilize piezoceramics.

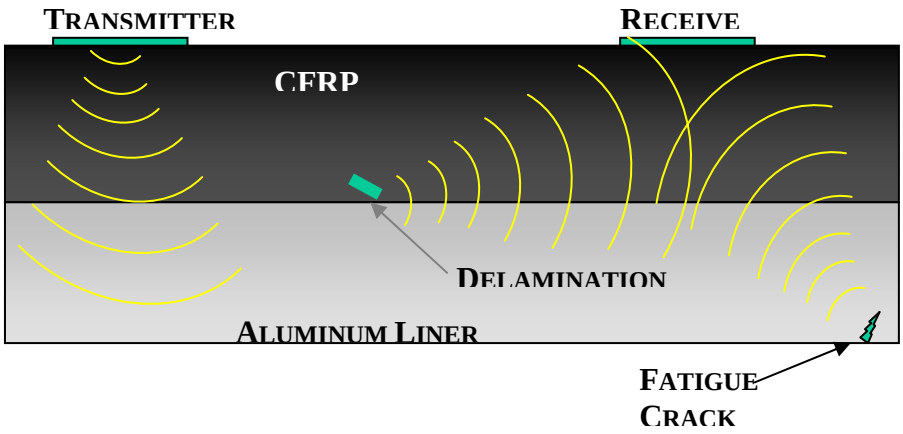

Figure 5.4: Acoustical Resonance System Schematic

The resulting analysis of this system becomes one of determining the difference between the transmitting and receiving sensors. This can easily be interpreted as: “If the structure changes in between the sending and receiving sensors, then the resulting waveforms will also change”.

The resulting waveforms in the system incorporate the following features of the overall system:

- sensor resonance frequency,
- carbon-fiber reinforced polymer resonance frequency and modulus,
- aluminum-liner resonance frequency and modulus,
- acoustical impedance between the sensors,
- boundary conditions,
- combined modulus and speed of transmitted sound in the structure,
- cracks, fatigue, delamination, heat, stress rupture, gouges and impact damage in the tank, and
- frequency-dependant coherence of the structure.

The selected data analysis method consists of the following series of calculations:

1. Measure waveform into working memory,
2. Filter data (17 to 85 MHz),
3. Windowed power spectrum density using Welch’s Method,
4. Frequency cutoff (filter data above and below the cutoff frequencies),
5. Transfer function estimate (output data over input data),
6. Comparison of transfer function estimates to baseline frequency division, and
7. Root-mean squared and scaling to a single number, or damage indicator.

In order to quantify the damage to the cylinder, the results need to be reduced to an indicator that can easily be used for comparison purposes. It was determined that a single

number indicator would be sufficient for this purpose. In the calculation of the empirical transfer function estimate, essentially a signature of the tank is created. In order to compare these signatures, division of the measured signature over the baseline signature was completed, resulting in a vector of comparison numbers as a function of frequency. Hence a value of unity is considered as no change, but changes in resonant frequencies in the signature can result in large-scale variations. Accordingly, the comparison vector was analyzed with a root-mean-squared analysis and then scaling by the length of the vector to bring the normal undamaged indication back to unity.

Note that this single number, as indicated in the analysis method, is scaled such that 1 is the baseline or normal operation. Damage is indicated with scaled numbers varying from this normal baseline of 1. The damage indicator thresholds of critical damage would not be necessarily defined as the critical damage level was not defined in this project. In this project, non-critical damage has been used as the detection criteria to allow for adequate sensitivity for real applications of this technology.

Details of a sample data set and its analysis are given in Appendix D.

5.3 Summary

This section has presented a brief outline of data management and signal processing, as well as illustrating some typical transient traces. Details of all analysis and methods are presented in Appendix D. The next chapter summarizes the various results.

CHAPTER 6. SUMMARY OF RESULTS

6.1 Introduction

The objective of this chapter is to summarize the results obtained from the sensors for the different damage mechanisms. These are presented from a single set of input-output sensors on the tank for a particular region. It is to be noted that, depending on the damage mechanism and location of the damage, not all damage is visible on every sensor; rather, the most effective mechanism for detecting damage to the structure was found when the damage was in between the transmitting and receiving sensors.

Three-dimensional plots are used to illustrate the typical damaged system results and contain the following data taken at varying pressure levels (plotted on the depth or 'y' axis), pressure cycle count (shown on the lengthwise or 'x' axis), and the "damage indication" (shown on the vertical or 'z' axis). The data, as plotted in this manner, maximize the amount of information that can be visibly presented, while maintaining the data for various structures to be easily distinguishable. The "damage indicator" is combined from a series of 2000 data points (refer to Chapter 5 and Appendix D for details), brought into a single value which shows relative 'changes' in the signature from the baseline case. These changes can be either positive (above 1.0), or negative (below 1.0). A positive change typically indicates a shift in resonance frequency or an increase in acoustical admittance at particular frequencies. This corresponds to a change in the modulus of the material being tested. A negative change in this signature will indicate a decrease in acoustical admittance, indicating that the structure does not have the ability to transmit sound at the same levels that have been baselined. This correlates to a net decrease in the modulus of the structure and could indicate that the structure may be 'falling apart' through delamination.

Note that the results shown in this thesis are only representative examples of typical damage mechanisms. In the process of developing the system, approximately 34 compact discs (each 700 MB in size) of raw signal data have been archived. Presentation in this thesis of all results for all collected data would be excessive. Typical examples are shown, with each plot consisting of approximately 5000 data readings through the test, and each data reading consisting of 2000 raw data points per channel. The plots shown were created as a balance to illustrate the results of the approximately 10 million data points used to construct each graph. Furthermore, an average surface (of three-dimensional spline curve fit) is plotted in between each of the points. This is the equivalent of placing a "blanket" over the plotted points, resulting in a surface that is much easier to visualize and observe general trending over the large number of data points.

6.2 Fatigue Damage

As mentioned in Chapter 4, the most difficult damage mechanism to identify is the presence of fatigue damage, which, in turn makes it most difficult to design the pressure vessel to relevant standards. The tank structure is thought to conform to conventional fatigue prediction and classifications of load-bearing structures. However, it is very difficult, if not impossible, to identify the life of a tank, as loading and life spans vary from one unit to the next.

Typical fatigue loading on a pressure vessel goes through the following stages throughout its life span:

1. Crack nucleation,
2. Crack initialization,
3. Crack growth, and
4. Crack failure.

When examining fatigue loading and failure of these composite pressure vessels, it is paramount to identify the crack presence in the initialization or growth stages of fatigue.

The presence of a crack in the aluminum liner will not cause a catastrophic failure of the tank (as all standards require a Leak Before Burst (LBB) criterion in the design and testing of the pressure vessels) [White, 2002]. However, the leakage of a combustible gas in an enclosed space will produce an undesirable critical condition that could result in catastrophic failure of the fuelling system.

Current standards examine fatigue loading and crack propagation by limiting the lifespan of the tanks [ANSI/CSA, 2000]. For example, in automotive use, tanks are limited to a lifespan of 15 years, and are tested to standards that parallel high-loading conditions for this lifespan of 15 years. The resultant system provides good safety to the end user as these tanks are significantly over designed for their actual use.

The fatigue failure of the tank G4604 is shown in Figure 6.1. These results are typical of fatigue failure, measured and identified by this acoustic signature analysis. Similar plots have been made from tank G4695 and G4646 and show the drop in the vertical axis at a pressure count of approximately 22000 (indicating a change in acoustical impedance and resonance frequencies). The tank was exposed to 28,000 pressure cycles of 0 to 310 bar (4500 psi). At 22,000 pressure cycles, the system indicates fatigue damage with a drop in the damage indication (or coefficient) from 1.2 to 0.7, and then the tank began to leak at 28,000 cycles due to liner fatigue. Note that this would be the equivalent of 77 years of operation if the vehicle was filled once per day.

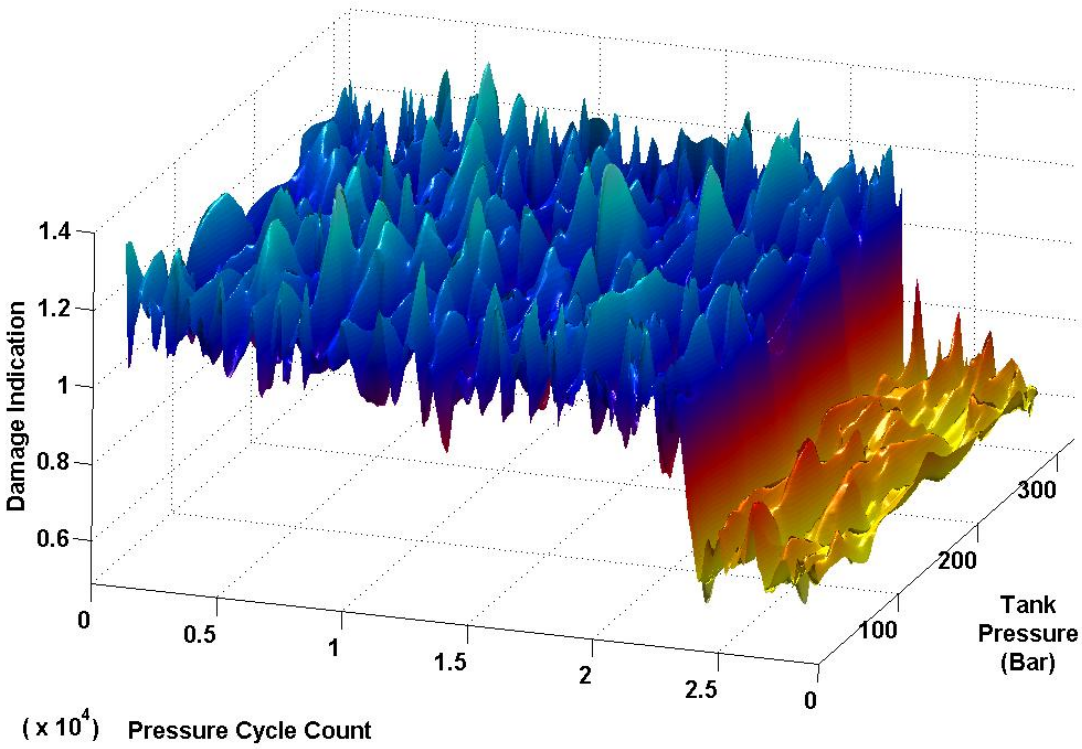

Figure 6.1: Typical Fatigue Failure (Image is Rotated for Visibility)

Figure 6.2 shows the actual fatigue failure mode of Tank G4604. The tank surface shows sweating and leakage through the fibers due to the failure of the aluminum liner on the bottom half of the tank. However, the composite overwrap did not show any deterioration in strength as surface flaws were not visible.

The fatigue properties for the composite structure are still not fully understood. The failure mode is a combination of stress-corrosion cracking, fracture mechanics, and fatigue in the aluminum liner. The difficulty is in the combination of the different materials – aluminum, epoxy and carbon fiber. Each has a different thermal expansion coefficient, and the amount of resin, carbon fiber and the aluminum liner for each tank is not exactly the same. Variations in the geometry, temperatures, load profiles, and loading amplitudes all influence the fatigue life of the tank. Furthermore, autofrettage

characteristics for the tank make the exact loading on the aluminum liner unknown. This autofrettage procedure stresses the tank to put the aluminum liner under compression when the tank is empty (much like preloading a bolt before loading it), and this results in placing the stresses on the composite in one direction (tension) only.

Figure 6.2: Tank Fatigue Failure

The interrelationship between the materials is what is observed in Figure 6.1. It is unlikely that the system can detect the initiation and growth of a fatigue crack in the tank. However, the system appears to be able to detect the changes in resonance, and hence in the wall structure, that result from the crack growing past a certain threshold. At the current state of the research, the threshold of the crack growth is unknown, and investigation of this subject would be of interest in future research.

6.3 Cut and Gouge Damage

Historically, cut and gouge damage has been difficult to identify on composite pressure vessels. This has been due primarily to the fact that these tanks are often hidden from direct view, underneath the vehicle undercarriage, beneath shrouds and covers, etc. Thorough visual inspection is currently the only mechanism for identifying cuts and gouges on these tanks.

The main cost associated with the visual inspection of tanks is the physical removal and extraction of the tanks from vehicles, storage racks, and other places where they are used. In the case of most vehicles, the tanks are most often inaccessible and can require major effort to remove.

Figure 6.3 shows the results of the cut and gouge damage inflicted on Tank G4642. The system was operated for the first 500 cycles to generate a normal operational profile. As can be seen for the first part of the tank life, the system operates with a nominal damage indicator coefficient value of 1.0. After the damage was inflicted, however, there is a noticeable change in the damage indicator with a jump in reading past 2.5. The tank damage consisted of two longitudinal cuts: 400 mm by 0.75 mm and 25 mm by 1.75 mm, as specified in the NGV2-2000 standard.

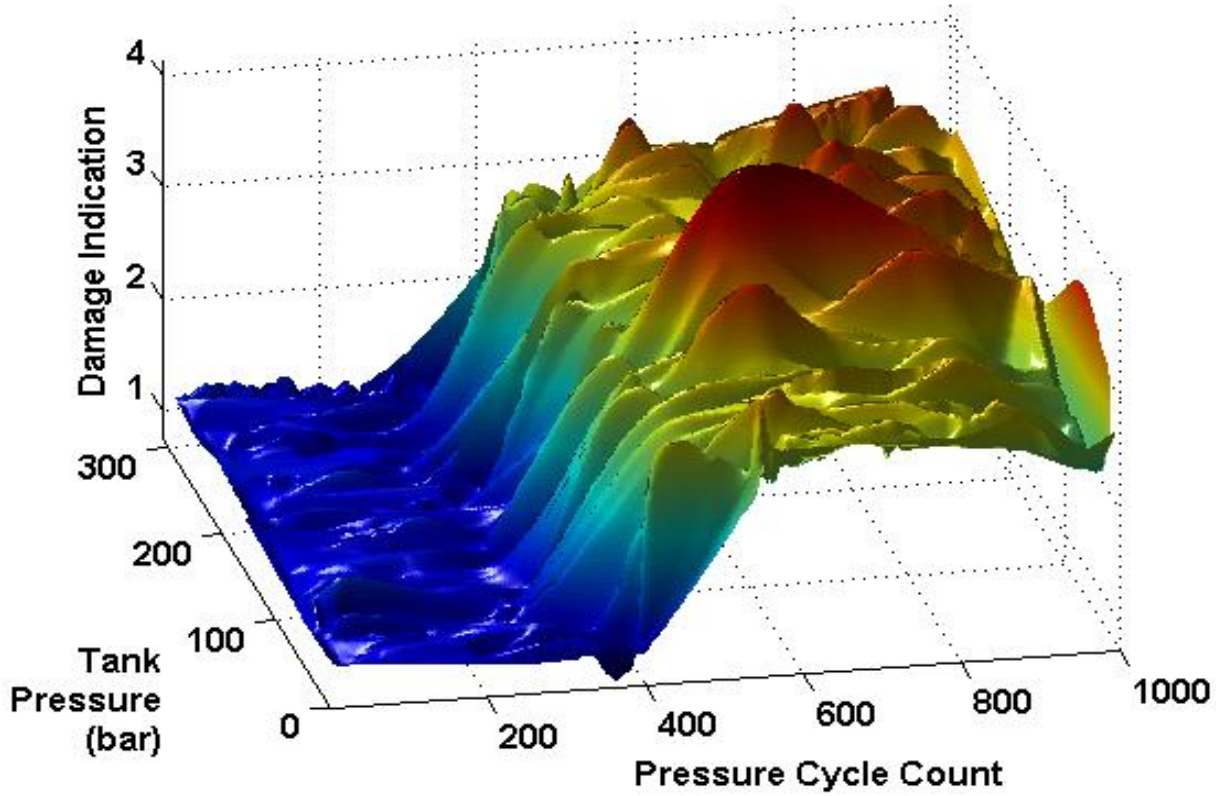

Figure 6.3: Cut and Gouge Damage Results

Figure 6.4 shows the mechanical damage imposed on the tank as per the NGV2-2000 specification. The NGV2-2000 cut specification was used to confirm the system sensitivity to damage, as it is the maximum design critical cut and gouge damage. As can be seen from the data, the system is very sensitive to cuts and gouges, and cut and gouge damage levels can easily exceed a damage threshold of 7 on the damage indicator scale. The damage shown in Figure 6.4 can easily be detected by the damage detection system, as shown in Figure 6.3, and the conclusion can be made that the system is sensitive to critical damage levels for this particular tank design. Smaller cuts and gouges will be picked up by the system, as well, which is a good design feature for this system to have.

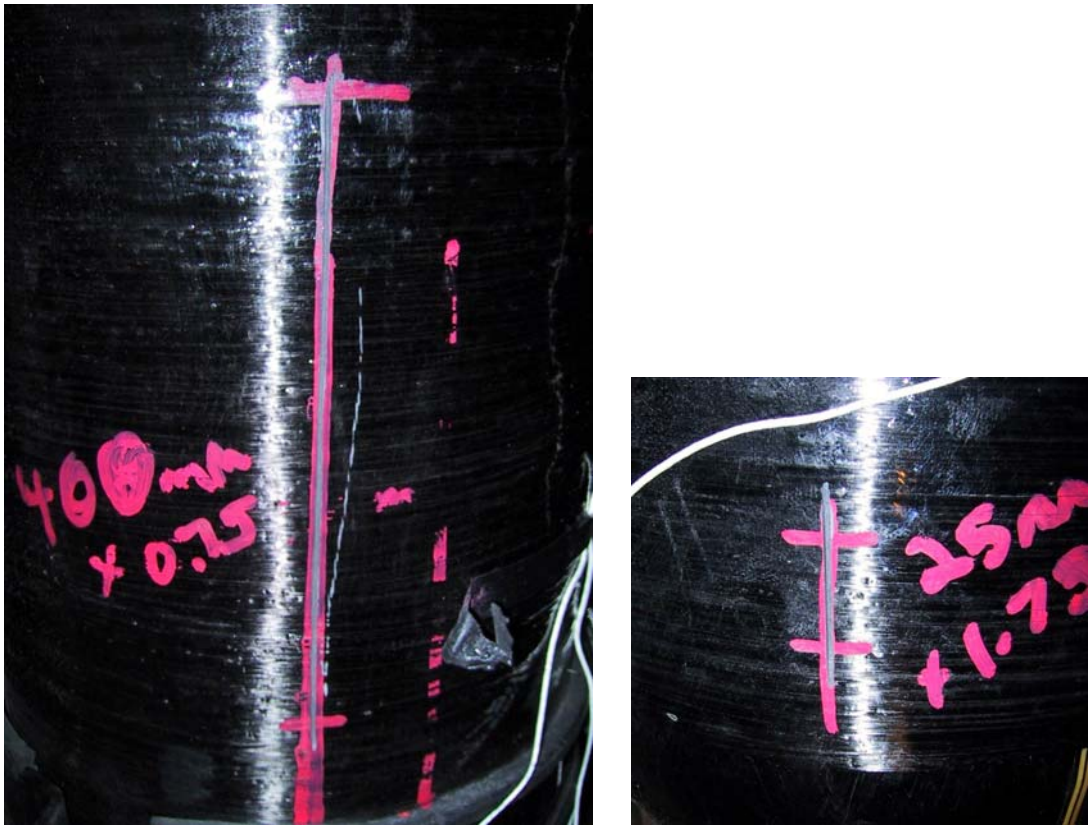

(a) (b)

Figure 6.4: Cut Damage on Tank (a) 400 mm (8 in.) by 0.75 mm (0.03 in.) and (b) 25 mm (1 in.) by 1.75 mm (0.07 in.)

The results of the damage detection system show a positive indicator, indicating shifts in resonant frequencies, and show consistency on the readings. The plot in Figure 6.3 is composed of 569 data measurements on the tank. The readings were taken independent of temperature and pressure, and the temperature and pressure were recorded at each sample point. It is evident in Figure 6.3 that the results indicate independent operation of the damage sensing mechanism from pressure (see pressure axis). Temperature was also not found to cause significant deviation of the measurements. The insensitivity to system and environmental variables is an important feature, as the measurements do not have to be compensated or corrected to prevent undesirable effects. Damage indicator consistency indicates error levels, accuracy, repeatability, as well as system reliability. The system performance appears to be well above the requirements for this test.

6.4 Drop and Delamination Damage

As mentioned in prior sections, delamination damage caused by drop and impact damage is one of the most undesirable forms of damage to composite tanks. Often damage can be significant, causing large, but unobservable, losses in structural integrity. Traditional damage detection is limited to ultrasonic or acoustic techniques, which can only be measured on a surface spot basis, and the entire surface of the structure must be examined to ensure structural integrity. This requires the removal of the tank from the vehicle, which can be an onerous task.

Figure 6.5 shows the results of drop and delamination damage on the tank. Tank delamination is the result of a 3 m (10 ft) drop onto concrete after 1000 pressure cycles. Delamination damage is detected immediately with an indicator reading of 2. After the test, a burst test was conducted to evaluate the integrity of the tank. The burst pressure was 900 bar (13,000 psi) (typical burst pressures) after the damage and significant more damage was inflicted. This additional damage is not shown in Figure 6.5. Typical test/design burst pressures for this particular design range from 760 bar (11,000 psi) to 900 bar (13,000 psi) were indicated by the manufacturer of the tanks. So, the drop/delamination damage was not severe enough to affect the burst pressure of the tank. It is not clear in the figure that the test starts after the drop (at a count of 0).

Figures 6.6 and Figures 6.7 show respective damage on the tank and the damage mechanism that has been used to inflict the damage on the tank. As has been previously indicated, the damage is not visible to the naked eye. However, the damage on the tank has been substantial enough to produce a pronounced change observable to the tank damage detection sensing system.

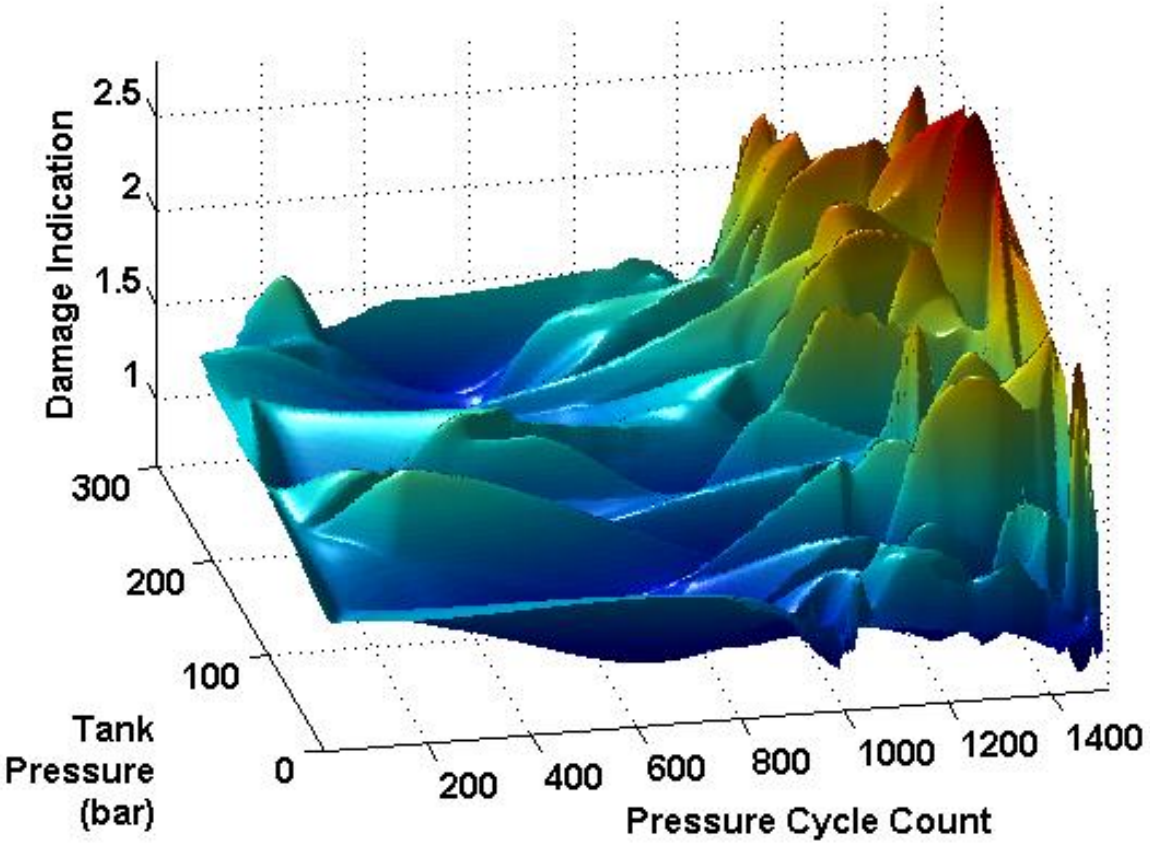

Figure 6.5: Drop and Delamination Damage

Figure 6.6: Tank Delamination Damage

Figure 6.7: Tank Drop Height of 3.05m (10 ft)

It has also been proposed to increase the impact energy by performing a test in which the tank is dropped from a height of 3 m (10 ft), half filled with water. Current knowledge of composite structures realizes that there are limitations on the material strengths of such structures. One typical point of interest of composite structures is that these structures are traditionally isotropic structures, and have directional strengths. The strength of the tank must be a function of the resistance to pressure and failure. Strengths in other directions, as observed after such tests as drop and delamination, are not high in composite materials. Accordingly, such a damage sensing system will become more important with proposals for higher working pressures of 700 bar (10,000 psi) with burst pressures of 1,850 bar (27,000psi).

The extreme sensitivity to delamination damage mechanism is where the real strength of the damage sensing system lies. Note that the damage detection system may not be able to prevent catastrophic failure, in cases where large amounts of damage are quickly

inflicted on the tank. This would correspond to cuts, large impacts and combinations of these damages, such as in an accident. However, extreme sensitivity to small amounts of damage may prevent significant damage and subsequent catastrophic failure of the tank.

6.5 Heat Damage

Heat damage has the potential to cause the tank to lose its structural integrity through the breakdown and loss of the outer carbon fiber wrap. The data combined into Figure 6.8 shows the tank damage system results from heat damage.

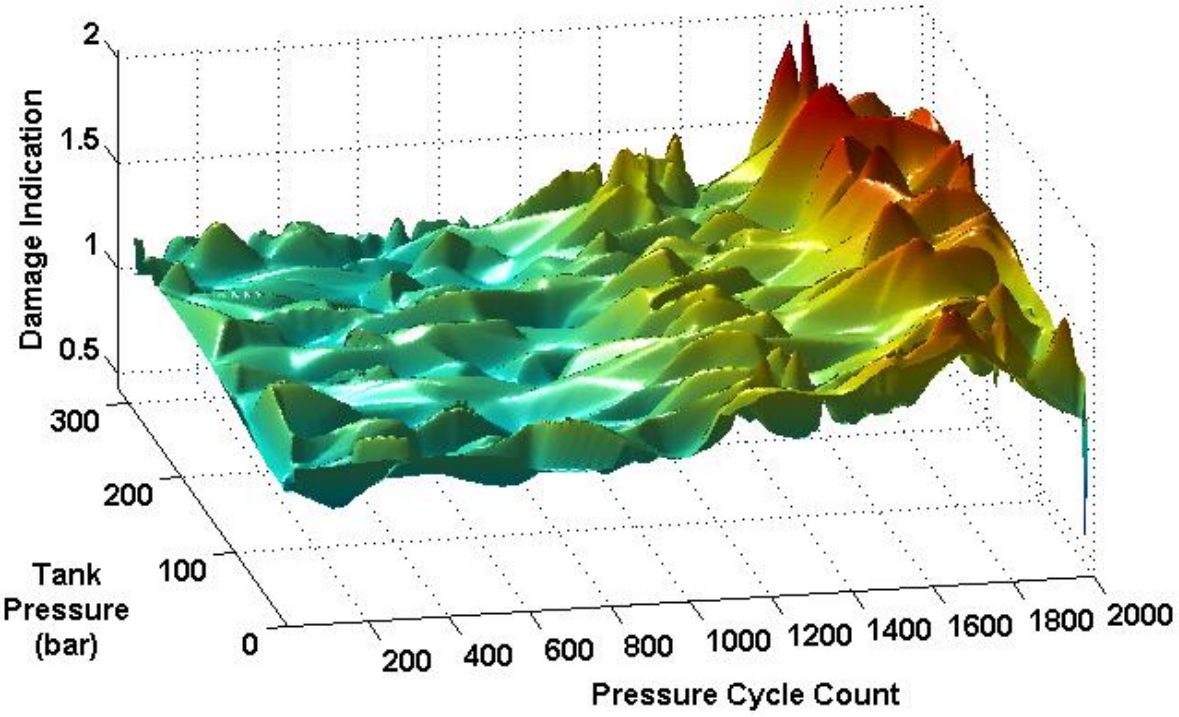

Figure 6.8: Heat Damage on Composite Structure

In the above figure, the tank was subjected to a small propane flame of temperature 1200^{o}F for 30 seconds. This was applied at 1000 pressure cycles, and then repeated again at 1500 pressure cycles. The heat damage is shown by an elevated damage

indication of 1.3 at 1000 pressure cycles and an elevated damage indication of 2 at 1500 pressure cycles.

The heat damage on the tank is shown in Figure 6.9 as a change in color on the surface of the tank. This is actually indicative of the loss of the epoxy matrix that holds the CFRP overwrap together.

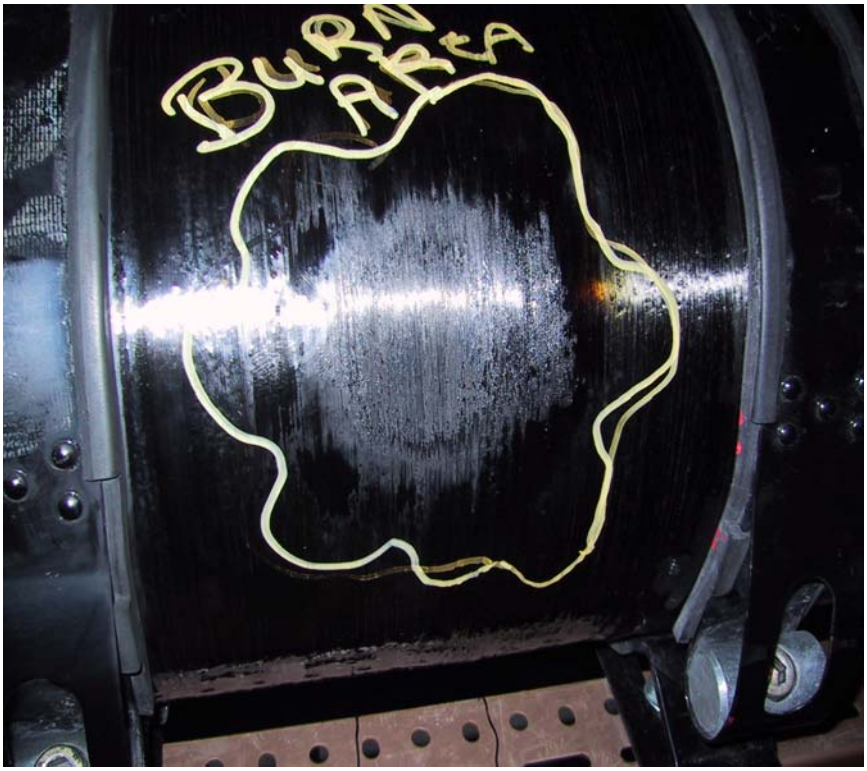

Figure 6.9: Heat Damage on Tank Sidewall

The small propane heat source is shown in Figure 6.10. This small torch was applied to the surface of the tank and was held for approximately 30 seconds. A localized area of heat damage was created from the torch, simulating the application of heat on a tank side wall from such operations as cutting a strap or a bolt off the mounting mechanism. Although the damage is visible to the eye, there is the risk that the tank will be subsequently installed with the damage hidden from view. As such, it is important to detect and manage this damage mechanism.

Figure 6.10: Propane Torch Used to Create Heat Damage

6.6 Stress Rupture

Stress rupture is a unique failure mode to composite materials. If, for example, a pressure vessel is subjected to elevated stress and temperature levels of a long period of time, then the structure can start to come apart. Furthermore, composite tanks are designed to withstand a certain amount of elevated stress conditions. As can be found experimentally, carbon-fiber composites tanks are less susceptible to this failure mode than other types of composites. However, elevated pressures in the tank can cause problems.

Examining the NGV2-2000 code presented in Appendix A, the code calls for hydrostatic pressurization to 1.25 times service pressure while at a temperature of 65°C (149°F). This condition must be maintained for 1000 hours and an evaluation of the burst pressure is used to detect structure deterioration, if any has occurred. The code indicates the trend observed — that over-pressurization can simulate stress rupture. A combination of stress, temperature, and time causes failure of the tanks. Increasing the stress levels has been found to accelerate the phenomena. Prior experience has indicated that tank pressure of three times the service pressure held for eight hours is a good indicator of this failure and was used for this test to indicate stress rupture damage.

Figure 6.11 indicates the test results from the simulated stress rupture testing. The tank was subjected to an elevated pressure three times its service pressure up to 630 bar (9100 psi) and let set for eight hours. This is further illustrated in Figure 6.12; however, the stress rupture damage is shown at 30 pressure cycles with an elevation in damage from 1 to 1.5. Note that the damage detection system was not activated during the over-stressing at three times it service pressure. The results shown in Figure 6.11 indicate damage indicator levels before the over-stressing and after the over-stressing.

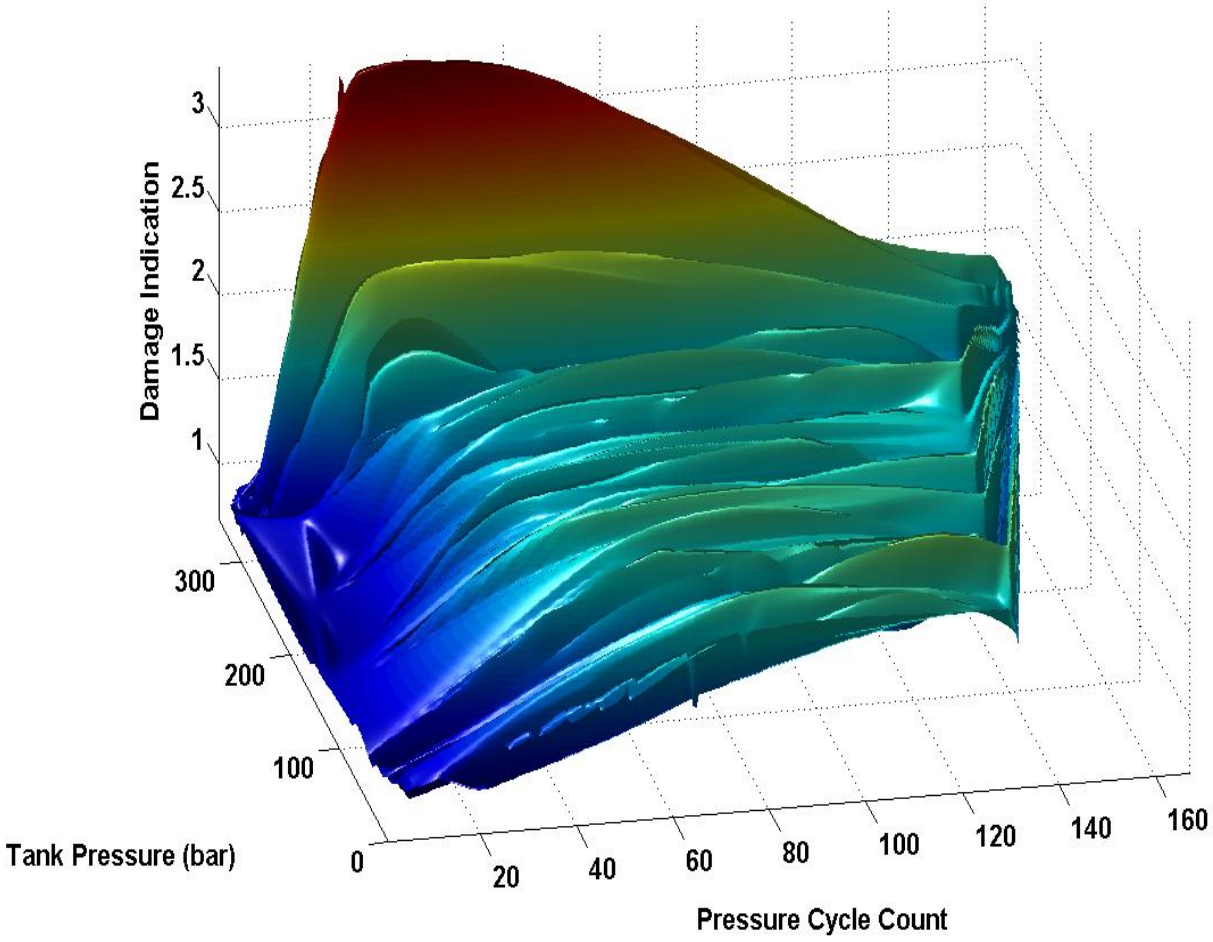

Figure 6.11: Stress Rupture Damage Plot

The stress rupture testing apparatus is shown in Figure 6.13, where the tank was pressurized inside a protective tank in the burst chamber.

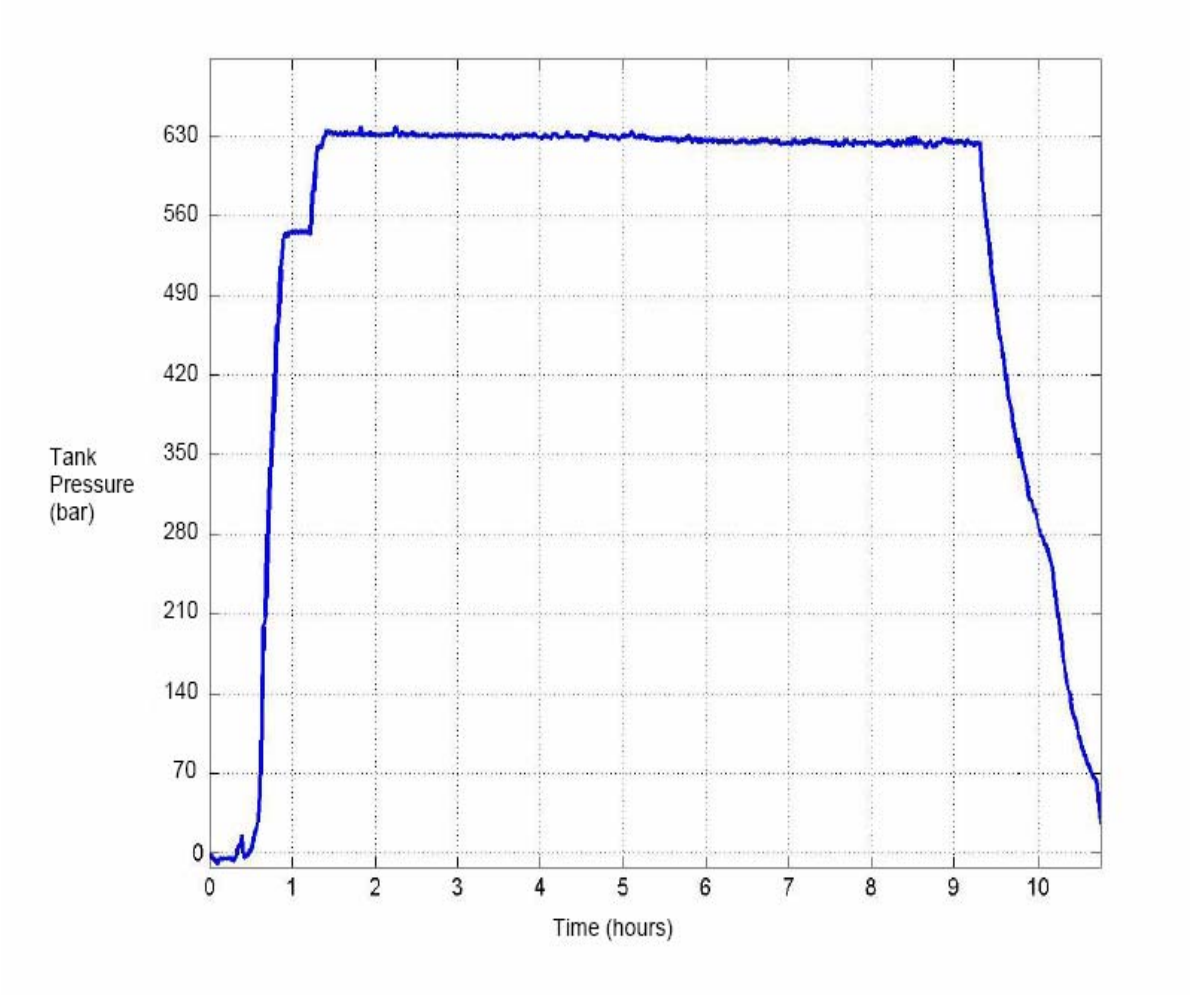

Fgure 6.12: Pressure Profile for Stress Rupture

As was to be expected, the over-pressurization of the tank resulted in a structural change in the tank as measured by the damage detection system. The over-pressurization effects also produced an expected, but interesting, phenomena. In particular, during over-pressurization of the tank (above two times service pressure), a noticeable change in signal quality and strength was observed from the sensors. As the structure became overstressed, the mechanical properties of the structure changed, and the carbon wrap held the sensors in place, producing a noticeable reduction in signal strength and

amplitude because the sensors were not moving as much.. Furthermore, the piezo-film sensors did not flex as much under high stress levels and capacitances of the sensors was reduced.

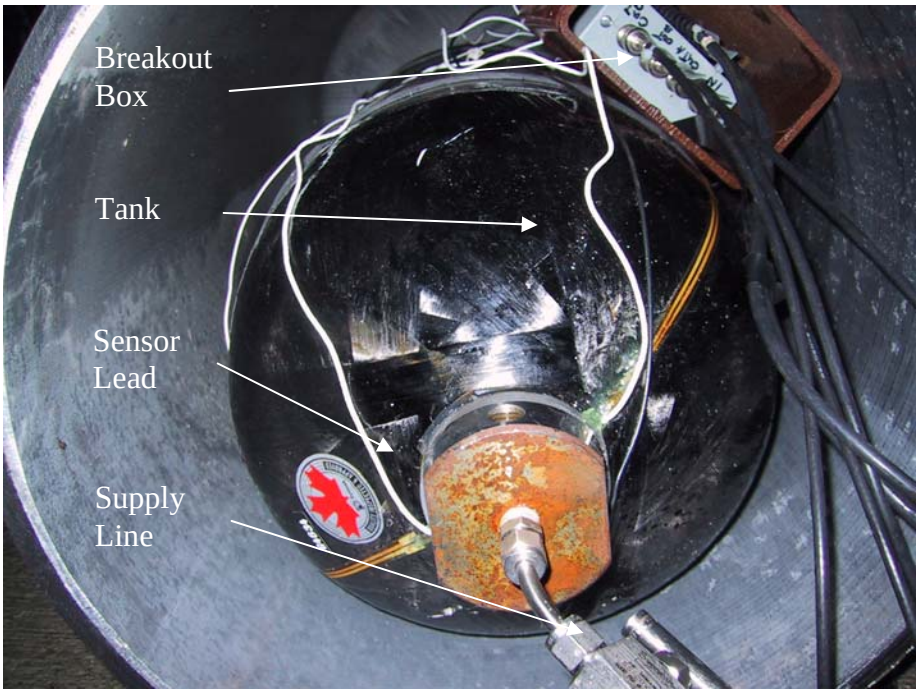

Figure 6.13: Stress Rupture Testing Apparatus

6.7 Combinational Damage

The investigation of the possible combinations of damage, including any of the aforementioned damage mechanisms, is discussed in this section. A tank was subjected to successive damage of drops, delaminations, and cuts, and was then cycled until the liner failed in fatigue.

Figure 6.14, and corresponding Table 6.1, shows the combinations of damage types with successive damages of drops and delaminations, cuts and liner fatigue. The forward axis indicates pressure cycle counts, as the tank pressure is cycled from minimal pressures to

1.5 times service pressure. One pressure cycle is considered as the tank pressure is raised

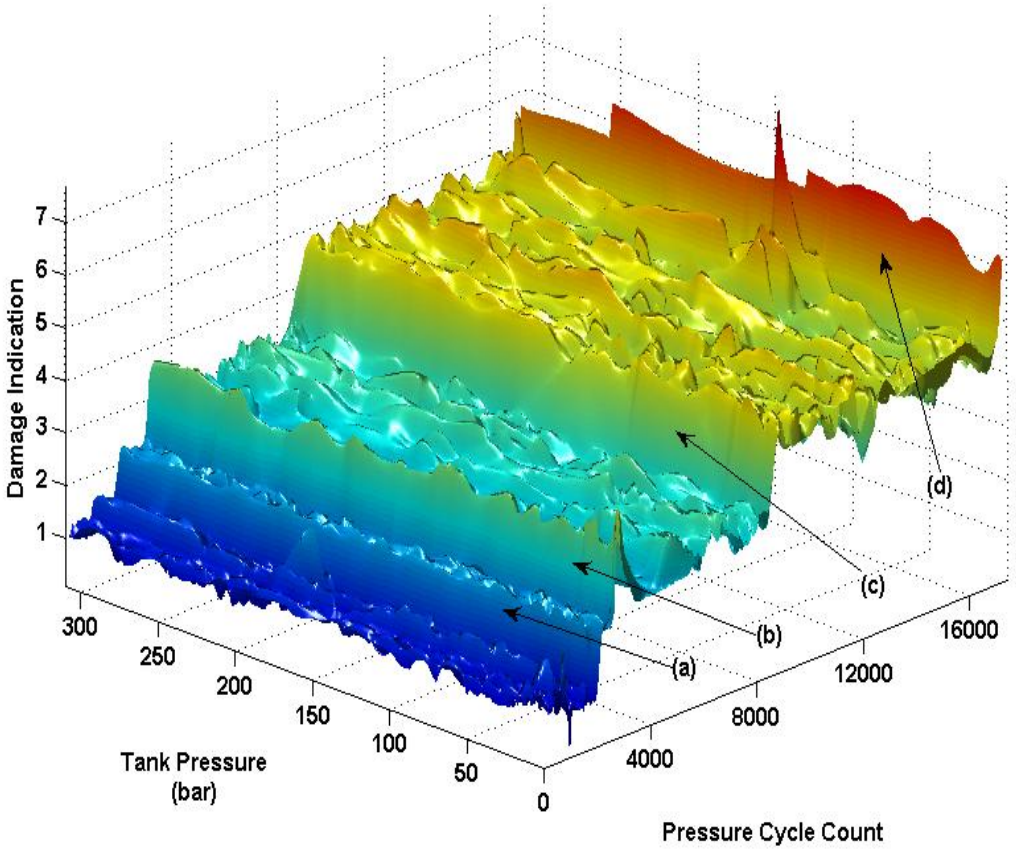

from near zero to 310 bar (4500 psi) and back down to zero.

Figure 6.14: Combinational Damage Plot

Table 6.1: Damage Profile Corresponding to Figure 6.14

Damage Type		Pressure Cycles	Indicator Level
(a)	Drop Impact	1,000	1.5
(b)	Cut #1	3,000	3.5
(c)	Cut #2	7,000	4.8
(d)	Liner Fatigue	17,500	6.0

A careful examination of the damage and subsequent changes in damage indication from the system shows good linearity, as well as a good indicator of damage to the tank. Of

interest, a series of drops, from 0.6 m (2 ft), 1.2 m (4 ft), and 1.8 m (6 ft) were done on this tank. The 0.6 m (2 ft) drop produced no noticeable delamination, the 1.2 m (4 ft) drop produced a delamination of the size of a dime, and the 1.8 m (6 ft) drop a delamination the size of a dollar coin. One can actually see the three drops on the plot, as slight ridges, independent of pressure, on the first 2000 pressure cycles. Of most interest is the 1.8 m (6 ft) drop, which produced a damage indication of 1.5 on the scale of 1 to 6.

Figures 6.15 and 6.16 show the drop site where the 1.8 m (6 ft) drop was conducted, and the subsequent damage to the tank. Note that this damage is considered minimal for the design with little or no reduction in burst strength of the tank.

Figure 6.15: Drop Impact from 1.8 m (6 ft) onto Smooth Concrete

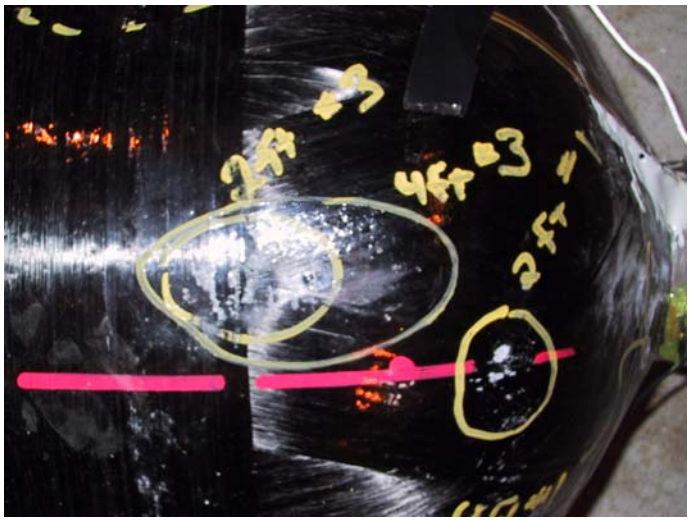

Figure 6.16: Delamination Damage from 1.8 m (6 ft) Drop

Figures 6.17 and 6.18 show the two cuts applied to the tank. The first cut, 100 mm (4 in.) long and 3 mm (0.11 in.) deep was applied to the tank at 3000 pressure cycles, producing a damage indication level of 3.5. Note that the damage indicator rises sharply and settles at the new level, giving indication of the damage inflicted on the structure, and not of a transient response that becomes immeasurable. The second cut, 100 mm (4 in.) long and 4.5 mm (0.18 in.) deep was inflicted at 7000 pressure cycles. Note that this was accomplished by cutting the tank at the same point as Cut #1, just making the cut deeper. This was done to show incremental damage levels on the tank. This produces a stable damage indication reading of 4.8.

Figure 6.17: Cut #1 – 100 mm (4 in.) Long by 3 mm (0.11 in.) Deep

Figure 6.18: Cut #2 – 100mm (4 in.) Long by 4.5mm (0.18 in.) Deep

Figure 6.19 shows the eventual fatigue failure of the tank after 17,500 pressure cycles, the equivalent of 48 years of operation at one fill per day. The tank fails under liner fatigue directly opposite the cut line.

Figure 6.19: Fatigue Failure of Tank after 17,500 Pressure Cycles

At 17,500 pressure cycles, the tank begins to leak, but not before the damage indication levels rise. When the tank starts to leak, the hydraulic system is not able to produce 310 bar (4,500 psi) in the test tank, and the system shuts down. The observations of the system at high pressure, and at a high damage indication (6.0) show that the system was able to pick up an elevated damage signal before the tank fatigued. This is important because the system has the potential to produce an early damage indication before eventual failure occurs. In field implementation, a single pressure cycle is typically observed in a day for most gaseous-fuelled vehicles, giving ample opportunity for the system to detect damage.

6.8 Other Damage Mechanisms

Other environmental effects were analyzed in this project. These included gravel testing (spray of high velocity gravel onto the surface of the tank), water penetration testing, and

environmental testing. These three tests were used to validate the performance of the damage detection system under field operation.

Gravel testing was done utilizing a venturi-style gravel accelerometer, where gravel pieces less than 12.5mm (1/2 in) were sprayed onto the surface of the tank. As these tanks are designed of this type of environment, they are able to withstand a large amount of surface impacts without damaging the integrity of the pressure vessel. The testing showed no apparent increase in damage level signal as a result of the gravel testing.

Water penetration testing was also incorporated into the project. Due to the nature of the damage detection system, water posed a threat to the electrical components, and potentially to produce not accurate damage indicators. In order to test this hypothesis, a fine mist spray was directed onto the surface of the tank for a period of 8 hours, while monitoring the tank. As the sensor leads were not designed for watertight applications, these leads were not exposed to the water mist, and were sealed externally. The testing, after 8 hours of slow pressure cycling the tank with the water mist, showed no change in damage indication. It was generally thought that the tank was too tightly wound, especially when the tank was under pressure, for water to penetrate into the carbon fiber structure. This agrees generally with the field experience, where water penetration and freeze-thaw cycling has not posed problems for these carbon fiber tanks.

Further examination into the effects of environmental conditions and stored fluid type were conducted in this project. An environmental chamber was utilized to test the tank under pressure, and varying levels of pressure, to observe the effects of temperature on the damage indication mechanism. In order to service the full automotive temperature range of –40°C to 80°C, nitrogen gas was used to test the tank. This further required verification of the effects of nitrogen on the damage detection system. In the end, no noticeable difference in damage indication was observed in the entire temperature range and for the change in gas, most likely due to the high frequencies used in the damage detection system

6.9 Summary

In this section, the results of the damage detection system have been presented. Positive results were obtained in all of the failure modes examined, which included fatigue, cuts and gouges, drops and delaminations, heat damage, stress rupture, and combinations of the above damage mechanisms. In the next chapter, a discussion of the indicated results is given.

CHAPTER 7. DISCUSSION

7.1 General

The features that allow for improved reliability and accuracy of the system are sensor design and installation. An embedded sensor design allows for mechanical and environmental protection of the leads and sensors. Iterative sensor design and environmental testing have allowed for the development of a trouble-free system. As well, the integration of the sensors into the tanks allows for radio frequency and electromagnetic noise protection.

The system has been designed to output a linear damage indicator reading (defined in Chapter 5 and Appendix D) that is consistent, accurate, and reliable as shown in the test results in Chapter 6. This linear reading is proportional to damage as indicated. Insensitivity to system pressure is shown in the three-dimensional plots. Other environmental influences, such as temperature and fluid type, were examined with negligible changes in the damage response.

One of the problems associated with this technology is the high bandwidth requirement. In this research, a sampling window from 17 to 85 MHz was used to evaluate and identify damage to the cylinders. This is currently beyond most off-the-shelf microprocessor capabilities. However, the development of future microprocessor Digital Signal Processing products will certainly reduce microprocessor costs.

The current technology has been developed primarily to detect changes in the cylinder structure. No work has been done to investigate the different damage mechanisms, and how to differentiate between them. Due to the nature of the pressure vessel, which is loaded uniformly (with gas pressure), the system was developed to identify faults in the structure, and not necessarily location or cause of the faults. Any damage indication

needs to be properly examined with a nondestructive evaluation technique that will ensure the structural integrity of the cylinders.

The development of the technology has also identified weaknesses in the damage detection system. In particular, tests show that sensor placement and the number of sensors used are critical. The final design, with sensor placement as shown in Figure 3.18, incorporates sensor coverage throughout the cylinder. As can be expected, the testing results indicated best damage detection when the damage is located between the transmitting and receiving sensors. Other sensors may or may not have picked up the damage, depending on location, sensor functionality, and lead attachments. Much difficulty was found with sensor leads, as a reliable and near indestructible lead was not used in the testing. These cylinders are often located on the outside of a vehicle, exposed to gravel, road dirt, salt, and spray. However, in the laboratory testing, they only have to withstand drop tests, cut tests, heat tests, environmental testing, moisture, and many other environmental and physical requirements.

The sensors require a very robust design. They are susceptible to damage, especially when handling cylinders full of water or some other fluid. Due to time and outsourcing variables, a conventional off-the-shelf sensor was selected for this application. Initial testing with the sensors mounted on the surface of the cylinder provided for adequate observations that the sensors could be easily damaged. However, incorporation of the sensors into the cylinder structure provided protection from physical damage, as well as protection from signal disturbances such as electromotive and radio-frequency noise. When the sensors were moved into the cylinder structure, the noise levels dropped dramatically, and repeatability was increased, as shown in Appendix D. Furthermore, the longest fatigue testing gave a good chance to evaluate the overall performance of the sensors to repeated usage. The sensors were tested to a life of approximately 5.4 billion cycles through accelerated life testing conducted jointly with tank fatigue cycling. This ensures a lifespan of well over 30 years (longer than the cylinder life) and sufficiently longer than most electronics packages last.

It also is imperative that the sensors remain small and thin, except when examining for delaminations in which case the exact sensor size is not critical. During the development of the cylinders, delamination studies were done to evaluate the impact of thin delaminations to the structure. As well, the test cylinders with embedded sensors showed no overall reduction in fatigue cycle life or burst pressure from the manufacture of the sensors into the tank. Sensor thickness is more important, due to the introduction of a stress concentration in the cylinder. This will affect sensor sensitivity, accuracy of readings, and may cause problems resulting in reduced cylinder life and reduced burst pressures.

A discussion of each damage mechanism is included in this section to evaluate results and conclusions for the current work, or as well as to identify future work.

7.2 Fatigue Damage

First and foremost, fatigue damage is very difficult to detect inside the tank. Fatigue damage is the result of a small fatigue crack penetrating the aluminum cylinder liner. Typical liner thicknesses at the point of fatigue are 3 mm (0.125 in.). Resultant crack lengths for a crack initiated on the inner liner wall will grow to 6 mm (0.25 in.) long. These cracks are not visible to the naked eye on the outer surface and are even difficult to detect with conventional ultrasonic testing. Ultrasonic testing for this application is limited to a surface-mounted ultrasonic probe, which would be required to pass over the entire surface of the tank.

Fracture mechanics [Bhuyan and Su, 1998] on fiber-reinforced aluminum-lined pressure vessels indicate that the crack growth stage lasts approximately 5000 pressure cycles until leakage occurs. This seems very consistent with that detected on the damage system. However, results should be repeated, and at the point of reduction in the damage calculated signal, the tank should be investigated for crack initiation and growth.

It has been expected and anticipated that the presence of the crack in the aluminum liner does produce a localized stress riser in the CFRP structure. As a result, it is believed that the damage detection system picks up this stress level change or motion, resulting in a different structure resonance and admittance. However, for the decrease in damage indication, this may be explained if the damage indicator is sensitive to the water passing through the structure as a result of the fatigue crack. This failure mode should be more thoroughly investigated in future work.

7.3 Cut and Gouge Damage

Cut and gouge detection are, in comparison to fatigue detection, one of the simplest damage mechanisms to detect on a tank. Depending on the severity of the damage, significant damage can normally be visible to the naked eye. Furthermore, after prolonged cylinder use with the damage, the fibers that no longer bear any load due to the damage tend to peel themselves off from the cylinder. This becomes visible as a section of fibers 'spring' loose from the surface of the cylinder.

Sensitivity testing for the cut and gouge testing was done through the use of the NGV2-2000 standard (see Appendix A). The required cuts for the test were two cuts, the first 25 mm (1 in) long and 1.25 mm (0.05 in) in depth, and the other cut were 200 mm (8 in) long and 0.75 mm (0.03 in) in depth. The cylinder minimum design calls for pressure cycling from empty to 1.25 times the service pressure for a minimum of 11,250 pressure cycles. Clearly, if this damage can be detected before a minimum of 11,250 pressure cycles, then the damage detection system is sensitive enough for industrial and automotive applications.

Tests were completed on cylinders with neck cuts, hoop cuts, longitudinal cuts and gouges made from impacts with an axe. Under all situations, a significant change in the tank resonance frequencies and admittance were observed.

7.4 Drop and Delamination Damage

Impact damage to the tank quite often causes delaminations in the CFRP structure. As previously discussed, these delaminations are often hidden to the observer, and some type of Non-Destructive Evaluation (NDE) mechanism must be utilized to identify the damage.

Testing conducted on the cylinder was done with a variation of impact damage, causing delaminations. The height at which the first measurable delamination (approximately 25mm (1 in) diameter) was produced with the tank at a 45^{o} angle was found to be 1.2 m (4 ft). The impact energy was approximately 270 Nm with this particular cylinder design. Tests were conducted below, and in incremental steps above this delamination height. Results showed a linear trend of delamination size with net changes in cylinder resonance frequencies and acoustic admittance.

Of further interest was the investigation of what normal cylinder use would do to damage level signals. It was observed that once the damage levels were established, they did not drop back to the initial value. The levels did remain stable at the new level. This is significant because this would only require sporadic and intermittent sampling of the structure, and not continuous monitoring, such as in acoustic emission. This adds a whole degree of flexibility because it does not require operation in times where power is not available (such as in transport, filling, and maintenance).

7.5 Heat Damage

Heat damage is one of the few damage mechanisms that tends to be often overlooked. In fact, localized heat damage rarely penetrates all but the outer layers of the CFRP on the pressure vessel. However, heat damage can pose a significant reduction in overall strength of the pressure vessel.

Visual inspection is the only NDE technique available for identifying heat damage in the composite pressure vessel. In terms of application and ease of implementation, a visual inspection is not a very reliable mechanism for NDE of cylinders in automotive applications. Visibility, access and costs all play a major role in the reliability of this method. The ability to detect heat damage to the cylinder is significant, as this failure mode is very unpredictable and important to identify in the early stage.

7.6 Stress Rupture Damage

The cylinder testing showed good correlation and results for the stress rupture testing. Of interest is the reduction in signal strength, shown by the large change in damage amplitude while the cylinder was at high pressure, as was shown in Figure 6.11. The damage to the tank structure is visible and is noticeably changed as the signal levels return to a level that is significantly higher than the original.

7.7 Combination Damage

As a part of the research, combinations of the above damage mechanisms were investigated to identify whether one damage mechanism could be separately identified from another, or if consecutive damage added, or was masked in previous damage signals. This testing involved a combination of drops, cuts and fatigue damage. The testing was successful, as damage levels were cumulative, indicating a linear output for the damage indication which was proportional to the actual level of damage. It was difficult to get a proper indication of the critical threshold of the damage in the tank, and a corresponding estimated tank life available. No effort was made in this project to identify and differentiate the different damage levels; rather the presence of damage was sought for identification.

7.8 Other Damage Mechanisms

As brought forward in Chapter 6, environmental testing was completed to evaluate the functionality of such a system under normal operating conditions. These tests included: gravel testing (spray of high velocity gravel onto the surface of the tank), water penetration testing, temperature testing, and testing with different media inside the tank. These tests were used to validate the performance of the damage detection system under field operation.

In summary, all of the environmental testing showed little or no significant problems in operation of the health monitoring system. Gravel testing showed no apparent increase in damage level signal, as the damage inflicted by the gravel was superficial damage to the surface of the cylinder. Water penetration testing also showed no problems with operation, although it is extremely important to design the electrical connectors and wiring able to handle such environmental stresses. It was generally thought that the cylinder was too tightly wound, especially when the cylinder was under pressure, for water to penetrate into the carbon fiber structure. This agrees generally with the field experience, where water penetration and freeze-thaw cycling has not posed problems for these carbon fiber cylinders. Finally, no noticeable difference in damage indication was observed in the entire temperature range and for the change from liquid to gas, most likely due to the high frequencies used in the damage detection system.

Such other damage mechanisms, such as acidity/alkaline environment, environmental extremes and radio-frequency/electromotive noise still require testing. These and other tests need to be completed to verify good repeatability and reliability of the system, as the potential for a false damage indication will make industrial acceptance difficult.

7.9 Summary

The system also shows the potential to identify manufacturing flaws and exhibit a level of quality control on the tanks. Currently, NGV and similar standards call for one tank from

every manufacturing batch to undergo quality control testing to identify poor material qualities, flaws, dry and insufficient wrap, autofrettage problems, as well as other manufacturing problems. This is a very time consuming and costly approach to quality control. The damage detection system has the potential to reduce these requirements, as every cylinder with the damage detection system is quantified at the time of manufacture, and correlations between the quality and the baseline characteristics might be found.

After the testing and development in this research project was completed, further work at Stanford and NASA, on the development of systems for the detection of flaws in composite structures was recently published by [Kumar et al., 2004, Kusaka and Qing, 2003]. This work, detailing systems that monitor the integrity of filament wound structures utilizing built-in sensor networks (Piezoelectric film), shows very similar application, method and results of the systems. The work entails development of a layer of built-in sensors that have a matrix of transmitting or receiving piezoelectric film sensors that can be utilized to detect flaws in composite structures. These sensor networks were demonstrated to detect delamination and crack growth in carbon fiber reinforced cylinders such as tested in this project. The results from these publications reaffirm the results presented in this work. It should be mentioned that the approach of using a single fault detection coefficient presented in this thesis was unique to this study.

In the next section, conclusions and recommendations are given to bring the health monitoring system into a commercial product.

CHAPTER 8. CONCLUSIONS AND RECOMMENDATIONS

8.1 Conclusions

A reliable, low-cost acoustical ultrasonic system to detect damage in high-pressure storage cylinders has been designed, developed, and tested. The technology can be deployed at a reasonable cost, and has been designed to accurately detect damage with little to no maintenance required. Thirty cylinders were used in a test matrix to examine all possible failure mechanisms of the tanks, including combinations of failure mechanisms. Furthermore, the damage sensing system has been shown to be insensitive to environmental effects, such as temperature, humidity, moisture, and electro-magnetic noise. However, further testing is still required to develop final products to meet relevant standards.

In specific, the conclusions that can be drawn from this work are as follows:

1. The failure modes for Type III composite pressure vessels that are relevant for the operation of a structural health monitoring system include fatigue, cuts and gouges, impact and delaminations, stress rupture and heat damage. It is important to be able to detect both individual failure modes and combinations of these modes of failure.

2. In order to effectively sense damage in a Type III composite cylinder, piezo-electric film sensors must be embedded into the tank structure. This allows major damage to be detected before the cylinder becomes pressurized. However, minor damage that is well below critical thresholds can be identified once the cylinder is pressurized, as changes in the resonant structure of the cylinder are more easily observed once the stresses in the cylinder change as it is pressurized.

3. Most damage types are indicated by changes in resonance of the composite structure. These changes have been identified as increases in the calculated damage indicator, and have been successfully identified for fatigue, cuts and gouges, impact and delaminations, stress rupture, heat damage, and combinations of these damage mechanisms. However, for fatigue, decreases in the calculated damage indicator may be sensitive to the water passing through the structure as a result of the fatigue crack.

4. The testing portion of this thesis indicates the effective safety factor used in the design and implementation of such composite pressure vessels. As was observed, in excess of 50 years of service can be extracted from a cylinder that is only rated for a 15 year service life. The potential for reducing safety factors, materials, and costs can be easily made with integration of an on-line damage detection system for these cylinders. The barrier to this implementation lies in changing and adapting the relevant standards to reflect new technology

5. It is concluded that the single number damage indicator factor is an effective approach to represent and detect failures modes in composite pressure vessels.

The novelty and uniqueness of this work has been affirmed with the award of a United States patent for the method to detect damage in composite pressure vessels, including examples of implementation of the technology. The tank damage system has been developed at the forefront of technology, and has been implemented in a cost-effective system that accurately detects damage.

A technique was developed to allow for the use of a low-cost piezo-film sensor to aid in structural health monitoring of composite pressure vessels. This technique utilizes a pulse – receive mode of operation with one transmitting sensor and three receiving sensors for the particular pressure vessel that was utilized in this work. This technique was demonstrated to identify all of the major failure modes for the tank well below the critical damage threshold. The reliability that has been demonstrated in this low-cost

system shows promise compared to all of the other techniques available. However, more work remains to be completed before this technology can be brought forward for commercialization. Such a technique, as developed in this work, needs to be fully tested and understood before it can be used in a commercial application.

8.2 Recommendations and Further Work

8.2.1 General

In order to bring the system to a commercial product, the following tasks need to be completed:

1. Proper identification of the sensing mechanism needs to be completed. Initial work suggests the presence of both electrical coupling as well as physical coupling between the sensors. Examination into resonant filters, capacitive couplings and electrical properties of composites should be conducted.

2. Extension of the damage detection system into a larger tank design: This will include sensor location selection, including transmission distances, resonant frequency analysis (to design the sensor resonance frequency) and full-scale trials of all failure modes. Further work should also be considered to optimize sensor location.

3. Fatigue Failure Analysis: Investigations into the fatigue failure mode need to be further studied. In particular, the cylinder needs to be fatigue cycled until the damage indicator shows that the tank is failing, and a proven non-destructive evaluation examination should be completed to identify the failure. This should be correlated to the damage detection results.

4. Evaluation of in-situational operation: This is critical to evaluate performance of the system under real operating conditions. A six-month testing and evaluation stage is recommended to fix all of the 'bugs' before sending out prototype units for evaluation. Potential problems include: salt spray, corrosion, dirt and residue buildup, on the external and internal tank components, sensor lead damage, and software and electronic hardware reliability.

5. Proper identification of the damage level threshold and what should be considered a minimum to warrant further NDE inspection of the cylinder.

6. Examination into further environmental effects such as noise, acids, alkalines, and other automotive fluids.

8.2.2 Recommendations for new tank design failure modes:

In order to further evaluate the damage detection system, the following design failure modes should be used for evaluation at future stages of the work. These recommended failure modes are the most relevant and prominent for the Type III cylinder design and provide the threshold for significant damage in the cylinder, although minor damage should also be detected.

8.2.2.1 Delamination and Impact Damage Testing

Depending on tank design, it is recommended that a test which utilizes 25%, 50%, 75%, and 100% of the drop energy that would provide a 50 mm (2 in) diameter bruise of the tank. This bruise can be found by tapping the surface to hear a change in pitch where the delamination has formed.

8.2.2.2 Cut and Gouge Testing

Typical minimum threshold cuts should be known for each particular cylinder design. For example, the tank design used in this project (L033 Series) has a cut threshold of 400 mm by 7.5 mm before the fibers start to pull or snap when they are cut. Once this action takes place, the tank is no longer able to withstand service pressure operation. It is recommended that the damage used for cut and gouge detection be based on longitudinal cuts of 1 mm deep and 400mm long, incremented by a single millimeter in depth until the surrounding fibers reach the breaking point.

8.2.2.3 Heat Damage

Heat damage is present on the tank when exposed to an over-temperature situation, such as a vehicle fire or oxy-acetylene torches used in the vicinity of the cylinder. Heat damage can reduce the overall strength of the cylinder if the heat penetrates past the outer (5mm to 10mm) surface into the sidewall or shoulder of the tank. Furthermore, the aluminum liner temperature cannot be increased past its annealing temperature ($415^{o}C$ for 6061T6 aluminum). Hence, it is recommended that heat damage threshold testing should be inflicted to a depth of 4 mm thickness into the sidewall. Heat damage penetration can be measured through penetration of the damaged area with a sharp object.

8.2.2.4 Stress Rupture

Stress Rupture is commonly found in an over-pressure situation, such as in a fire or elevated temperature situation. Most systems will not have pressure relief valves inside the fuelling system, and simply rely on the fill system not to overpressure the storage system. Typical fill pressures causing stress rupture are in the three times service pressure range. Note that this failure mode is almost identical to that of stress corrosion cracking; however, carbon fiber is not susceptible to stress corrosion cracking. Hence, it is recommended that stress rupture tests should be tested for an estimated 100 hours at three times service pressure.

REFERENCES

ASTM E070403-95/1: *Proposed ASTM Standard – Test Method for Examination of Gas-Filled Filament-Wound Composite Pressure Vessels using Acoustic Emission,* January 2001.

ANSI/CSA NGV2 *Basic Requirements for Compressed Natural Gas Vehicle (NGV) Fuel Containers*, Prepared by CSA International, Cleveland Ohio, June 2000.

Avallon, E. and Baumeister T. *Mark's Standard Handbook for Mechanical Engineers.* McGraw Hill, Boston, 1996.

Bar-Cohen, Yoseph, Chang, Z., and Mal, A. *Characterization of Defects in Composite Material Using Rapidly Acquired Leaky Lamb Wave Dispersion Data*. NDT.net (On-line Journal), September, 1998, Vol. 3, No.9.

Bar-Cohen, Yoseph, Xue, T, and Lih, S. *Polymer Piezoelectric Transducers for Ultrasonic NDE*. NDT.net, September, 1996, Vol. 1, No. 9.

Bar-Cohen, Yoseph. *Emerging NDE Technologies and Challenges at the Beginning of the 3rd Millennium, Part I*. NDT.net, January 2000, Vol. 5, No.1.

Bar-Cohen, Yoseph. *Emerging NDE Technologies and Challenges at the Beginning of the 3rd Millennium, Part II*. NDT.net, February 2000, Vol. 5, No. 2.

Bhuyan, G. and Su, B. *Influence of Hoop-Wrap Composite Materials on Fracture Behaviors of Aluminum Lined Hoop-Wrapped Cylinders with Cracks*. Proceedings of the Sixth Annual International Conference on Composites Engineering, Florida, 1999.

Bossel, U. *The Physics of the Hydrogen Economy*. European Fuel Cell News, July, 2003, Vol. 10, No. 2.

Deutsch, W., Deutsch, K., Cheng, A. and Achenbach, J. *Defect Detection with Rayleigh and Lamb Waves Generated by a Self-Focusing Phased Array*. NDT.net, December 1998 Vol. 7, No. 9.

Dode, A. and Rao, M. *Pattern Recognition of Acoustic Emission Signals from PZT Ceramics*. NDT.net, September, 2002, Vol. 7, No. 9.

Duvall, P. *Natural Gas Vehicle Tank Life Sensor and Control*. United States Patent No. 5,522,428. June, 1996.

Foedinger, R., Rea, D., Sirkis, J., Baldwin, C., Troll, J., Grande, R., Davis, C. and Vandiver, T., *Embedded fiber optic sensor arrays for structural health monitoring of filament wound composite pressure vessels*, Proceedings On Smart Structures and Materials: Sensory Phenomena and Measurement Instrumentation for Smart Structures and Materials, 1999, SPIE Vol. 3670, pp. 289-301.

Finlayson, R., Friesel, M., and Carlos, M. *Health Monitoring of Aerospace Structures with Acoustic Emission and Acousto-Ultrasonics.* Proceedings of the 15th World Conference on Non-Destructive Testing, Rome, October, 2003.

Graps, Amara. *An Introduction to Wavelets*. IEEE Computational Science and Engineering, Summer 1995, Vol. 2, No. 2.

Holroyd, T. and Randall, N. *Use of Acoustic Emission for Machine Condition Monitoring*. British Journal of NDT, February, 1993, Vol. 35, No. 2, pp 75-78.

Javed, M. and Littlefair, G. *An Intelligent Condition Monitoring System Using Acoustic Emission*. Proceedings of the Artificial Neural Networks in Engineering Conference, St. Louis, MO, 1993, Vol 3., pp 775-780.

Johns, R and Kaufman, A. NASA TMX-52171, Lewis Research Center, 1964.

Kotsikos, G., Evans, J., Gibson, A., and Hale, J.. *Use of Acoustic Emission to Characterize Corrosion Fatigue Damage Accumulation in Glass Fiber Reinforced Polyester Laminates*. Polymer Composites, October 1999, Vol. 20, No 5, pp. 689-696.

Kusaka, T and Qing, P. *Characterization of Loading Effects on the Performance of SMART Layer Embedded or Surface-Mounted on Structures.* Proceeding of the Fourth International Workshop on Structural Health Monitoring, Stanford University, September, 2003.

Kumar,A., Beard, S., Qing, P., Chan, H., Ooi, T., Marotta, S. and Chang, F. *A Self-Diagnostic Structural Health Monitoring System for Composite Structure*s, SEM X International Congress, California, June, 2004.

Martin, Peacock. *Acoustic Emission for Detection of Process-Related Damage in Pressure Vessels and Piping*. SPIE, November, 1996.

McGrail, T. and Smith, C. *Acoustic and Ultrasonic Techniques for Condition Monitoring*. Colloquium on Monitoring Technologies for Plant Insulation. Institution of Electrical Engineers, London, November,1994.

Measurement Specialties Inc (MSI). *Piezo Film Sensors Technical Manual*, Document 1005663-1. April 1999.

Nesvijski, Edouard and Sarkis, Paulo. *Acoustic Emission and Failure Prediction of Composites*. NDT.net, March 2000, Vol. 5. No. 3.

Osamu, Haga. *Acoustic Emission Analysis of AL/CFRP Multi-Layerd Hybrid Composite Materials*. Journal of Materials Science, 1990.

Perez, I.,Cui, H. and Udd, E. *Acoustic Emission Detection Using Fiber Bragg Gratings*. SPIE, 2001, Vol. 4328, pp. 209.

Proakis, J. and Manolakis, D. *Introduction to Digital Signal Processing*. Macmillan Publishing. New York 1988.

Rose, J. *A Baseline and Vision of Ultrasonic Guided Wave Inspection Potential.* Journal of Pressure Vessel Technology, August, 2002,Vol. 124, pp. 273-280.

Sulatisky, M. *Intelligent Control Systems for Fuel Cell and Natural Gas Vehicles.* Saskatchewan Research Council, Publication 11305-1E02, September, 2002.

Teply, J. and Herbein, W. *Failure Modes for Filament Wound Aluminum Natural Gas Cylinders*. (Alcoa Labs, Alcoa Center, Pennsylvania). Paper presented at ASM International Conference on Fatigue, Corrosion Cracking, Fracture Mechanics and Failure Analysis, Utah, December 1985.

Tsimogiannis, A., Nikolaidis, V., Anastassopoulos, A.and Filho, P. *Hydrogen Cylinder Acoustic Emission Testing and Data Evaluation with Supervised Pattern Recognition*. NDT.net, September 2002, Vol. 7, No. 9.

Udd, E., Shulz,W., Seim, J., Haugse, E., Trego, A., Johnson, P., Bennett, T., Nelson, D. and Makino, A. *Progress on Multidimensional Strain Field Measurements using Fiber Optic Grating Sensors.* Presented at the SPIE Smart Structure Symposia Conference, Newport Beach, March 2000.

Van de Loo, P. *How reliable is Acoustic Emission (AE) Tank Testing? The Quantified Results of an AE Usergroup Correlation Study*. NDT.net February, 1999, Vol. 4, No. 2.

Walters, J. *Hoop-Wrapped, Composite, Internally Pressurized Cylinders: Development and Application of a Design Theory*. ASME Press, New York, 2003.

Webster, C. *Assessment of the Use of Acoustic Emission as an Inspection Method for FRP Wrapped Cylinders.* Internal Document 11633-34. Powertech Labs Inc. September, 1999.

White, N. *A Safety Analysis of High-Pressure Fuel Storage Systems That Use Active Controls*. Final Report. Charonic Canada Inc. March, 2002.

Zhang, D., Venkatesan, G., Kaveh, M. and Tewfik, M., *Fault Monitoring using Acoustic Emissions,* Proceedings of SPIE Conference on Sensory Phenomena and Measurement Instrumentation for Smart Structures and Materials, 1999,Vol. 3670, pp.392-402.

APPENDIX A. NGV2-2000, SECTION 18

This appendix summarizes relevant sections from the ASI/CSA NGV2-2000 code (Natural Gas Vehicle Code, United States of America), required pressure vessel certification procedure for Type 3 and 4 composite cylinders.

A.1 Ambient Cycling Test.

The ambient cycling test consists of hydraulically pressure cycling the cylinder between 10% and 125% of service pressure for 45,000 cycles. In this testing the cylinders must not burst and the composite overwrap must not break or separate.

A.2 Environmental Testing

Environmental testing is completed in several steps. In summary, these steps are:

1) Pendulum Impact Pre-conditioning: a 30 Nm (22 ft-lb) impact of a steel pyramid shaped pendulum while the tank is unpressurized.
2) On the sites of Preconditioning, each of the following five chemical substances are soaked on a wool pad for the duration of the testing:
   - Sulfuric acid - 19% solution by volume in water
   - Sodium hydroxide - 25% solution by weight in water
   - Methanol/gasoline - 5/95% concentration of M5 fuel meeting the requirements of ASTM D4814, Automotive Spark-Ignition Fuel
   - Ammonium nitrate - 28%o by weight in water
   - Windshield washer fluid (50% by volume solution of methyl alcohol and water).
3) Hydraulically pressure cycled from 10% to 125% of service pressure for 3,000 cycles
4) Hydraulic pressure hold for 48 hours at 125% of service pressure

A.3 Extreme Temperature Cycling.

The extreme temperature cycling calls for the following tests:

(a) Hydraulically pressure cycle between 10% and 125% of service pressure for 4,000 cycles at 82±5°C (180±10°F). for 4,000 pressure cycles.

(b) Hydraulically pressure cycle between 10% and 125% of service pressure for 4,000 cycles at -40±5°C (-40±10°F) for 4,000 pressure cycles.

A.4 Hydrostatic Burst Test.

When hydrostatically burst, the containers must exceed 2.25 times the service pressure before bursting.

A.5 Composite Flaw Tolerance Test.

The composite flaw tolerance test is conducted with the application of two flaws in the longitudinal direction in the composite sidewall. One flaw is made 25 mm (1 in) long and 1.25 mm (0.05 in) in deep, while, the other flaw is made 200 mm (8 in) long and 0.75 mm (0.03 in) deep. The cylinder is then hydraulically pressure cycled from 10% to 125% of the service pressure for 11,250 cycles, without the cylinder bursting, and without the cylinder leaking for 3,000 cycles.

A.6 Drop Test

The drop or impact test is conducted simulating handling impacts on installation of the cylinder while the cylinder is empty. The drop tests are made to the following specifications:

- Horizontally from 1.8 m (72 in)
- Vertically on each end from 1.8 m (72 in)

– At a 45º angle such that the center of gravity is at 1.8m (72 in)

Following the four impacts, the cylinder is then hydraulically pressure cycled from 10% to 125% of the service pressure for 11,250 cycles, without the cylinder bursting, and without the cylinder leaking for 3,000 cycles.

A.7 Bonfire Test.

The bonfire tests are used to evaluate if the finished cylinders will prevent rupture under a fire condition. The cylinders are tested with pressurized natural gas at 25% of the service pressure. The flames must impinge across the cylinder diameter and must average at least 430°C (800°F). For the duration of the tests, the gas must vent through the pressure relief device without the tank bursting.

A.8 Accelerated Stress Rupture Test.

For accelerated stress rupture testing, the cylinder is hydrostatically pressurized to 1.25 times service pressure at a temperature of 65°C (149°F) and held at the pressure and temperature for 1,000 hours. On subsequent burst testing, the cylinder must exceed 169% of the service pressure.

A.9 Penetration Test.

For the penetration testing, the cylinder is penetrated by an armor piercing bullet fired at a 45º angle from the sidewall. With compressed gas at the service pressure, the cylinder can leak but cannot rupture.

A.10 Leak Before Break.

For leak-before-break testing, the cylinders are pressure cycled from 10% of service pressure to 150% of service pressure. The cylinders must either leak or exceed 45,000 pressure cycles.

APPENDIX B. MANUFACTURING SPECIFICATIONS

This Appendix contains the manufacturing specifications for the second batch of tanks, used in the validation testing. The manufacturing data is presented for each of the tanks.

Dynetek Industries Ltd.

Dynecell Summary of Manufacture

Cylinder Model: L033NG200G8 Batch #: 235B

No.	Test Date (DD/MM/YY)	Serial Number	Volume (Water ltrs)	Empty Weight (kg)	Liner Weight (kg)	Laminate Weight (kg)	Perm. Exp After A.F.P. (cc)	Exp at T.P. (cc)	Perm. Exp After T.P. (cc)	Perm Exp After t.P. (%)
1	05/10/01	G4604	32.63	14.95	8.25	6.69	132	338	0	0
2	04/10/01	G4606	32.52	14.85	8.25	6.6	116	337	0	0
3	04/10/01	G4607	32.27	15.25	8.2	7.05	121	335	0	0
4	04/10/01	G4609	32.67	15	8.25	6.75	119	332	0	0
5	04/10/01	G4634	32.68	15	8.15	6.85	128	331	0	0
6	04/10/01	G4635	32.58	15	8.2	6.8	126	332	0	0
7	04/10/01	G4636	32.72	14.85	8.15	6.7	123	336	0	0
8	05/10/01	G4637	32.74	15.2	8.2	7	139	341	0	0
9	04/10/01	G4638	33.04	15.05	8.2	6.85	133	337	0	0
10	04/10/01	G4642	32.63	15.3	8.25	7.05	133	339	0	0
11	04/10/01	G4646	32.82	15	8.25	6.75	121	330	0	0
12	04/10/01	G4676	32.46	15.05	8.25	6.8	N/A	331	0	0
13	05/10/01	G4678	32.53	14.95	8.25	6.69	132	339	0	0
14	04/10/01	G4686	32.82	15.05	8.25	6.8	121	336	0	0
15	04/10/01	G4694	32.65	15.25	8.2	7.05	144	340	0	0
16		G4695	NOT AUTOFRETTAGED - TEST CYLINDER ONLY							
17	04/10/01	G4697	32.67	15.1	8.25	6.85	120	331	0	0
18	05/10/01	G4721	32.63	14.85	8.3	6.55	125	336	0	0
19										
20										

Approved By: Wanda C Date: Oct 17/01

APPENDIX C. SENSOR ASSEMBLY AND MANUFACTURING

In this appendix, details on the manufacture of the cylinders are given, and particularly, the manufacture of the sensors into the cylinder is detailed. This involves inserting the sensors into the composite structure as the tanks are being wound. On September 30, 2001, the tanks were manufactured at Dynetek Industries Ltd., in Calgary, AB. The liners were composed of stock L033 series liners. The wrap pattern was a type G5N8N, designed to 200 bar (2900 psi).

The sensors used were piezo-film sensors manufactured by Measurement Specialties Inc. The model was a FDT-052K W/MALE sensor with a 150 mm (6.0 in.) lead (part number: 2-1002785-1), and a male terminator on the end. This sensor has electrode dimensions of 12 mm (0.49 in) by 30 mm (1.2 in) and 85 μm thickness. The capacitance of the sensor is 0.74 nF. However, it is important to be aware that the carbon fibers in carbon fiber reinforced polymer structures are conductive. The epoxy matrix is an insulator, but because the tanks are wound with tension in the fibers, this tends to pull the carbon fibers onto the sensor surfaces. Accordingly, the sensors are then insulated to remove this problem. The sensors were coated with a pre-primer coat of a two-part epoxy. A Teflon-coated coaxial wire was then connected onto the male terminator, and then coated with a perchloroethelyne compound known as Marine Goop. This was done to protect the connections, while also providing adequate electrical isolation of the connectors.

The manufacturing process of the sensors was completed at Dynetek Industries during the winding of the cylinders. The liners, shown in Figure C1, were preformed, and had the end-bosses machined before the winding was completed. These liners are composed of seamless Aluminum 6061-T6 heat-treated to optimize the fatigue life of the cylinder.

Figure C.2 shows the computer controlled winding machine used in the winding process. The machine requires a pre-programmed winding scheme based on a particular cylinder

design. Further to this, this winding machine has been specifically designed and manufactured to this application.

Figure C.1: Aluminum Liner Before Winding

Figure C.2: Computerized Winding Machine

Figures C.3 and C.4 illustrate the winding process, where combinations of hoop (Figure C.3) and helical wraps (Figure C.4) are used to wrap the cylinder. This combination is designed and is required to undergo testing to meet or exceed the relevant standards, such as the NGV2-2000 standard summarized in Appendix A.

The sensors were placed just under the final hoop wrap on the shoulder of the tank as illustrated in Figure C.4. The final wrap, of approximately 6 mm (0.236 in) thickness, was wrapped over the sensors, providing protection and embedding the sensors into the structure.

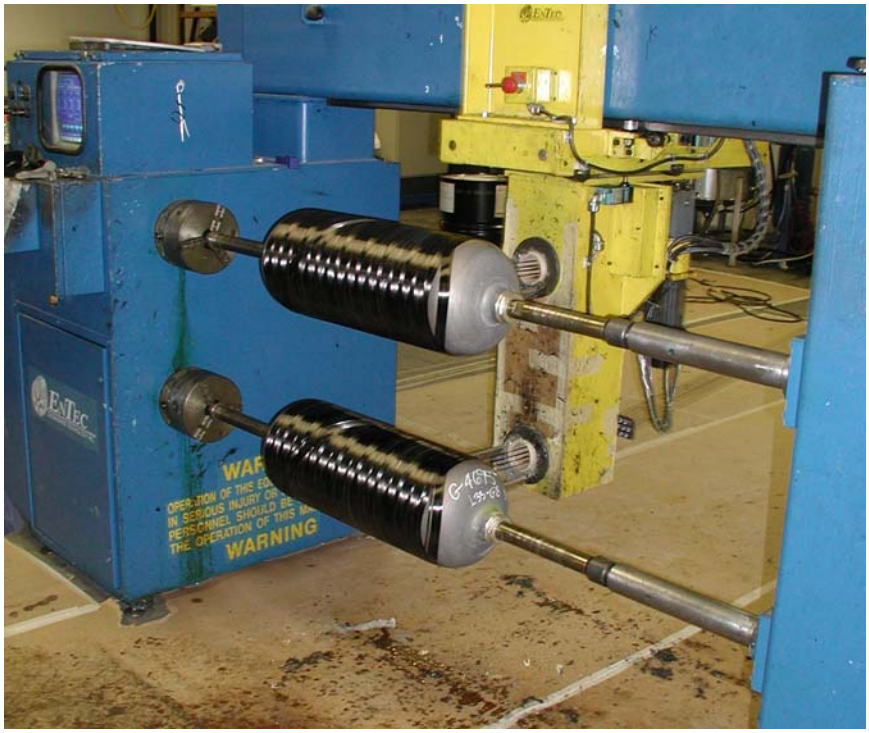

Figure C.3: Initial Hoop Wrapping

Figure C.4: Helical Wrapping and Sensor Placement

Figure C.5 shows the assembly used for curing the resin on the cylinders after winding has been completed. The cylinders are placed on a rack that has a mechanism for rotating the cylinders while being placed in an oven at elevated temperatures. The purpose of rotating the cylinders is to prevent drips and large pockets of resin from forming on the surface, which will tend to crack once the cylinder is put into service. Any drips or surface epoxy will crack due to the large deflections that the cylinders undergo when pressurized (between 1 and 3% strain longitudinally, and up to 5% strain in the hoop direction).

Figure C.5: Curing Assembly

APPENDIX D. METHOD OF ANALYSIS
EVALUATION OF ACOUSTICAL SIGNATURES

D.1 New Tank Signal Analysis

The signatures of a new tank and signatures of a tank that has entered into a failure mode and their analysis are examined in this appendix. The objective of this discussion is to detail the scanning and analysis methods used in this thesis. It is important to note that the objectives of this work were to identify failures in the composite structure before they become critical – the mode and identification of which failure mode has not been examined in any detail.

First, looking at the input and output signals, the measured transmitted (input) signal is shown in Figure D.1.

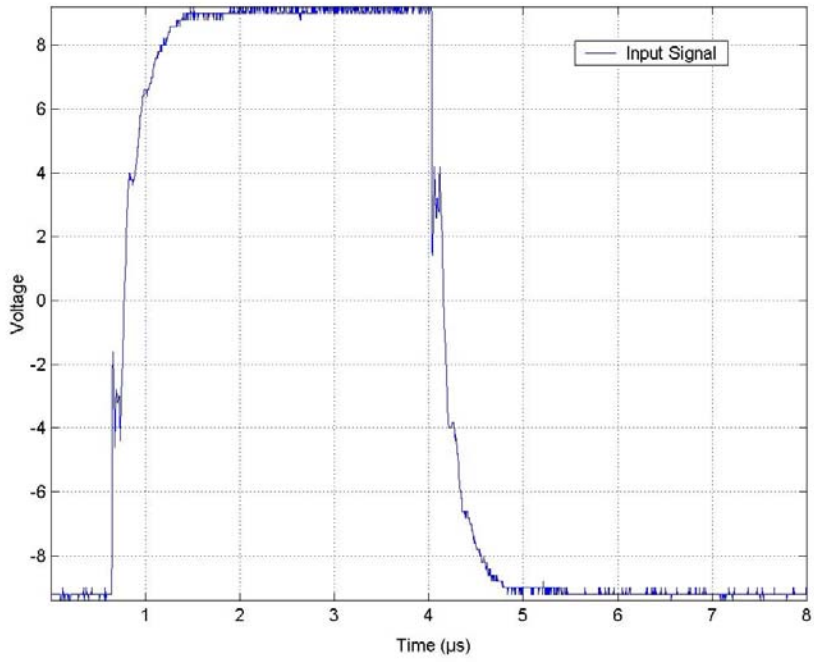

Figure D.1: Input Signal

And the output signals as received are shown in Figure D.2.

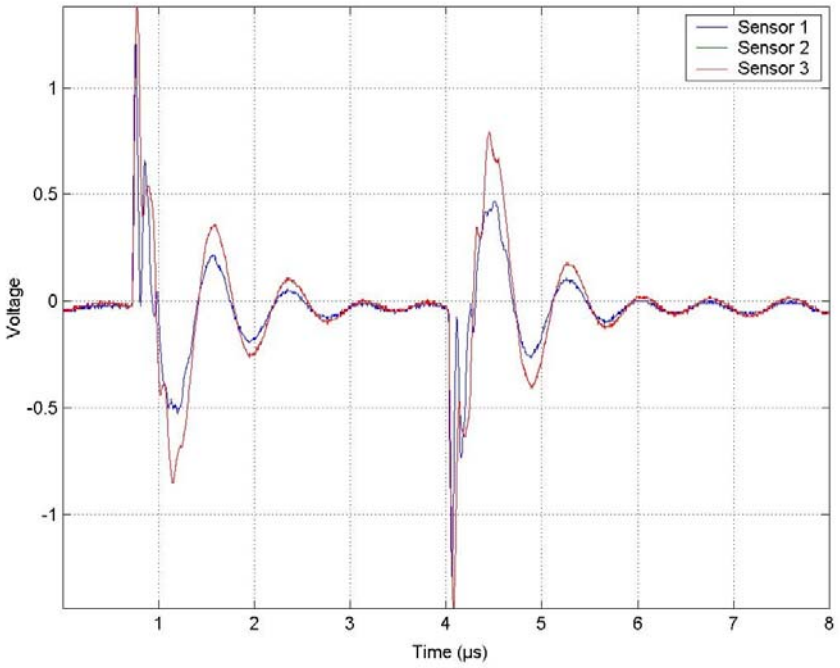

Figure D.2: Received Raw Signal

Note the similarities between the three signals received. As well, there are other subtle differences. But most importantly, one can see higher frequencies superimposed on top of lower frequency signals.

The first area of examination is in the input signal, as shown in Figure D.1. Note that the sensor used for the input signal is also a receiving sensor. Each or any sensor can be used to send or receive simultaneously. This feature can be used later for advanced error checking, but for now the system is just using one input signal and 3 received signals (one sensor is located in each quadrant of the pressure vessel as illustrated in Chapter 3). The input sensor also shows a received reflected signal in both the rise and fall of the impulse, which is predominantly a received compression wave reflecting through the thickness of the sensor. These features can be seen at 0.8 µs and 4.1 µs on Figure D.1.

In Figure D.2, the high frequency can also be seen in the received signals; again, at 0.8 μs and approximately 4.1 μs in Figure D.2. This corresponds to the high frequencies found in the input signal. The high-frequency content generally is indicative of the compression wave as it travels through the tank. Furthermore, the variation in sensor locations from the input signal can be seen in the received signals. If the signals are closely examined, one sensor actually receives the wave just slightly before the other sensors.

The second component of the signal can be found as a lower frequency content (of around 1 MHz) as shown in Figure D.2. Notice that this frequency is found in all of the receiving sensors, and are in phase with each other. There exists also a directionality which corresponds to the rising and falling signal waveforms in the input signal.

The derivation of the analysis is presented in this appendix. In order to show the method of the analysis, it is important to demonstrate what each signal looks like and the relevant information that can be extracted from each signal. The first component that is examined is the fast-fourier transform (FFT) of each signal [Proakis and Manolakis, 1988]. This is indicative of frequency content of the signals, and is shown as Power on the vertical axis and frequency on the horizontal axis. This is shown in the following four graphs, Figures D.3, D.4, D.5 and D.6.

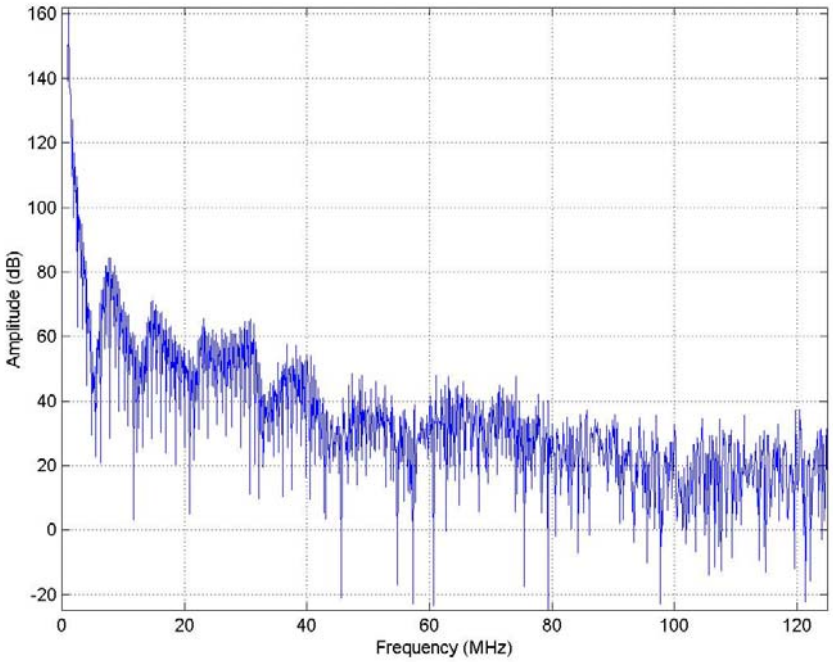

Figure D.3: Frequency Content of Transmitting Sensor

As can be expected from an impulse type of input signal, there exists relatively high frequency content, from near zero, upwards to 100 MHz. As can be seen near 1 MHz, 8 MHz, 16 MHz, and upwards, there is indication of the resonances of the sensor and circuitry in which the sensor is connected. These resonances can be used to verify operation of the transmitting sensor for fault detection. In the analysis of the tank structural health monitoring, these frequencies will be utilized to aid in the identification of faults. In particular, investigation into coherence, empirical transfer function estimates and other features will be made utilizing these resonant frequencies.

As can be seen in Figures D.4, D.5 and D.6, the frequency content of these signals seem to be relatively uniform. Certainly the resonant frequencies of the receiving sensors can be seen at frequencies of near 1 MHz, 8 MHz, 22 MHz and at other frequencies above these. These resonances are very uniform between the sensors. As the frequency increases, the resonances and information contained in the signal decrease. As such, it

becomes apparent that the relationship between the input and output signals must be examined.

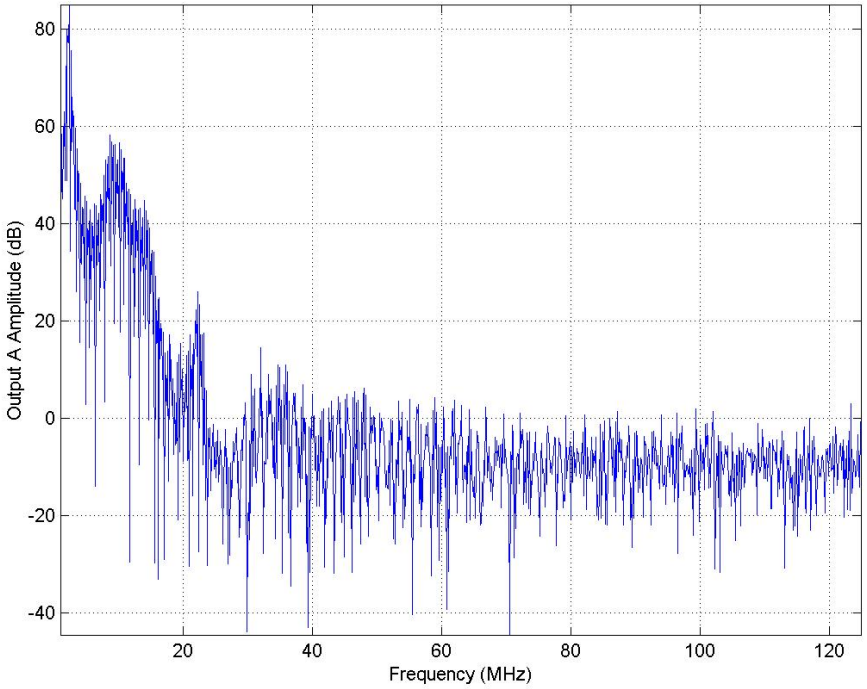

Figure D.4: Frequency Content of Receiving Sensor A

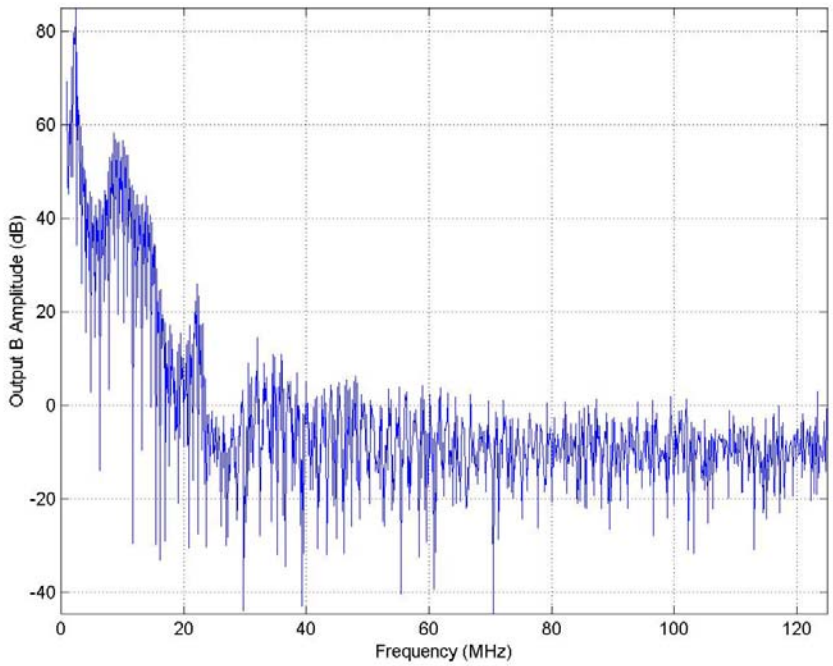

Figure D.5: Frequency Content of Receiving Sensor B

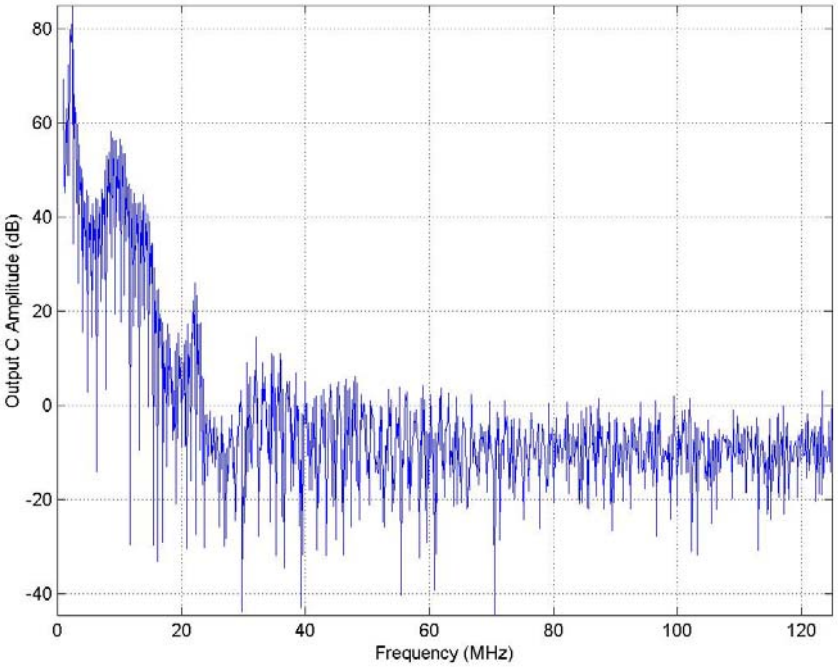

Figure D.6: Frequency Content of Receiving Sensor C

In order to examine the relationship between the input and output signals, as measured, different techniques will be utilized. For example, the relationship between the input and output should be examined at areas of resonance, such as near 8 MHz. The next three graphs illustrate the transfer function potential (as an Empirical Transfer Function Estimate (ETFE) calculated as a smoothed, normalized ratio between the frequency spectra of the output signal to the input signal). The ETFE is computed as the ratio of the output to the input Fourier Transforms and is expressed in terms of frequencies. Note that in the following graphs, the frequency range of 2 to 200 MHz are being examined. Looking between 1 MHz and 30 MHz, the three ETFE plots shown in Figure D.7 for signal A, Figure D.8 for signal B, and Figure D.9 for signal C, show very strong similarities. In particular, the same shape of the ETFE can be seen in all three ETFEs. Above 30 MHz, repeatability and reliability of the signals is shown to be poor.

The data shows that below 30 MHz, a uniform frequency plot is generated from the ETFE. However, to more fully examine the signal, it is of use to examine a time–frequency plot of a Morlet Wavelet [Graps, 1995].

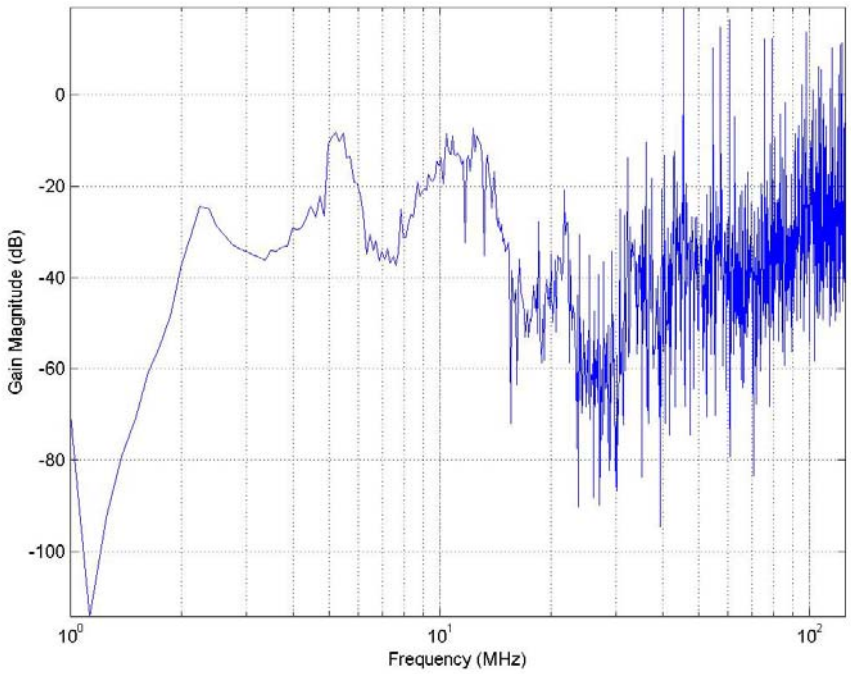

Figure D.7: ETFE of Received Signal A

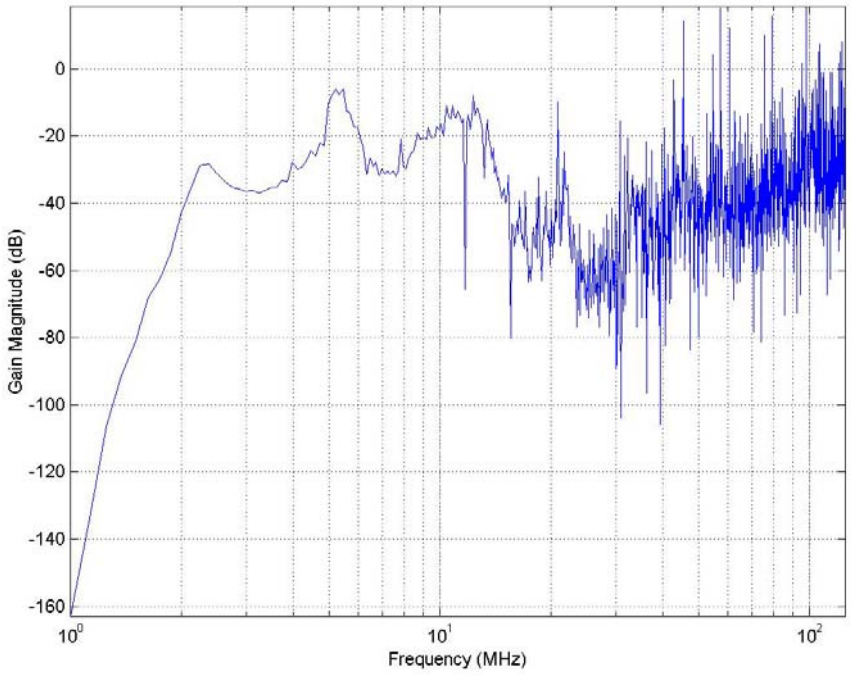

Figure D.8: ETFE of Received Signal B

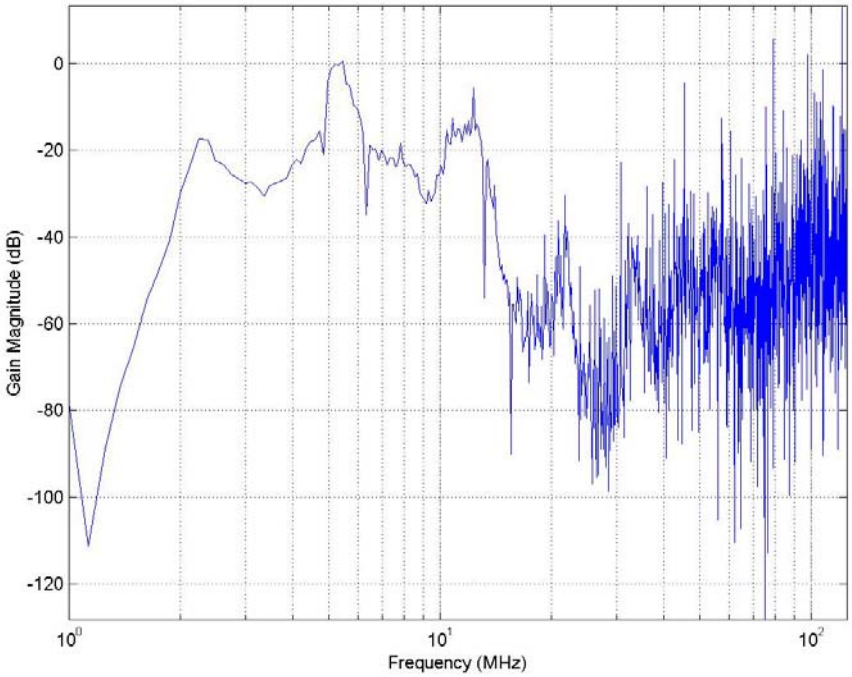

Figure D.9: ETFE of Received Signal C

The time-frequency spectrum of the signals are generated in the following plots, first the input signal, followed by the three output signals. A 128-point fast-fourier-transform is used to window the wavelet and analyzed at 2000 points corresponding to each time step.

In the wavelet plot shown in Figure D.10, the frequency content is shown on the vertical axis and the time scale is shown in the horizontal axis. The indication of the time-based frequency content is given as an indication of colour; where the intensity of the signal is indicated in the following order: blue, green, yellow, orange and red, where blue has the least intensity, and red has the highest intensity.

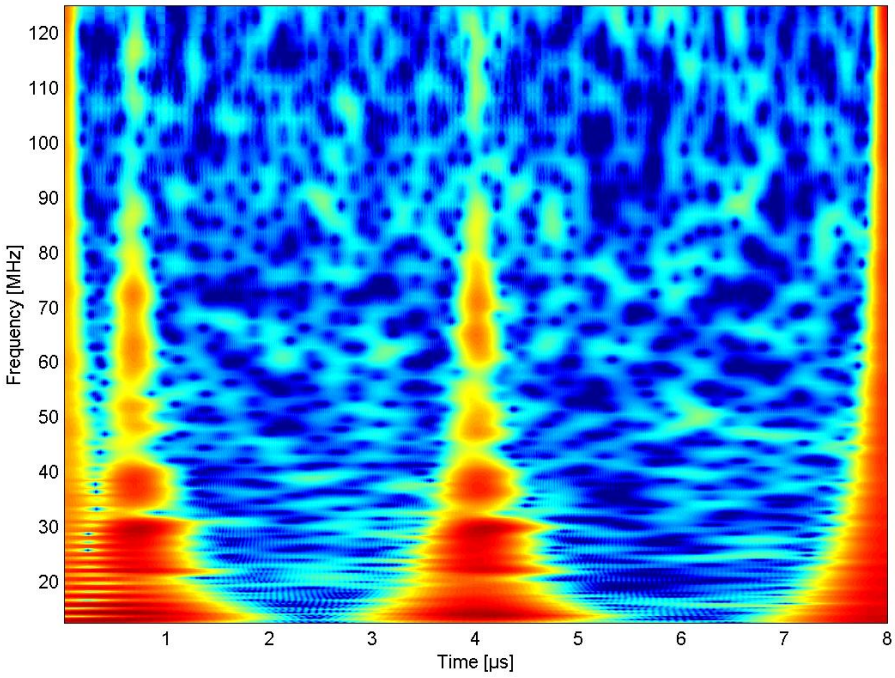

Figure D.10: Input Signal

In Figure D.10 the rising and falling signals are very clearly shown, such as in Figure D.1. These features are shown as the vertical bands of increased frequency at 0.8 µs and 4 µs. The frequency content at 0 µs and 8 µs are shown as artifacts resulting from the starting and stopping of the analog-to-digital converter used to sample the waveforms. Note that the resonant frequencies appear to be similar on the rising and falling sections of the signal. As well, the resonant frequencies are shown as wider

portions of the signal, as shown in Figure D.10 at below 40 MHz, where the resonance appears like an island in the plot.

Although the high frequency is present in the input signal, Figures D.11, D.12 and D.13 show the time-frequency plots for channels A, B, and C, respectively. Likening these to the other analyses, the time-frequency plots are very comparable in shape and illustrate that the frequency content of the rising and falling signals of the input have very similar frequency content. Only partial signals of high frequency are transferred to the received signal. This suggests a correlation can be made through the use of coherence.

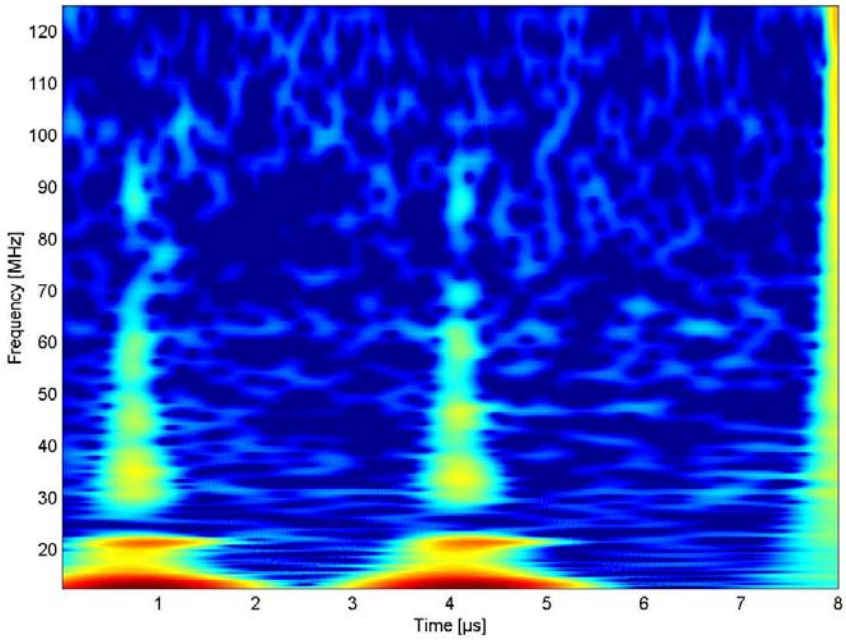

Figure D.11: Output A – Time-Frequency Plot

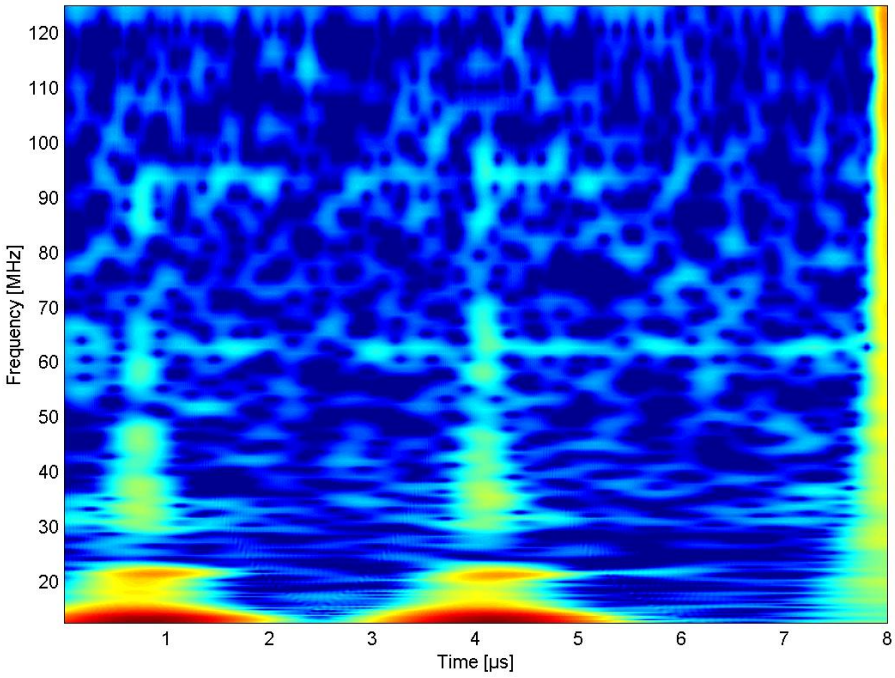

Figure D.12: Output B – Time-Frequency Plot

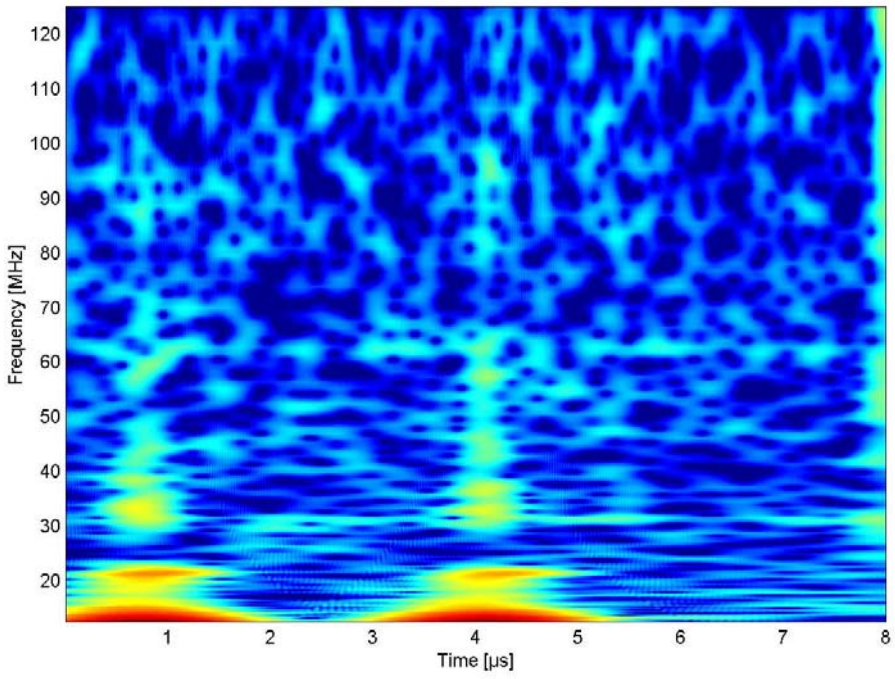

Figure D.13: Output C – Time-Frequency Plot

The coherence between two signals, x and y, can be given as a function of frequency and calculated by the following function:

$$C_{xy}(f) = \frac{|P_{xy}(f)|^2}{P_{xx}(f)P_{yy}(f)}, \qquad \text{(D.1)}$$

where,

x and y are the two corresponding signals to input and output, and

P designates the periodogram calculated as the Power Spectral Density.

This coherence can be defined as a relationship between the input and output signals, and as the coherence approaches unity for a particular frequency, then good energy transmission at the frequency in question is observed.

The coherence of the signals is shown in Figure D.14. This coherence once again is very similar in between the receiving sensors. Below 20 MHz, the coherence is very strong (as it is near unity). As the frequency increases, the transmission strength (coherence) decreases proportionately.

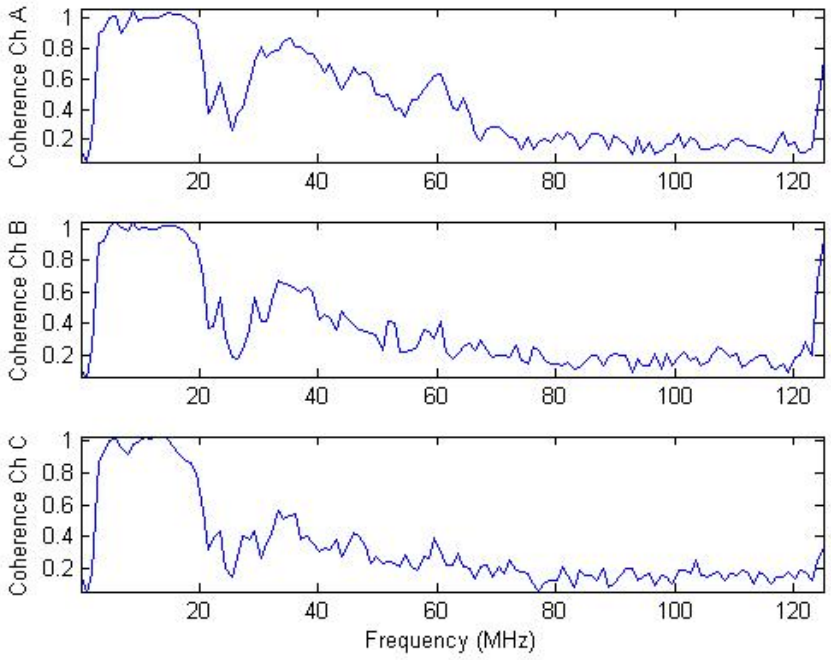

Figure D.14: Coherence of Output Signals

This analysis is used to examine the signals that are sent and received on a damaged tank, as given in the next section.

D.2 Damaged Tank Signal Analysis

A similar analysis as shown in Section D.1 is given for a damaged cylinder. This includes time domain, frequency domain, time-frequency domain and coherence correlations. The changes in signals that are relevant in order to observe noticeable changes are used to develop a proper mechanism for analyzing the structural integrity of a cylinder.

Similar to Figure D.1, the input signal is shown in Figure D.15. The rising component of the impulse is found at 0.8 μs, with the falling component at approximately 4 μs.

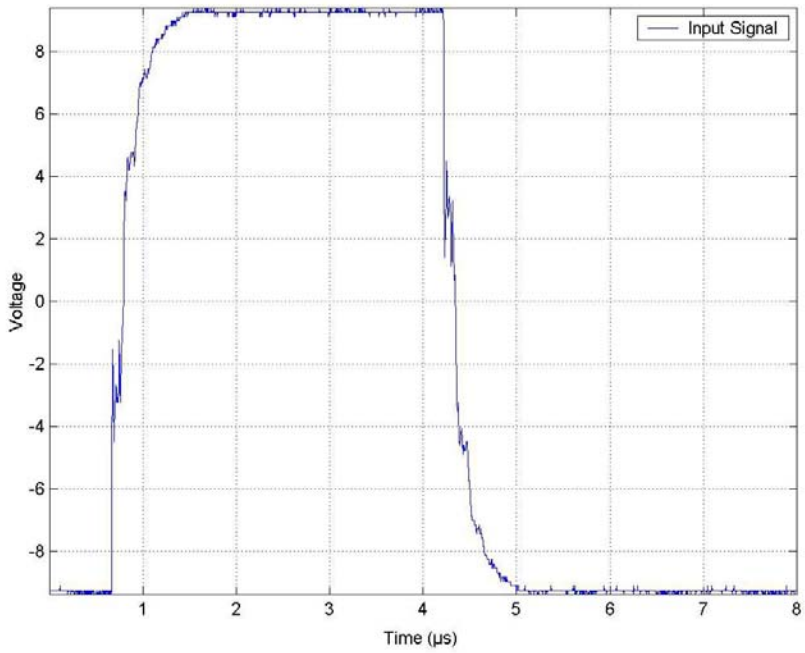

Figure D.15: Input Signal

The received signals are found in Figure D.16. As is seen in Figure D.2, the differences between the new and damaged signals can be observed. Both high frequency components have changed, while the amplitudes of the lower frequency components have dropped. These changes can be further quantified in the frequency domain.

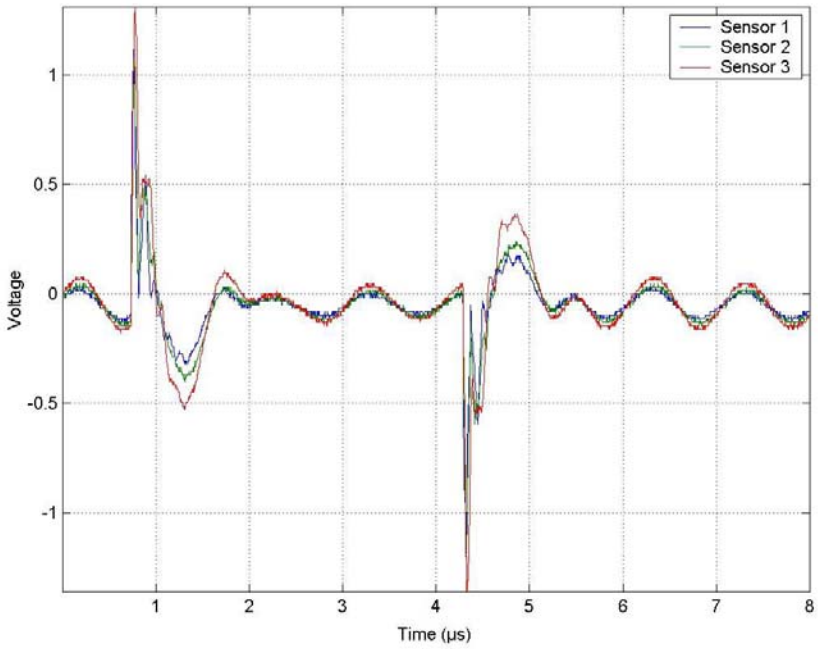

Figure D.16: Output Signal

Figure D.17 gives the input frequency content of the transmission sensor. This frequency content has not changed significantly from the new tank, as shown in Figure D.3.

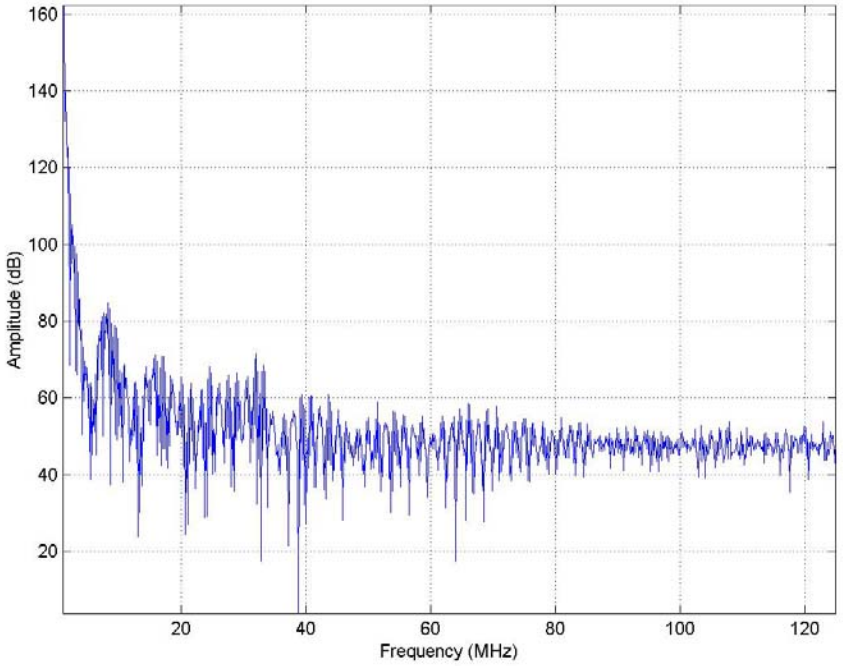

Figure D.17: Frequency Content from Input Sensor

The frequency-domain plots are given in Figures D.18, D.19 and D.20 for the receiving sensors A, B, and C, respectively. As compared to Figures D.4, D.5, and D.6 for the new tank receiving sensors A through C, the frequency content has shifted slightly, especially noted at around 22 MHz. At higher frequencies, the frequency content has not deviated significantly between the new and damaged tanks.

In order to further quantify and identify these changes, the ETFE will be examined between the input signal and each of the receiving sensors.

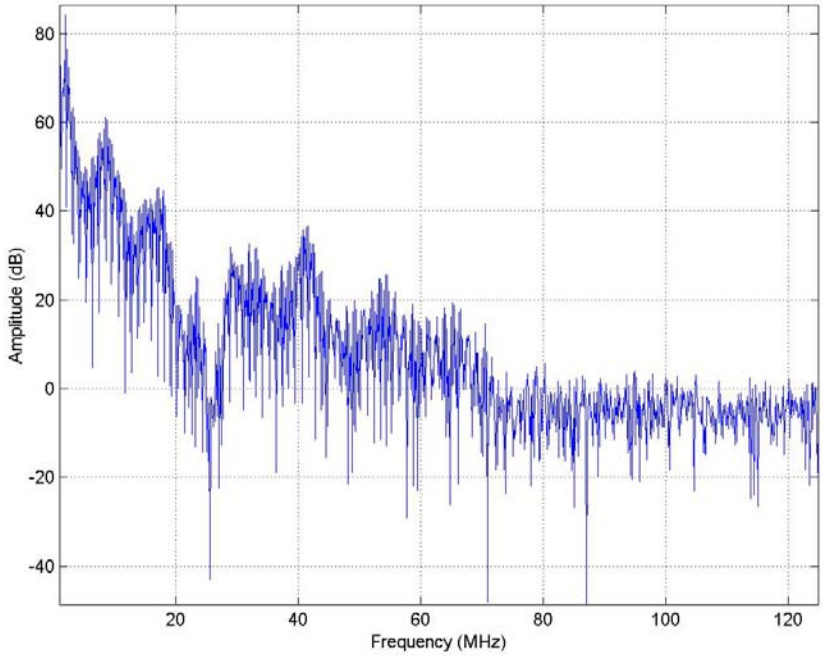

Figure D.18: Frequency Content from Receiving Sensor A

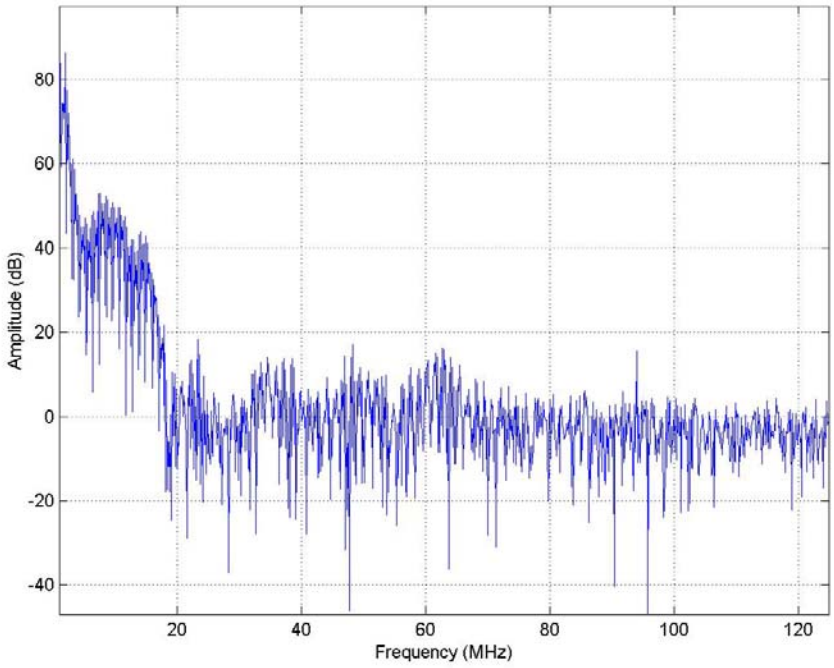

Figure D.19: Frequency Content from Receiving Sensor B

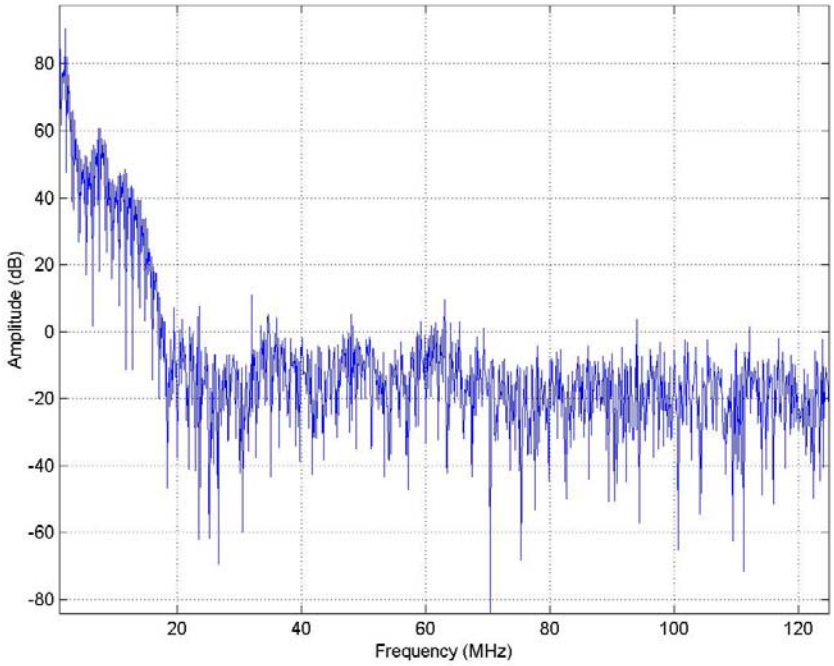

Figure D.20: Frequency Content from Receiving Sensor C

The empirical transfer function estimate has changed significantly from the new tank analysis, given in Figures D.7 through D.9, to the damaged tank ETFE shown in Figures D.21, D.22, and D.23 for the receiving sensors A, B, and C, respectively. One can see that overall transmission from the transmitting sensors to the receiving sensors has improved with larger amplitude gains in the damaged tank at certain frequencies (for example at under 10 MHz). The higher frequencies above 40 MHz do not show relevant information or changes between the new and the damaged cylinder.

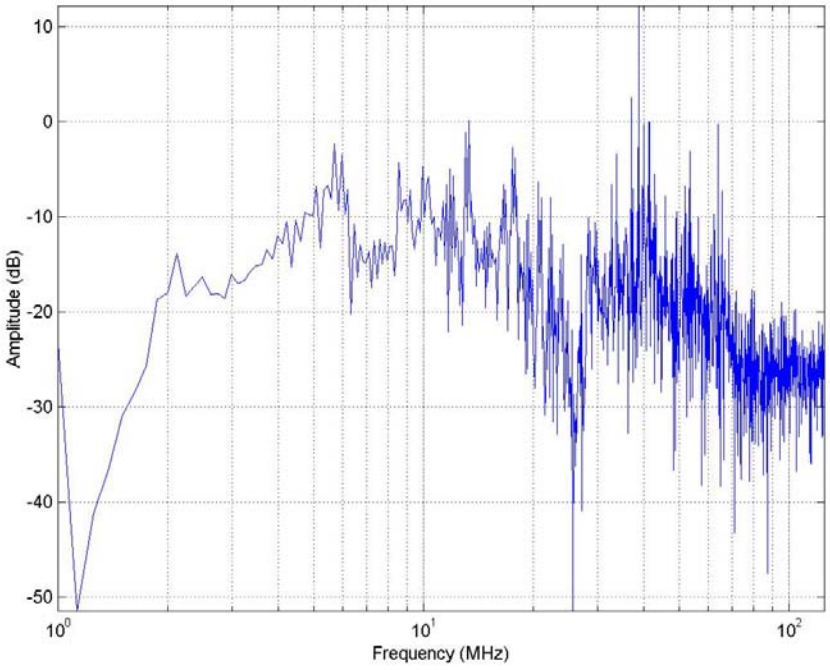

Figure D.21: ETFE from Receiving Sensor A

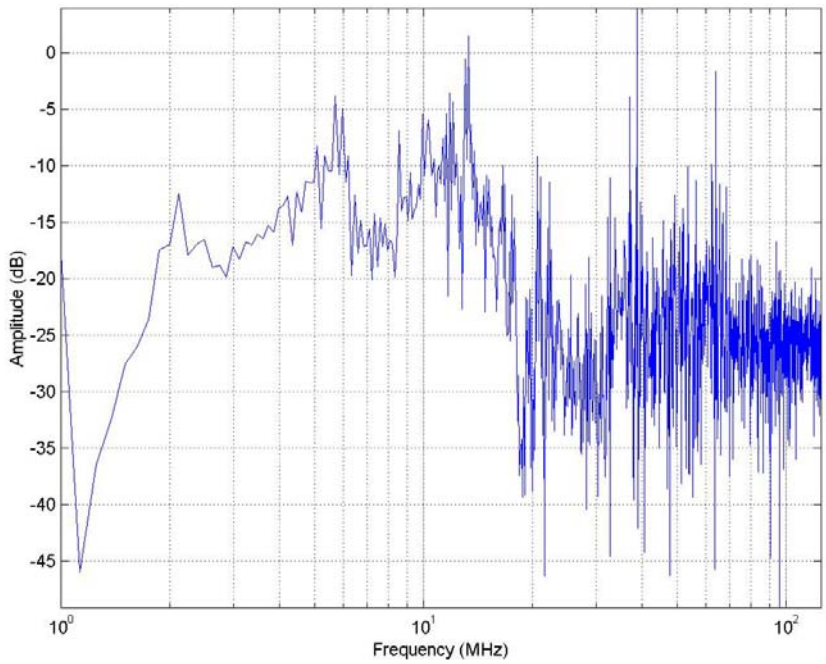

Figure D.22: ETFE from Receiving Sensor B

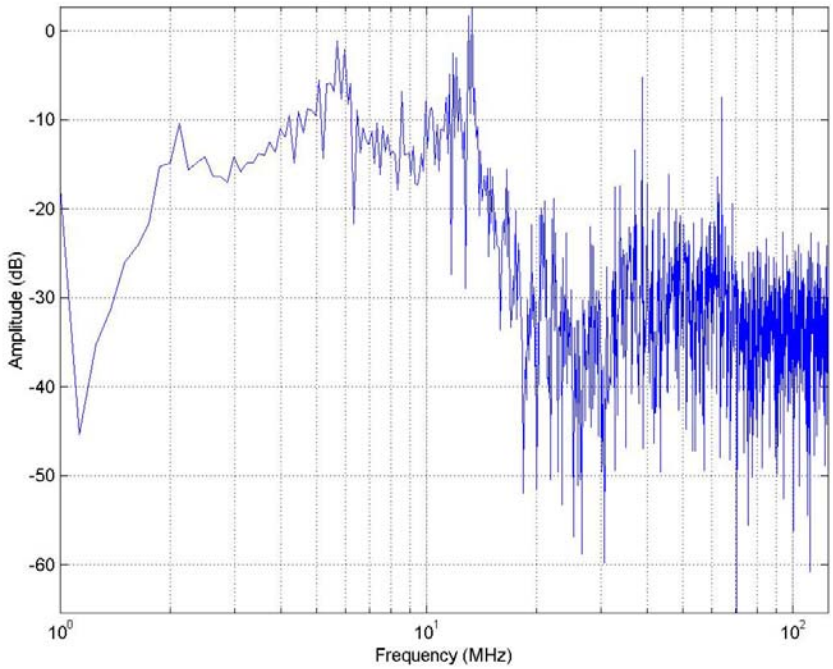

Figure D.23: ETFE of Receiving Sensor C

It is also important to identify if there are significant differences between the rising and falling signals as well as any other variations in the signals. This can be done by utilizing Morlet Wavelet analysis in a time-frequency breakdown of the signals [Graps, 1995].

The time-frequency breakdown of the damaged signals is given in Figures D.24 for the input and Figures D.25, D.26 and D.27 for the received signals for channels A, B, and C, respectively. Comparisons of these waveforms to the new damaged tank signals in Figures D.10 through D.13 generally indicate stronger coherence and transmission through the tank of these frequencies measured. In summary, the output characteristic frequencies of a damaged tank mimic the input frequencies closer than a new tank.

As well, the frequency content at 0 μs and 8 μs is indicative of the start and stop of the analog-to-digital converter used in the acquisition of the signals. There are distinct bands of transmission between the input and receiving sensors, shown as distinct islands in the time-frequency plots. This distinction can be further observed by examining the coherence of the signals.

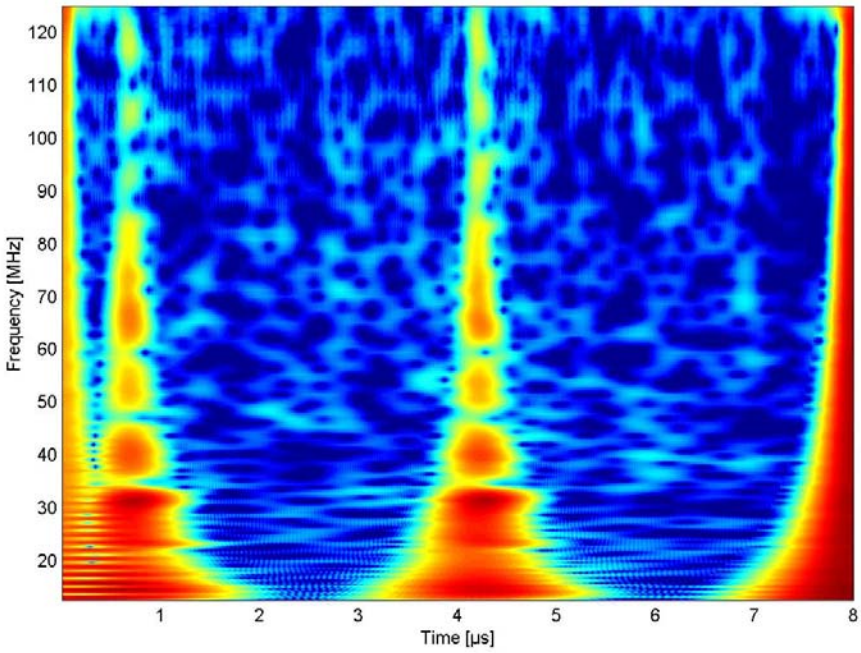

Figure D.24: Time Frequency Breakdown from Input Signal

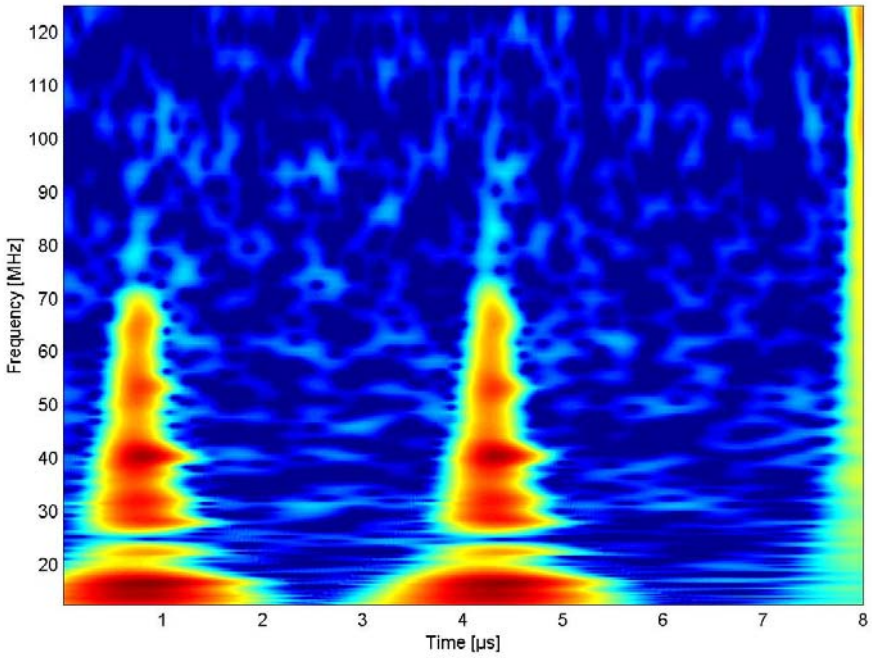

Figure D.25: Time Frequency Breakdown from Damaged Channel A

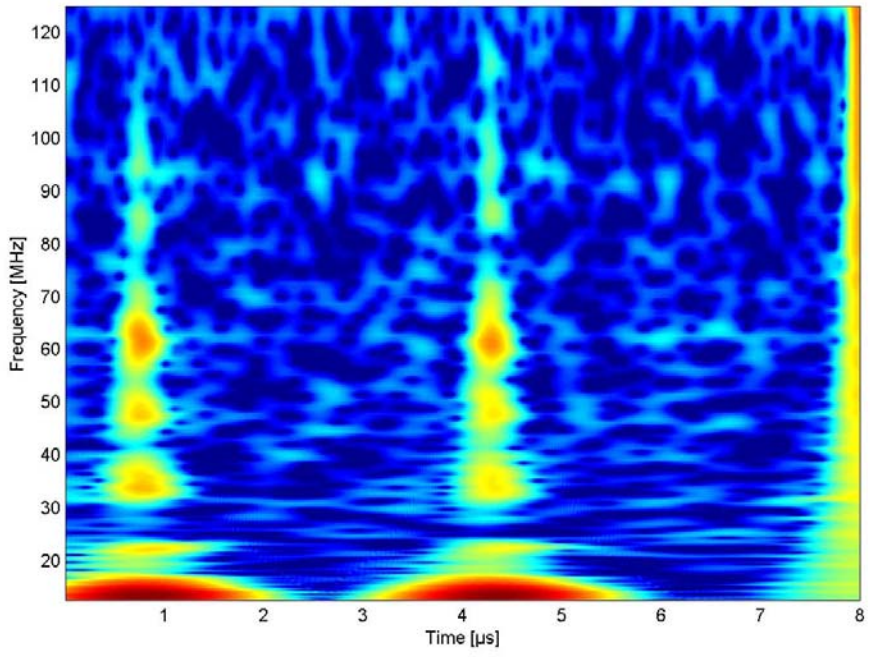

Figure D.26: Time Frequency Breakdown from Damaged Channel B

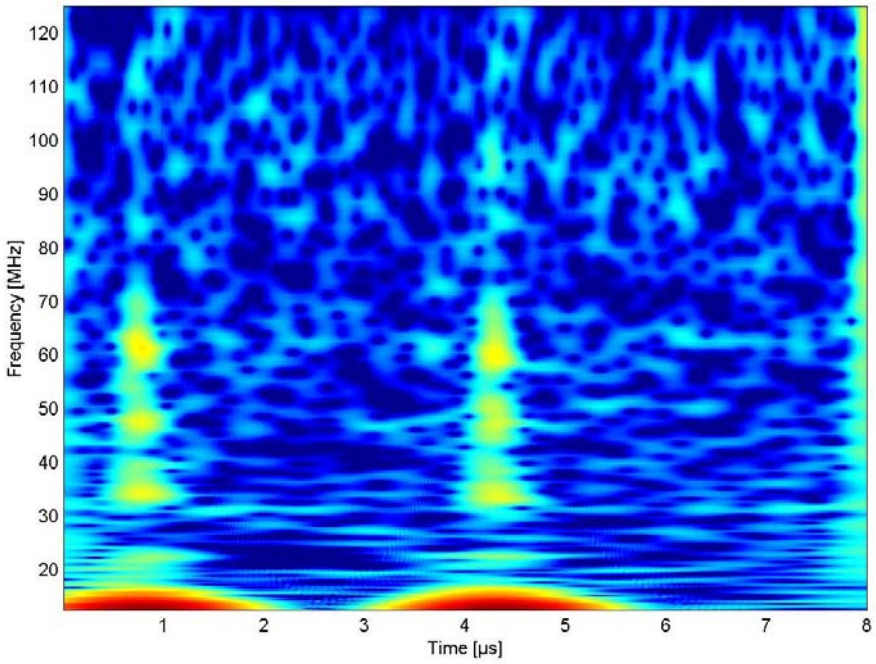

Figure D.27: Time Frequency Breakdown from Damaged Channel C

The coherence for the damaged tank signals is given in Figure D.28. The coherence is shown as significantly higher – up to 70 MHz – when compared to the new tank coherence, given in Figure D.14. The coherence is indicating significantly stronger transmission strength at most frequencies below 70 MHz. Under 20 MHz, the coherence drops at specific frequencies.

A direct comparison of the output signals to the input signals can be made to correlate the tank structure. We can see the same signal change occurring in all three types of plots: ETFE, time-frequency and coherence. At certain key frequencies, particularly between 17 and 85MHz, we can see large changes in the received signals. A direct comparison of these changes becomes the basis for the calculation and signal analysis. In fact, as the tank is damaged, we start to see more and more frequencies shift, with resonance frequencies changing and shifting.

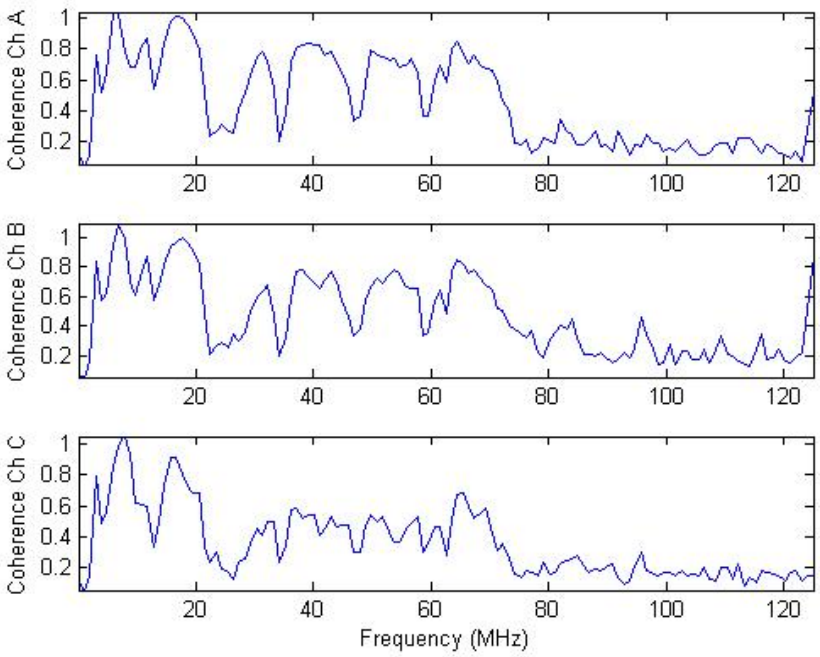

Figure D.28: Coherence from Damaged Tank

Further extension of the work can be done by examining other frequency ranges, by examining damage mechanisms and changes in the signal. However, for this particular application, the analysis of the damage is not a requirement; rather the detection of the presence of damage is as much information that is required.

Although the coherence shows a much larger variation at most frequencies, the analysis will focus predominantly on frequencies below 80 MHz. It is easiest, cheapest and the most useful to keep the frequencies as low as possible to maximize the information used, while keeping electronics simpler, as higher frequency sampling and analysis is often more difficult.

Observations lead to results indicating that there can be substantial changes in the received signal at very low and very high frequencies due to mounting conditions, stored fluid type, and other various environmental and modifying parameters.

This requires a filter design for the system, and has parametrics in the Laplacian domain as shown in Figure D.29.

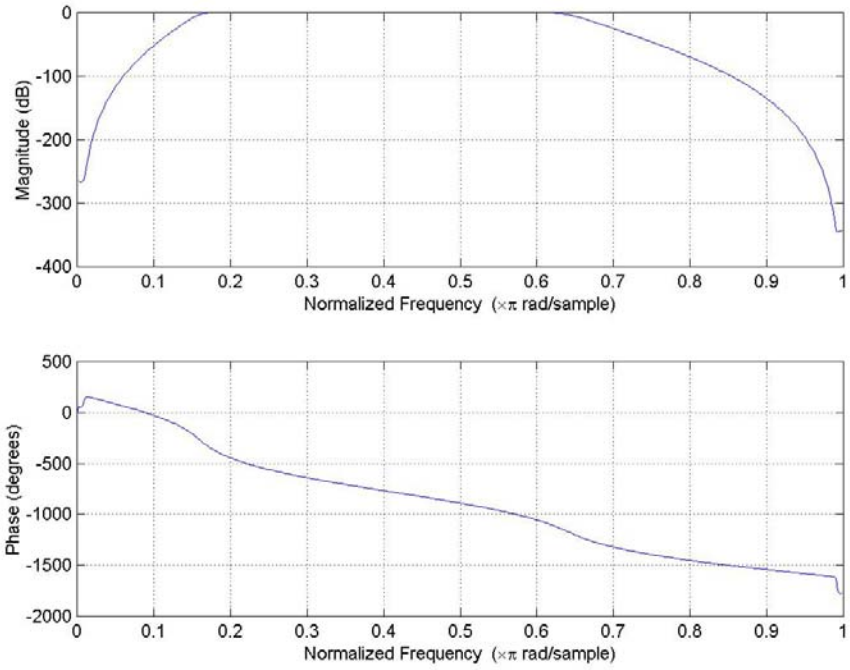

Figure D.29: Filter Characteristics

Phase transition and lag problems are circumvented by filtering twice, the first in the forward direction, and the second in the reverse direction, to cause zero nominal phase shift on the data.

The next step is to evaluate the signals independently through what is known as a Power Spectral Density (PSD) estimate. This was accomplished through the use of a 256 point Hamming Window (on a 2000 point sample, or 1/8 length). The hamming window is calculated by the following equation:

$$w[k+1] = 0.54 - 0.46\cos\left(2\pi\frac{k}{n-1}\right), \qquad k = 0, \ldots, n-1 \tag{D.2}$$

where,

w is the characteristic of the window,

k is the index of the window which is calculated iteratively from the previous window index, and

n is width of the window, in this case 256 points of calculations long.

The characteristics of the 256 point Hamming window are shown in Figure D.30. This windowed filter is applied through convolution of the window and the data in which the filter is applied.

Figure D.30: 256 Point Hamming Window

The result of such a convolution of the filter and the data is that the signal becomes very clean in the frequencies of interest. The PSD method that is used is known as Welch's Method, which is the averaged modified periodogram method of spectral estimation. This can be computed through the following function:

$$S(e^{j\omega}) = \frac{\frac{1}{n}\left|\sum_{l=1}^{n} w_l x_l e^{-j\omega l}\right|^2}{\frac{1}{n}\sum_{l=1}^{n} |w_l|^2}, \quad \text{(D.3)}$$

where,

S, is the spectral estimate as a function of frequency,

w is frequency,

n is the length of the data, and

l is the index used for the summation.

Once the spectral estimate is completed, the key frequencies of interest are observed. This correlates to a frequency bandwidth of 17MHz to 85.3MHz, for the particular tank design used in this analysis. The frequencies above and below are dropped, while looking at the results in between. Finally, the output data is divided by the input data at each frequency. This corresponds to the matrix division of the output frequency vector by the input frequency vector of the frequencies of interest.

This method of analysis is now covered in detail.

D.3 Selected Data Analysis Method

The selected data analysis method consists of the following series of calculations:

1. Measure waveform
2. Filter data
3. Windowed power spectrum density using Welch's Method
4. Frequency cutoff
5. Transfer function estimate
6. Comparison of transfer function estimates through baseline frequency division
7. Root mean squared and scaling to a single number

A close examination of the method used in the above process is now given in detail with examples on three waveforms.

For each step of the analysis, the new tank, the normal tank, and the damaged tank are shown. This is done to illustrate the differences between the new tank and the normal tank, which would be done under normal operating conditions. However, if the tank were damaged, then the differences between the new tank and the damaged tank signals would be used for calculations. The point of this method and analysis is to show how the tank health monitoring system is able to distinguish between a normal, non-damaged tank and a damaged, faulted tank.

For this example, the damage inflicted on the tank was cut and gouge damage, and is representative of typical new, normal and damaged tank signals. The measured waveforms are given to indicate these typical signals in the following section.

D.3.1 Measure Waveform

The new tank transmitting and receiving signals are given in Figures D.31 and D.32 respectively. These signals will be used as the baseline to compare the normal tank signals and the damaged tank signals to monitor the health of the cylinder.

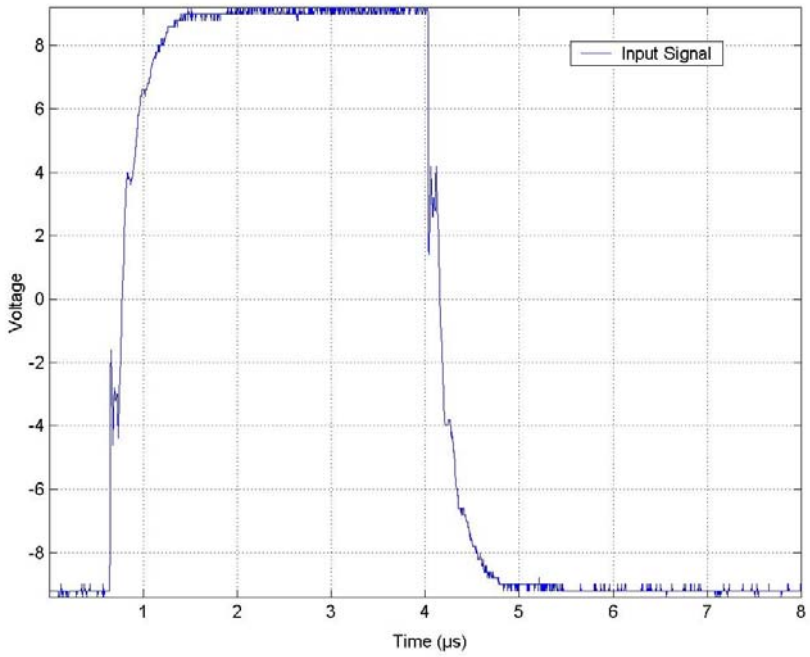

Figure D.31: New Tank Input

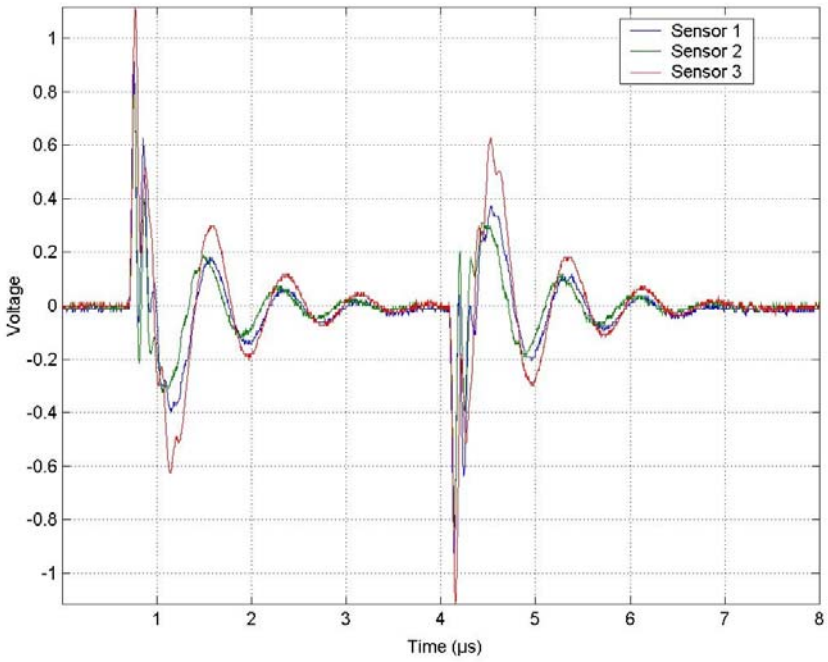

Figure D.32: New Tank Output

The normal tank transmitting and receiving signals are shown in Figures D.33 and D.34, respectively. These signals are characteristic of normal operation of the cylinder, and used to show the signals transmitted and received from a healthy tank.

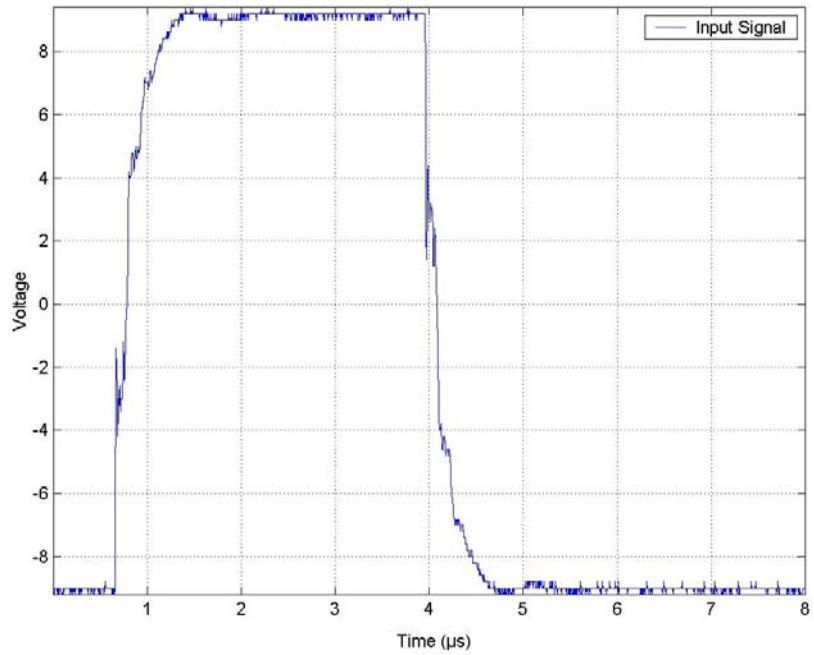

Figure D.33: Normal Tank Input

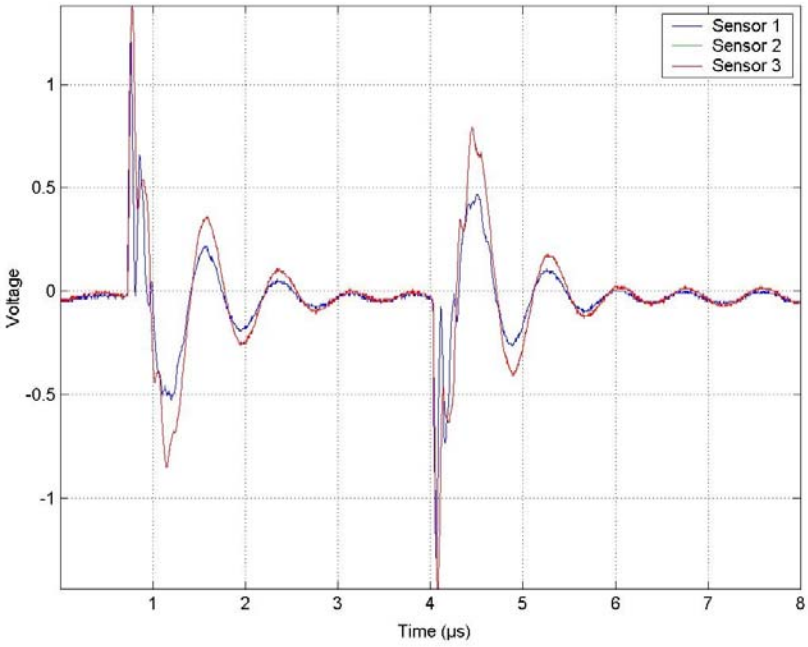

Figure D.34: Normal Tank Output

The damaged tank has transmitted and received signals as shown in Figures D.35 and D.36, respectively. The differences between the signals of a new, normal and healthy tank are visibly different. These differences will be characterized and quantified in the following sections. However, the first step is to sort out the relevant information through filtering.

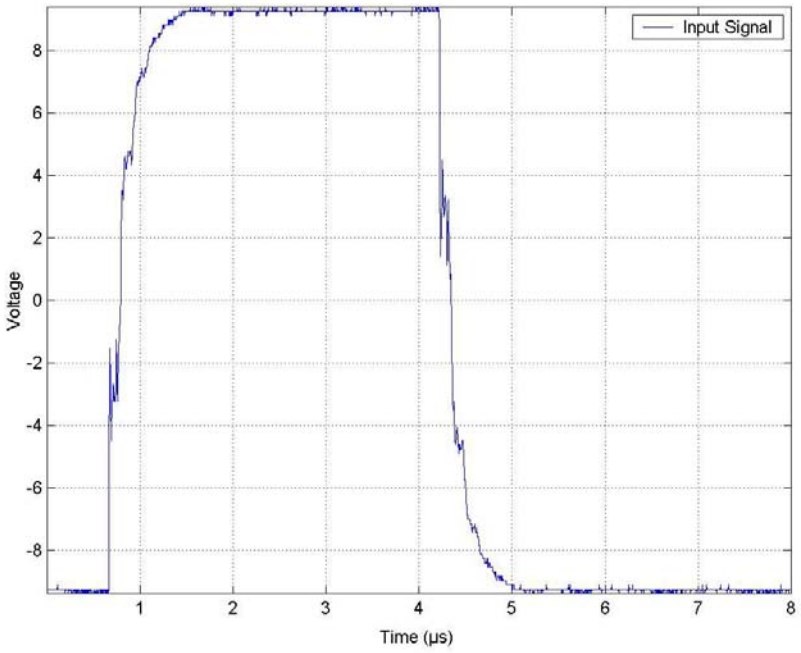

Figure D.35: Damaged Signal Input

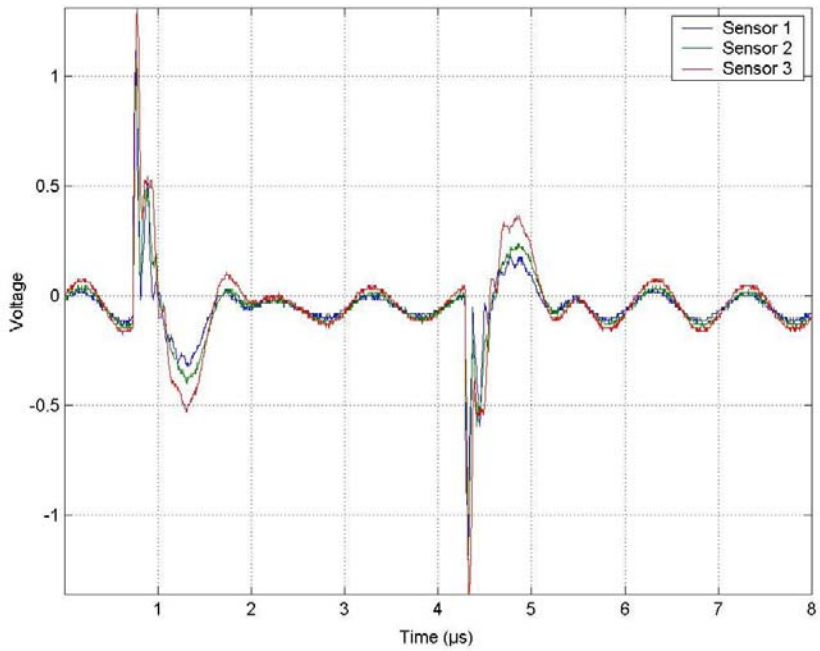

Figure D.36: Damaged Tank Signal Out

D.3.2 Filtered Signals

Using the filters described in Figure D.29 and Section 2, the data have been reduced by removing both the low and the high frequencies. This leaves the signal portions considered relevant for comparison and analysis purposes.

The new tank signals are shown in Figures D.37 and D.38 for the transmitted and received signals, respectively. More or less, little or no information is left in the new tank received signals. Significant information is left in the transmitted signal.

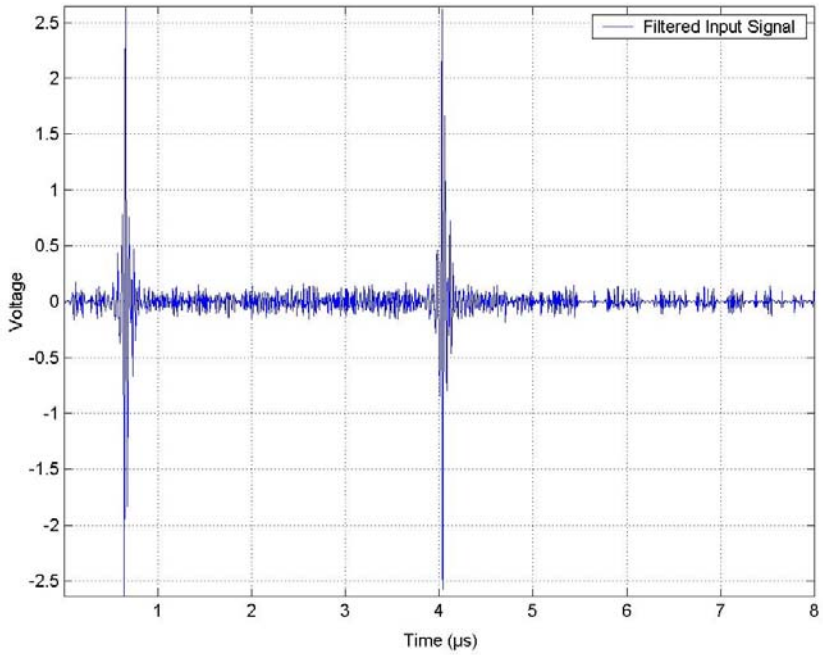

Figure D.37: Filtered New Tank Signal In

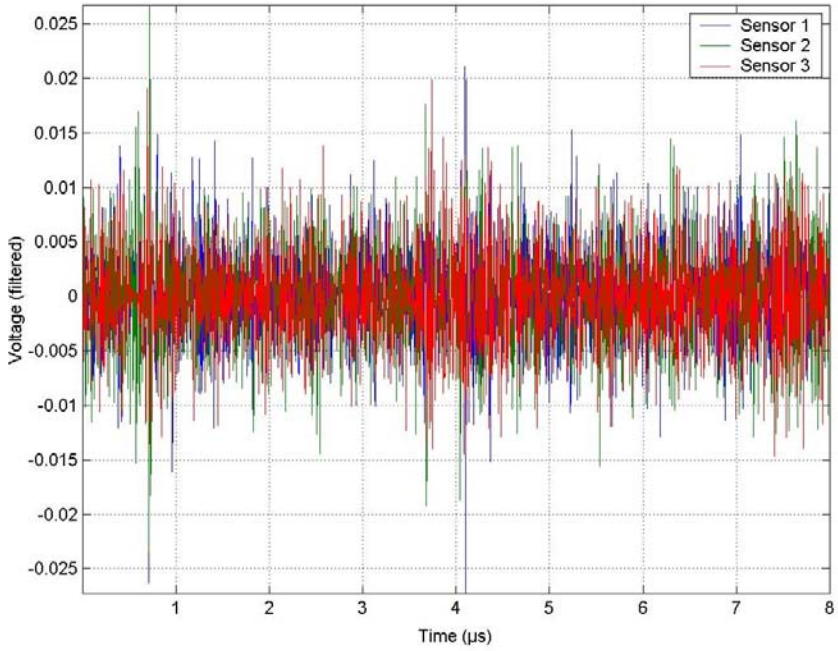

Figure D.38: Filtered New Tank Signal Out

Figures D.39 and D.40 illustrate the normal, healthy tank signals for the transmitted and received signals, respectively. The higher frequency components associated with the impulse rise and fall remain as the major components of the signal after filtering. Notice the amplitude increase between the new tank and normal tank received signals.

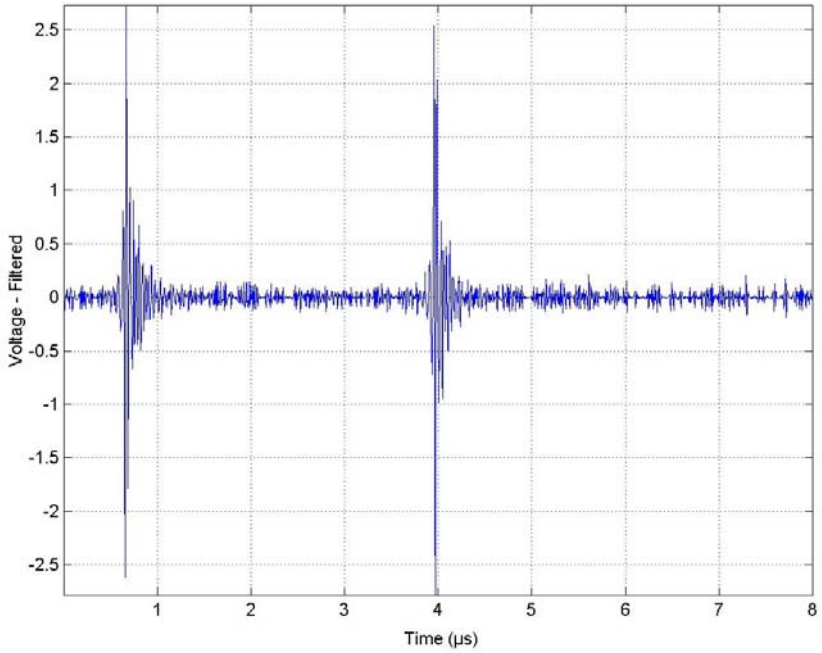

Figure D.39: Normal Tank Filtered Signal In

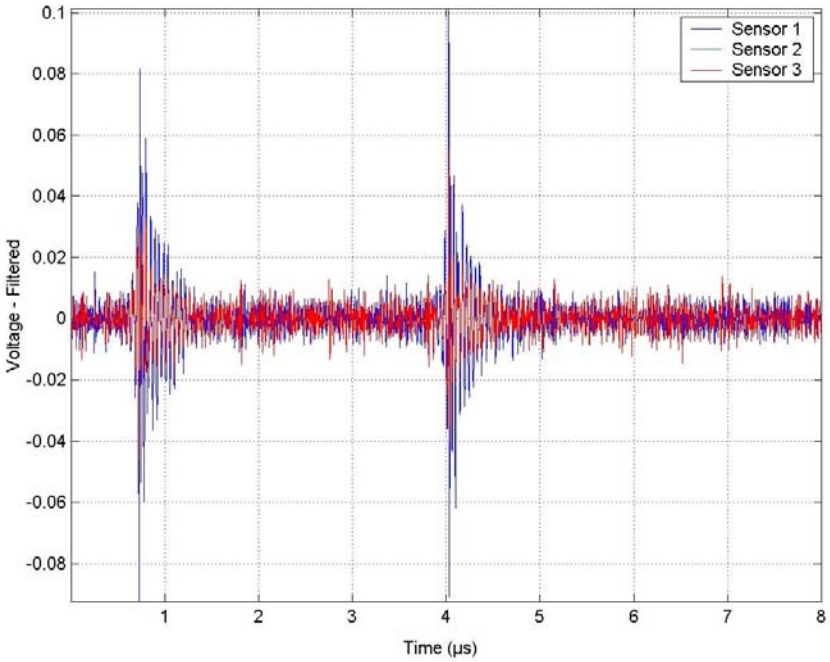

Figure D.40: Normal Tank Filtered Signal Out

Figure D.41 and D.42 illustrate the filtered time signals from the transmitted and received sensors, respectively. Notice the increase in amplitude of the received signal strength when compared to the normal tank received signals.

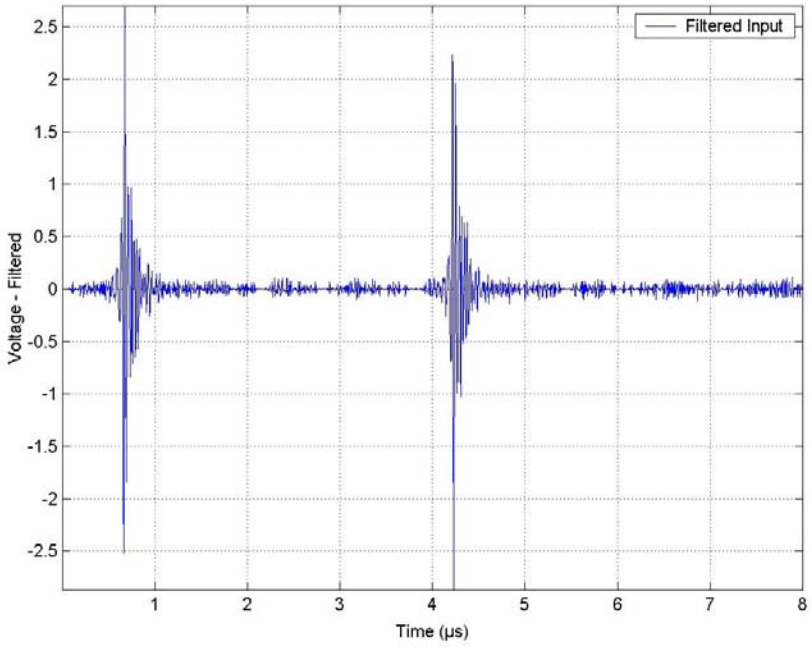

Figure D.41: Damaged Tank Filtered Signal In

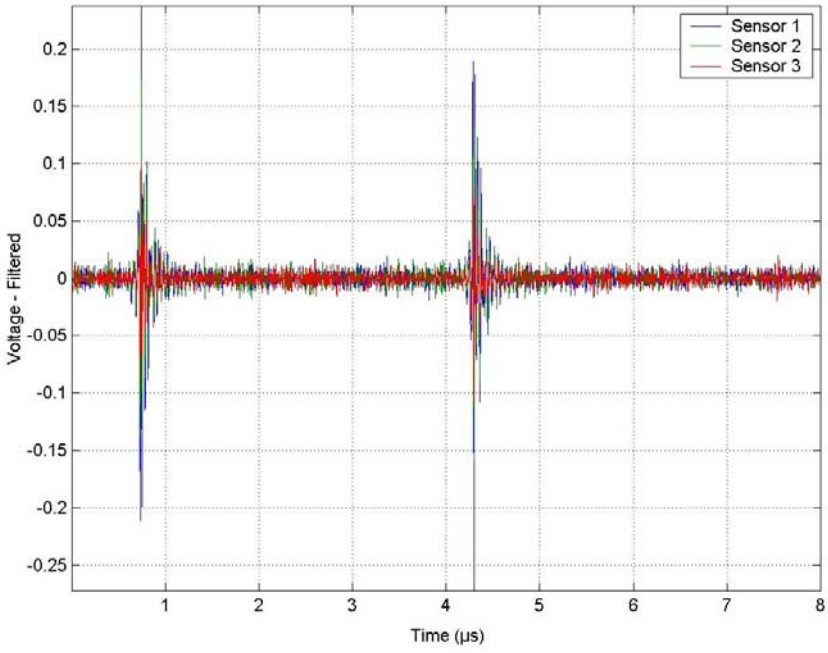

Figure D.42: Damaged Tank Filtered Signal Out

As the amplitude of the signals is easily observed to change as the tank is damaged, the frequency content of the signals also change. This is addressed in the following section.

D.3.3 Windowed PSD Through Welch's Method

The power spectral density (PSD) is an accurate method to analyze and compare frequency content of signals. The PSD provides a dimensionless power indicator on the vertical axis as a function of frequency, found on the horizontal axis. The PSD information is compared from a new tank to a normal tank and a new tank to a damaged tank.

Figures D.43 and D.44 show, respectively, the PSD information for the transmitted and received signals on a new tank. As can be seen in both figures, the filtering process is very effective at removing frequency content above the 80 MHz cutoff and below the 20 MHz cutoff. As can be expected, for the new tank there is significant power in the transmitted signal in these frequencies; however, little power is received in all of the receiving sensors.

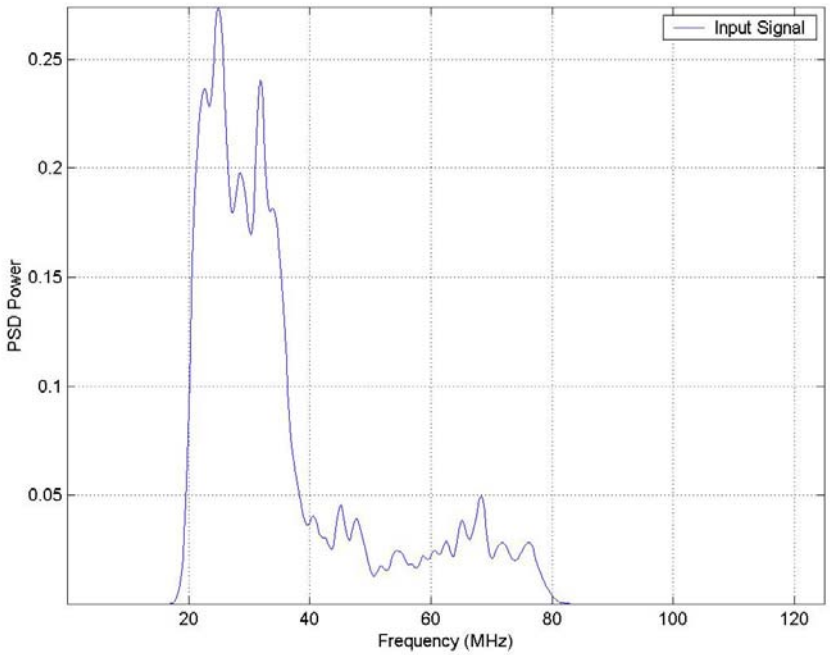

Figure D.43: New Tank Input Signal PSD

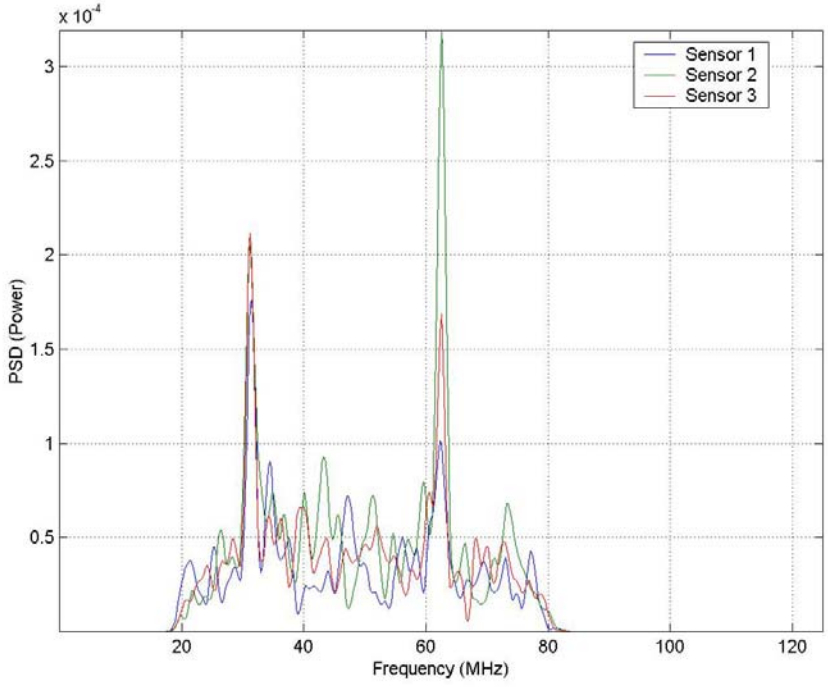

Figure D.44: New Tank Output Signal PSD

Figures D.45 and D.46 show the PSD information for the normal tank transmitting and receiving sensors, respectively. Again, the PSD power is very effectively filtered for frequencies above and below the filter cutoffs. The power is observed to increase from the new tank PSD on the received signals.

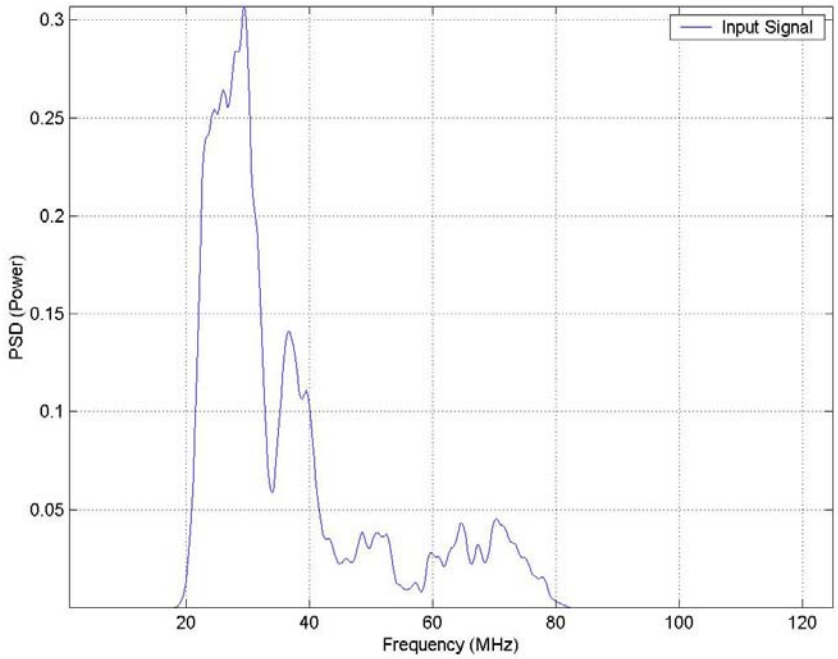

Figure D.45: Normal Tank Input PSD

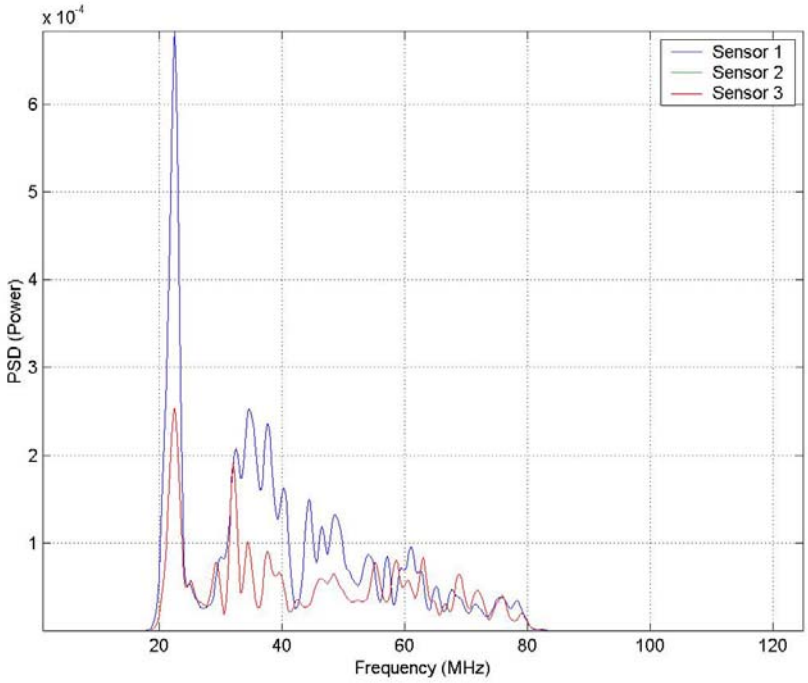

Figure D.46: Normal Tank Output PSD

Figures D.47 and D.48 show the input and output PSD for the damaged tank, respectively. The input PSD for the damaged tank does not significantly deviate from the new tank input PSD, shown in Figure D.43. However, the output PSD varies significantly, and, in fact, the PSD signals vary inbetween receiving sensors, which indicates proximity to the damage. However, it is the objective of this work to examine tanks only for the presence of damage, not the cause and location of the damage.

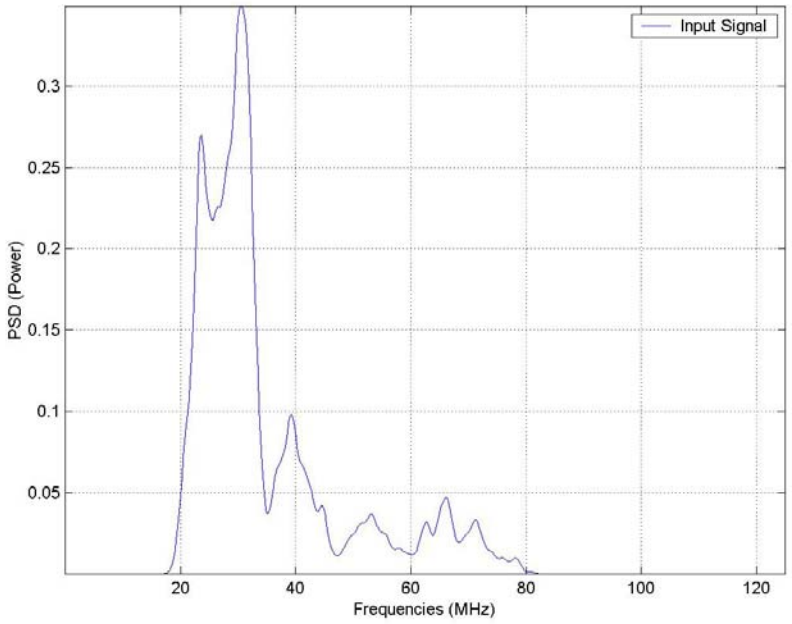

Figure D.47: Damaged Tank Input Signal PSD

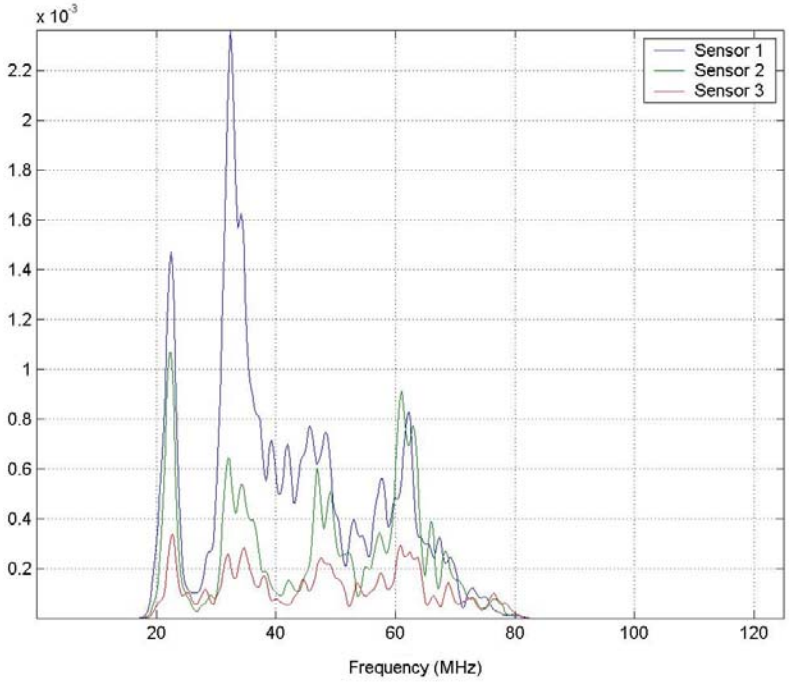

Figure D.48: Damaged Tank Output Signal PSD

In order to ensure a reliable and trouble-free analysis method, the PSD will be further windowed.

D.3.4 Frequency Window (Cutoff)

Utilizing the 256 point Hamming Window, illustrated in Figure D.30, the PSD information is windowed next to ensure that only reliable information is being used in the analysis calculations. This is an important step to ensure removal of noise and other influences that can cause errors in operation.

In the following figures, the Hamming Window has been applied to the PSD diagrams for the new, normal and damaged tanks. Figures D.49 and D.50 show the new tank PSD windowed information for the input and output signals, respectively. Figures D.51 and D.52 show the normal tank PSD windowed information for the input and output signals, respectively. Similarly, Figures D.53 and D.54 show the damaged tank PSD windowed information for the input and output signals, respectively.

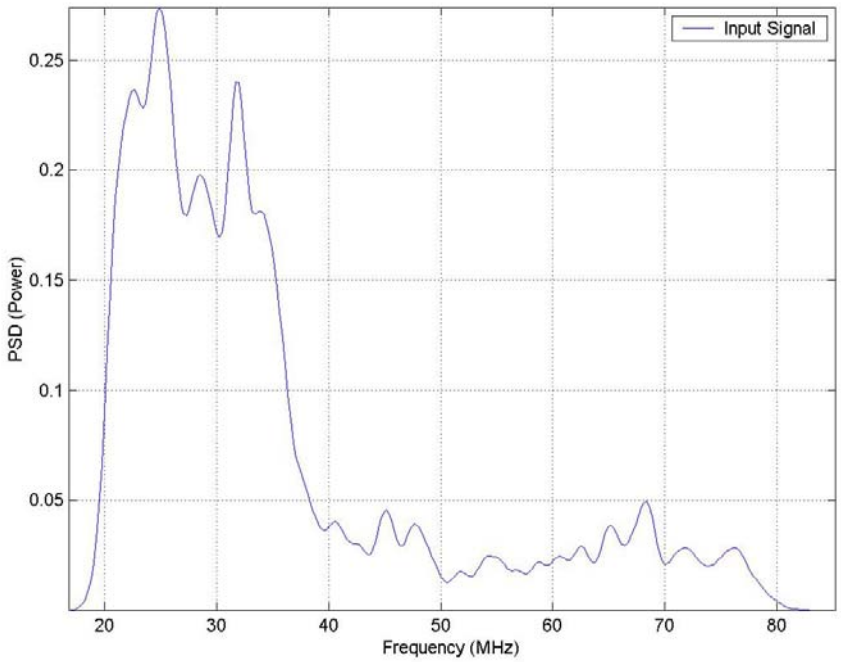

Figure D.49: New Tank PSD Window Signal Input

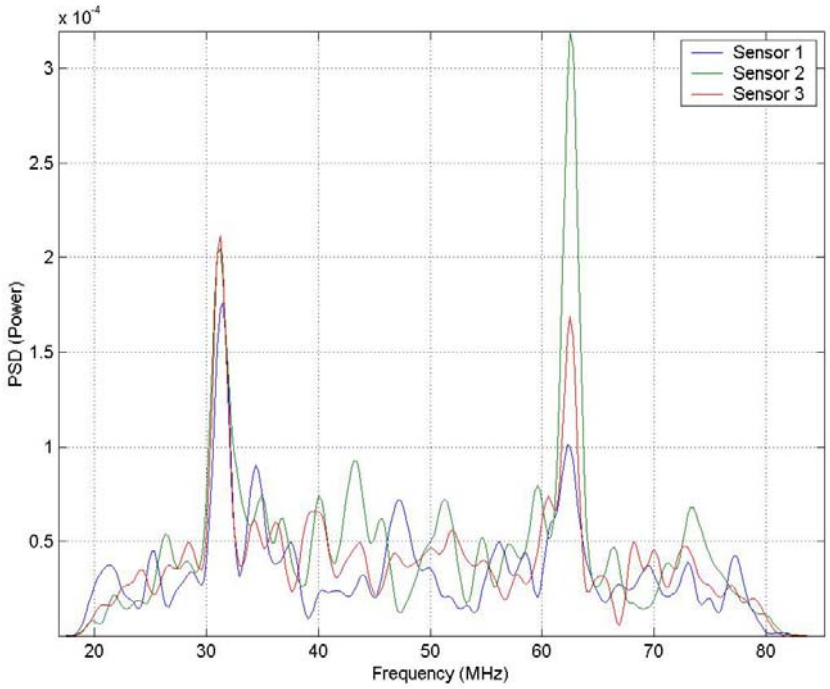

Figure D.50: New Tank Signal Output Windowed PSD

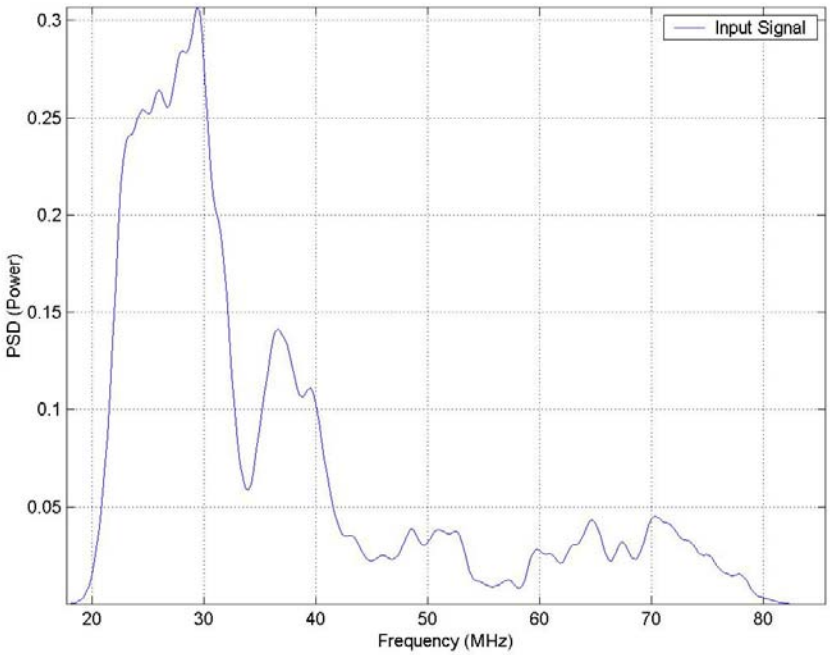

Figure D.51: Normal Tank Signal Input Windowed PSD

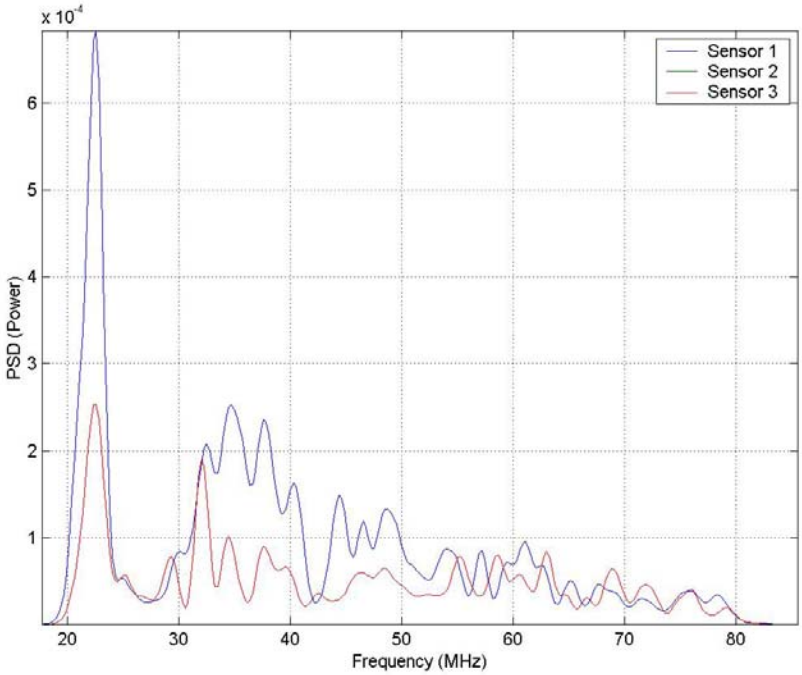

Figure D.52: Normal Tank Signal Output Windowed PSD

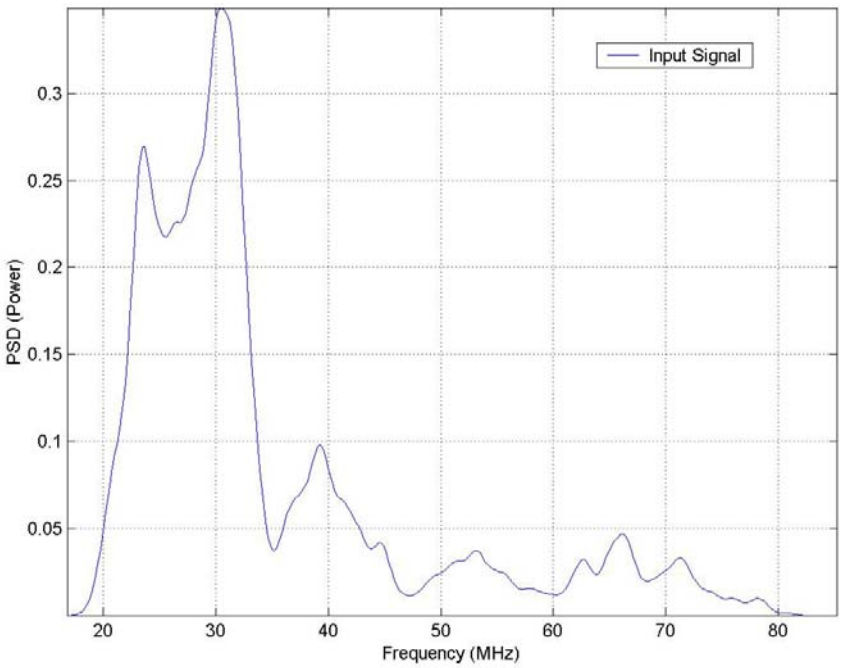

Figure D.53: Damaged Tank Signal Input Windowed PSD

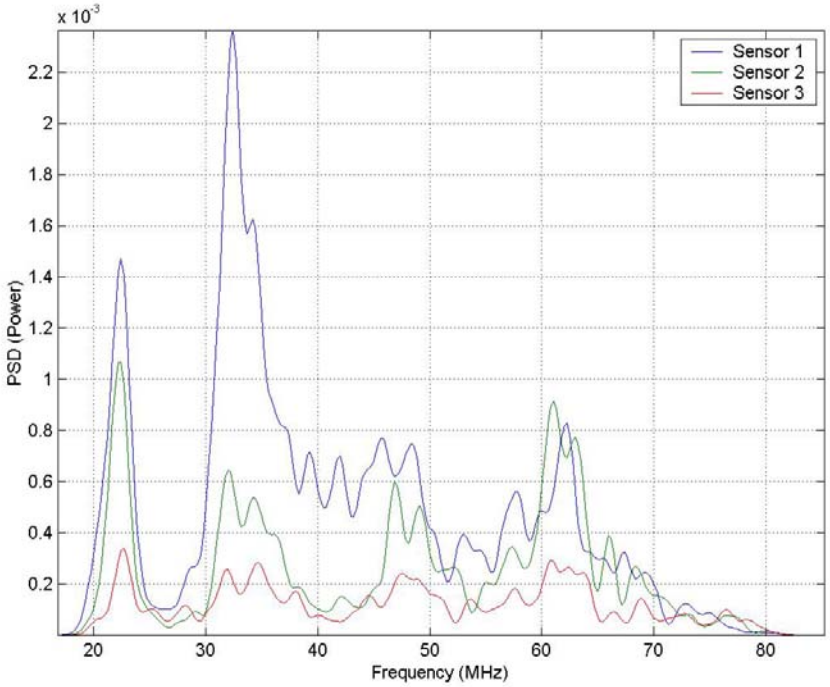

Figure D.54: Damaged Tank Signal Output Windowed PSD

In all of the above figures, they are similar to their non-windowed counterparts as they are windowed which cuts off the frequencies above and below the windows.

These windowed PSD diagrams will be used to compare normal and damaged tanks through the use of ETFE's.

D.3.5 Transfer Function Estimate

The empirical transfer function estimate as defined in previous sections is used to compare the relationship between input and received signals. In particular, the ETFE allows for a frequency-dependent comparison to be made which represents the signature of the tank.

Figure D.55 shows the ETFE given for a new tank. Peaks in the frequency are shown in the normalized ETFE on the vertical axis. These peaks represent the frequency-dependent features of the tank.

Figure D.56 shows the ETFE as calculated for a normal tank from the windowed PSD. The normalized ETFE shows low amplitude features of the normal tank ETFE.

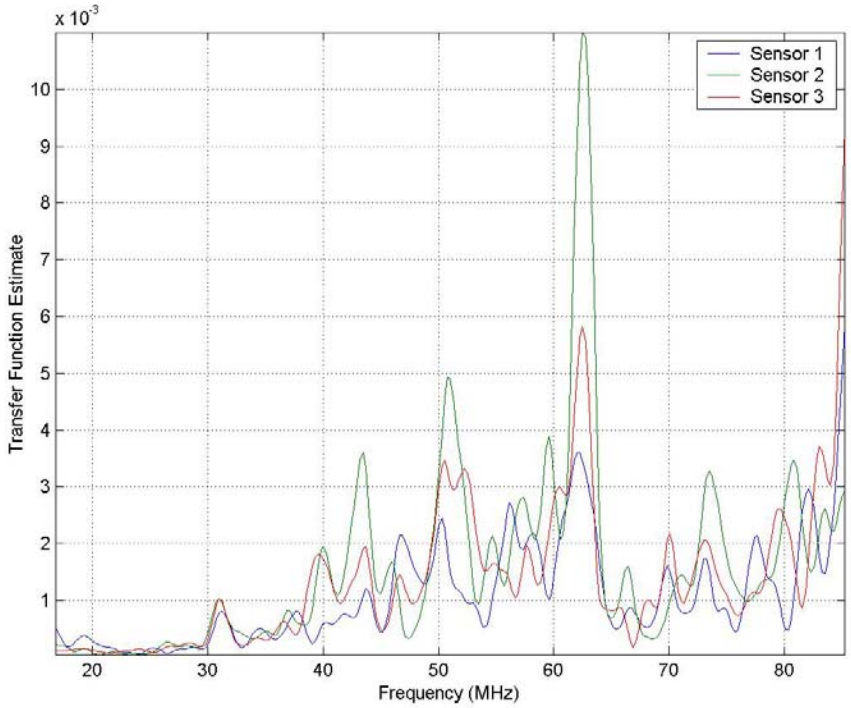

Figure D.55: New Tank Transfer Function Estimate

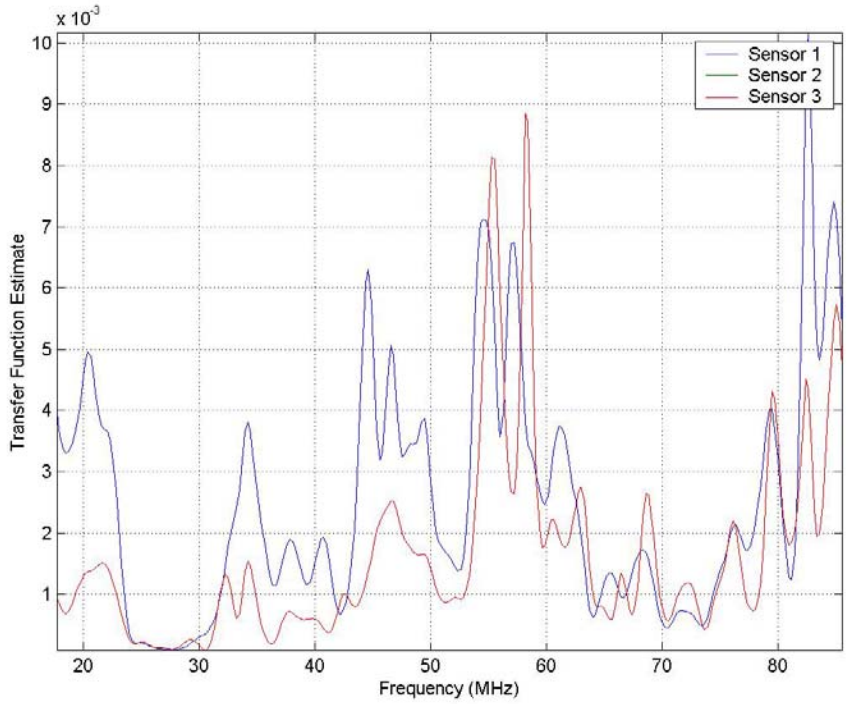

Figure D.56: Normal Tank Transfer Function Estimate

Figure D.57 shows the damaged tank ETFE, based on the windowed PSD calculations. Notice the increase in ETFE amplitude for the damaged tank when compared to a normal tank's signatures (almost a factor of 10). These variations in amplitude need to be quantified in order to assess the health of a tank.

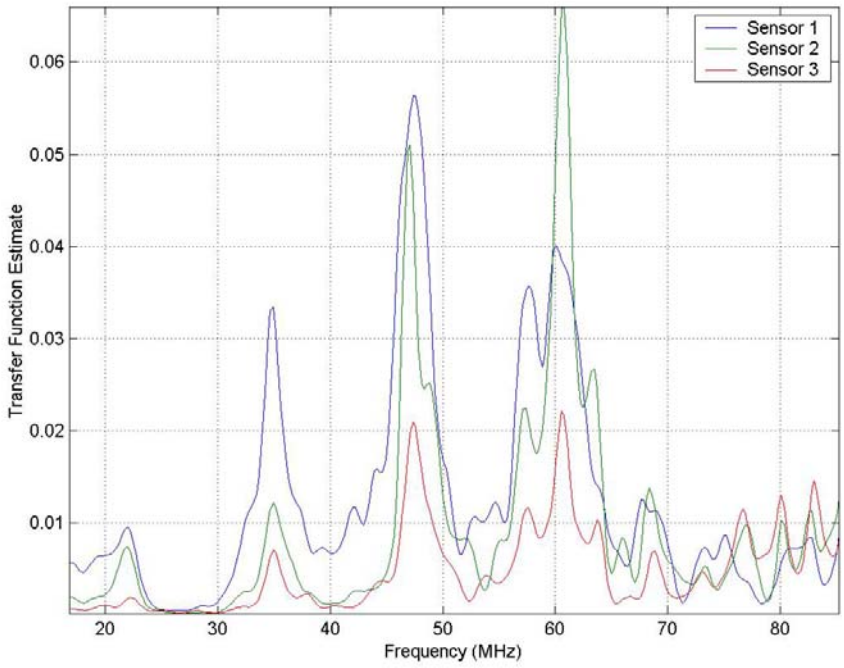

Figure D.57: Damaged Tank Transfer Function Estimate

D.3.6 Comparison of Transfer Function Estimates

Figure D.58 gives the comparison of the ETFEs of a new tank and the normal tank. This is done through a vector division of the ETFE of the current signal from the tank by the ETFE as baselined from the tank when new. This is done for each of the three receiving sensors. As a result of this matrix division, changes are shown as spikes or peaks in division of the normalized transfer function estimates.

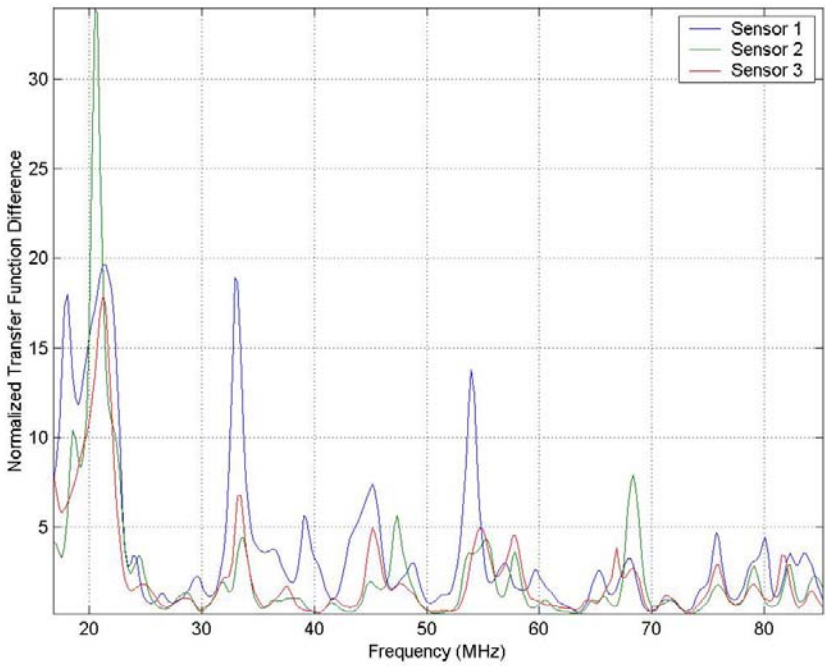

Figure D.58: Normal Tank Comparison of Empirical Transfer Function Estimate

Similar to the normal tank, the damaged tank's ETFEs can be compared to the new tank's ETFE. This comparison is shown through the division as given in Figure D.59. As can be seen in this figure, the normalized transfer function difference from the damaged tank is significantly larger than that from the normal tank's signals.

These differences can be seen from sensor to sensor, and are quantified into a single number for indication of the structural integrity of the tank.

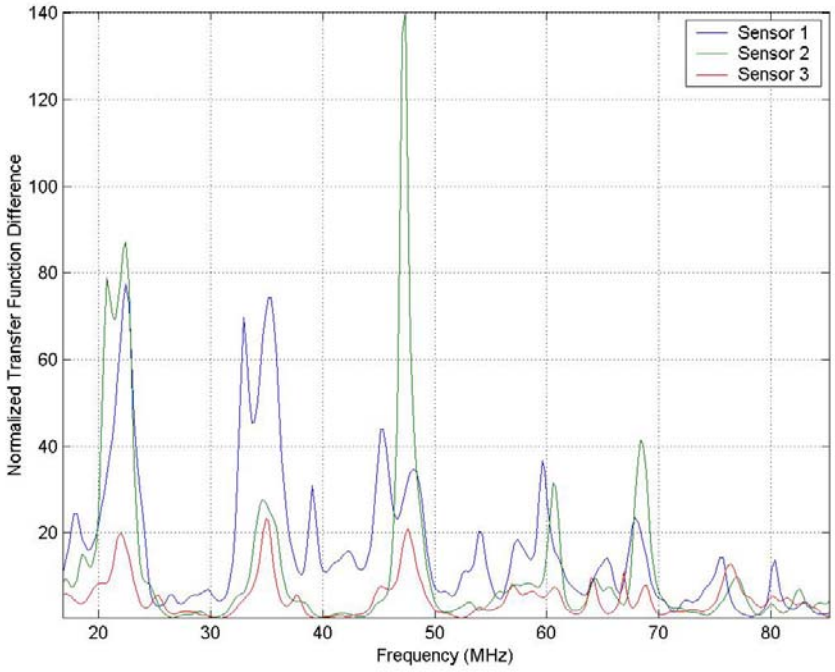

Figure D.59: Damaged Tank Comparison of Empirical Transfer Function Estimate

D.3.7 Root Mean Squared and Scaling

The final step of analysis is the reduction of the normalized transfer function difference into a single number. This is done through a root mean squared calculation, or as:

$$y_j = \sqrt{\frac{\sum_{i=1}^{M} u_{ij}^2}{M}} \tag{D.4}$$

where,

y is the rms at time j,

u is the normalized transfer function difference, and

M is the number of data points in the 17 MHz to 85 MHz region.

In order to quantify the damage to the cylinder, the results need to be reduced to an indicator that can easily be used for comparison purposes. It was determined that a single number indicator would be sufficient for this purpose. In the calculation of the empirical transfer function estimate, essentially a signature of the tank is created. In order to compare these signatures, division of the measured signature over the baseline signature was completed, resulting in a vector of comparison numbers as a function of frequency. Hence a value of unity is considered as no change, but changes in amplitude at the resonant frequencies in the signature can result in large-scale variations. Accordingly, the comparison vector was analyzed with a root-mean-squared analysis and then scaling by the length of the vector to bring the normal undamaged indication back to unity.

Note that this single number, as indicated in the analysis method, is scaled such that 1 is the baseline or normal operation. Damage is indicated with scaled numbers varying from this normal baseline of 1. The damage indicator thresholds of critical damage would not be necessarily defined as the critical damage level was not defined in this project. In this project, non-critical damage has been used as the detection criteria to allow for adequate sensitivity for real applications of this technology.